BRNO UNIVERSITY OF TECHNOLOGY

VYSOKÉ UČENÍ TECHNICKÉ V BRNĚ

CENTRAL EUROPEAN INSTITUTE OF TECHNOLOGY BUT

STŘEDOEVROPSKÝ TECHNOLOGICKÝ INSTITUT VUT

THERMOMECHANICAL RESPONSE OF POLYMER NANOCOMPOSITES WITH PREPARATION PROTOCOL CONTROLLED NANOPARTICLE DISPERSION

TERMOMECHANICKÉ CHOVÁNÍ POLYMERNÍCH NANOKOMPOZITŮ S DISPERZÍ NANOČÁSTIC KONTROLOVANOU POMOCÍ PŘÍPRAVNÉHO PROTOKOLU

DOCTORAL THESIS
DIZERTAČNÍ PRÁCE

AUTHOR
AUTOR PRÁCE

Ing. František Ondreáš

SUPERVISOR
ŠKOLITEL

prof. RNDr. Josef Jančář, CSc.

BRNO 2018

Abstract

This thesis is focused on a fundamental investigation of nanoparticle self-assembly in polymer liquids and on properties of the prepared polymer nanocomposites with controlled nanoparticle dispersion. Despite recent progress in understanding polymer nanocomposites, there are still unfilled gaps in the fundamental knowledge of relaxation phenomena and mechanical properties of various nanostructures that would provide key information for designing hierarchical or multidomain nanocomposites processable by additive manufacturing technologies. The emphasis was put on the investigation of the preparation protocol influence on the final dispersion state, preparation of various nanostructures – individually dispersed NPs, chain bound clusters, and contact aggregates at a constant composition, and determination of their relaxation and mechanical properties. Moreover, nanoparticles were utilized as "probes" in polymer matrix that affect the segmental ordering and the relaxation dynamics of polymer chains. This approach can help to derive the relationship between the nano scale segmental dynamics and macro scale mechanical properties of polymer glasses. It is a challenging fundamental scientific problem with an extreme technological importance. Non-grafted ceramic nanoparticles and polymer glasses were used to avoid the focus to deflect from the study of the nanoparticle–polymer interaction influence towards the influence of the graft–polymer interaction or the altered crystalline structure. A thorough investigation was performed for the PMMA/SiO_2 model system and subsequently broadened to systems with different matrices (PC and PS) and nanoparticles (ZnO_2 and Fe_2O_3) in order to generalize the obtained results. Nanostructure, volume fraction, and composition dependences of relaxation – glass transition temperature, reptation time, plateau modulus, number of entanglements, and mechanical properties – yield stress, yield drop, elastic modulus, strain hardening modulus, and creep response were determined. Achieved results were interpreted by means of the recent models. The determined relaxational and mechanical properties were connected to provide information about the molecular processes responsible for the mechanical response of the polymer nanocomposites.

Key words

Polymer nanocomposites, nanoparticle self-assembly, relaxation properties, mechanical properties

Abstrakt

Tato dizertační práce je zaměřená na základní výzkum procesů samouspořádávání nanočástic v polymerních kapalinách a na vlastnosti připravených polymerních nanokompozitů s řízenou disperzí nanočástic. Navzdory současnému pokroku v porozumění polymerních nanokompozitech, stále chybí mnohé fundamentální znalosti relaxačních a mechanických vlastností polymerních nanostruktur, které by mohly poskytnout klíčové informace pro návrh hierarchických funkčních kompozitů zpracovatelných aditivními výrobními technikami. Hlavní důraz byl kladen na výzkum vlivu postupu přípravy nanokompozitu na finální stav disperze nanočástic, přípravu řízených nanostruktur – individuálně dispergované nanočástice, řetězci vázáné klastry a kontaktní agregáty - a určení jejich relaxačních a mechanických vlastností. Navíc byly nanočástice využity jako „sondy“ v polymerní matrici, které ovlivňují segmentální uspořádání a relaxační dynamiku polymerních řetězců a mohou poskytnout o těchto dějích zásadní informace. Tento přístup může pomoci nalezení vztahů mezi segmentální dynamikou na nano škále a mechanickými vlastnostmi polymerních skel na makro škále, což je náročný fundamentální problém s extrémní technologickou důležitostí. Neroubované keramické nanočástice a polymerní skla byly použity, aby se minimalizoval vliv silných interakcí mezi nanočásticemi a řetězci. Podrobný výzkum byl vykonán na modelovém systému PMMA/SiO_2 a následně rozšířen na systémy s jinými matricemi (PC a PS) a jinými nanočásticemi (ZnO_2 and Fe_2O_3) za účelem zobecnění obdržených výsledků. Byla určena závislost relaxačních a mechanických vlastností (teplota skelného přechodu, reptační čas, modul kaučukovitého plata, počet zapletenin, napětí na mezi kluzu, pokles napětí po mezi kluzu, elastický modul, modul deformačního zpevnění a odezvy při toku za studeny) na nanostruktuře, objemovém zlomku a složení. Získané výsledky byly interpretovány za použití současných modelů. Stanovené relaxační a mechanické vlastnosti byly propojeny, aby poskytli informace o molekulárních deformačních procesech řídících mechanickou odezvu makroskopických kompozitních těles.

Klíčová slova

Polymerní nanokompozity, samouspořádávaní nanočástic, relaxační vlastnosti, mechanické vlastnosti

ONDREÁŠ, F. *Termomechanické chování polymerních nanokompozitů s disperzí nanočástic kontrolovanou pomocí přípravného protokolu.* Brno: Vysoké učení technické v Brně, Středoevropský technologický institut VUT, 2018. 102 s. Vedoucí dizertační práce prof. RNDr. Josef Jančář, CSc..

Declaration

I declare that this thesis has been compose solely by myself under the supervision of prof. RNDr. Josef Jančář, CSc. and that all quotations of the literary sources are accurate and complete. The presented results are the property of Central European Institute of Technology at Brno University of Technology and all commercial uses are allowed only if approved by both the supervisor and the director of the Central European Institute, BUT.

Brno …… ...……

(author´s signature)

Acknowledgment

I would like to thank prof. RNDr. Josef Jančář, CSc. for his supervision. My deepest appreciation is addressed to my colleague Ing. Petr Lepcio for the close collaboration on the topic, particularly on the structuring phenomena of polymer nanocomposites, with whom I shared experimental samples, results and wisdom. I also highly value the collaboration with Ing. Klára Zárybnická and Ing. Marek Zbončák. I am grateful for the assistance provided by my colleagues at the Central European Institute of Technology, especially for the USAXS measurements by Mgr. Ondřej Caha, Ph.D. and the inspiring discussions with Ing. Jakub Sadílek. Part of the work was carried out with the support of CEITEC Nano Research Infrastructure, CEITEC Brno University of Technology. Many thanks to Dobromila Klemová and Ing. Ladislav Ilkovics from the Institute of histology and embryology at the Medical faculty of Masaryk University in Brno for the collaboration on the transmission electron microscopy. I thank prof.dr.ir L.E. Govaert for supervising me during the internship at the Eindhoven University of Technology and Leoind Pasthukov for his aid. I would like to express special gratitude to my wife her support and patience. Finally, I thank my family and friends for the support.

Table of Contents

1. General introduction into polymer nanocomposites

Progress of human society is connected with new technologies, which are closely related to the level of sophistication of the available materials and manufacturing processes. To meet recent challenges, novel bottom-up material platforms must be developed capable of adding end-use specific functions to their ever-enhancing physico-chemical properties and environmental friendliness. Synthetic and natural polymers and composites are increasingly utilized as functional materials in fields ranging from aerospace to medicine. Nanocomposites, i.e., composite materials with one or more nano-structured components may open a path for new-generation nano-devices. "Bottom-up" self-assembly approaches are limited only by size of the building block, if nanoparticles are used current design limits can be overcame. With aid of this approach, structures with tailored shape and internal structure can be prepared. Development of "bottom-up" fabrication platforms to generate 1-D, 2-D, and 3-D precisely ordered nanoparticle arrays may increase understanding of the physical properties of this new family of materials, develop structure-property function, and led to fabrication of next-generation nanoparticle-based devices including memory storage devices, batteries, photonic crystals, plasmonic waveguides, optical lens, photovoltaics, and nanoelectronic circuits. The "bottom-up" self-assembly approach taking the best of small molecules, nanoparticles and polymers is schematically shown in the Figure 1[1].

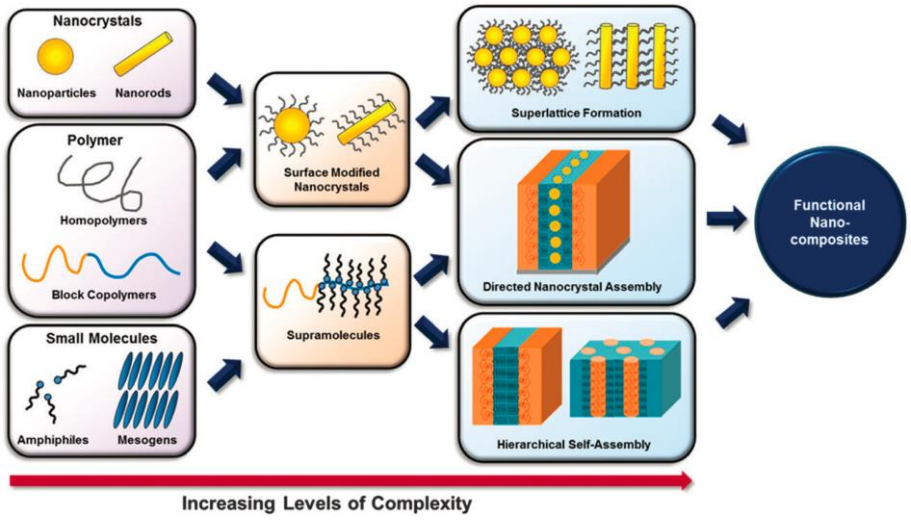

Figure 1: Schematically illustrated bottom-up self-assembly approach taking the best of small molecules, nanoparticles, and polymer to create next-generation materials. Reproduced from[1] with permission of The Royal Society of Chemistry.

As reported many times[2-4], polymer nanocomposites can provide properties unachievable by traditional composites. Rigorous investigation of common natural materials[2, 4-8] have shown that nature can create materials with advanced properties, for example simultaneous high stiffness and toughness or combined functionality and tailored mechanical properties. Nature can control self-assembly process to create hierarchical structures where original building

blocks – molecules or nanoparticles, are assembled into structures that are again used as building blocks during creating more complex structure on larger scales. Typical example of often studied natural system with extraordinary mechanical properties combining high stiffness and toughness is nacre[4-6]. Nacre consists of 95 vol. % of aragonite $CaCO_3$ and 5 vol. % biopolymers. These components form organized structures – platelets with bridges at micro scale that are organized further into brick and mortar structure at meso scale. Structure of nacre is shown in Figure 2. Brick and mortar architecture have been imitated on some systems at micro and meso scale without first hierarchical level of bricks[5, 9]. It was found that brick and mortar architecture lead to highly torturous crack paths that dissipate a lot of energy, however only brick and mortar architecture is insufficient for the extremely high amount of experimentally measured energy dissipation in the case of nacre. It highlights importance of the first hierarchical level – chain bound clusters of primary nanoparticles. On the other hand, man-made polymer nanocomposites contain usually from 0.1 to 20 vol. % of filler without hierarchical assembly. Higher filler volume fractions, typically more than 10 vol. %, in man-made polymer nanocomposites lead to worsening of filler dispersion, creating contact aggregates with weak interparticle interactions, and finally to significant embrittlement.

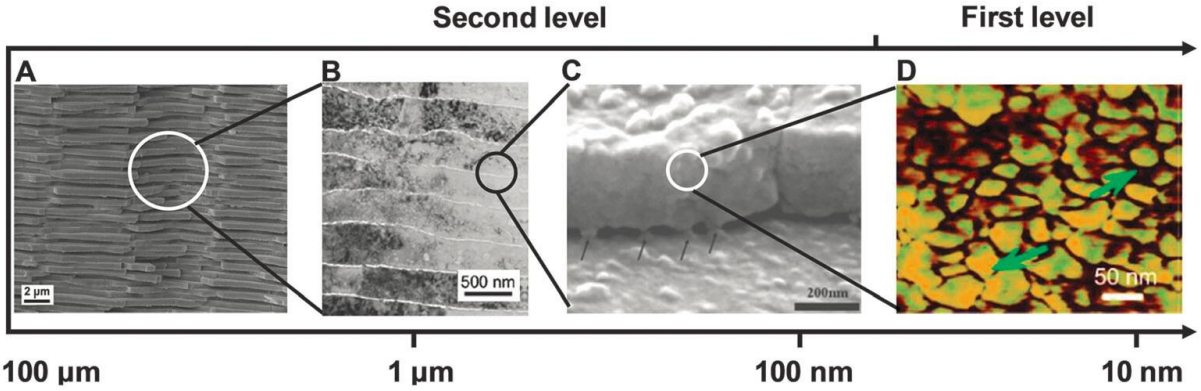

Figure 2: structure of nacre at various length scales and hierarchical levels. Reproduced from[5] with permission of The Royal Society of Chemistry.

Current experimental approaches are meeting only challenge of preparation of simple nanocomposite systems. Partial progress was achieved in the case of self-assembly of grafted nanoparticles resulting in strings and sheets[10-15]. Another successful approach was utilizing of micro-phase separation of block copolymers filled with specifically grafted nanoparticles[1, 12]. However, enthalpy interactions between nanoparticles and polymer chains are suppressed in the systems with grafted nanoparticles. Therefore, majority of variables that can affect dispersion and properties vanishes and the whole physics is reduced to graft squeezing. Then, two variables control the final dispersion state – density and length of grafts. It significantly simplifies the situation, which can be helpful in achieving desired nanostructure, but, on the other hand, diversity of variables that can influence nanostructure formation is lost.

Constructing precisely defined system with desired structure features and properties is still far from being achieved. The way, how to reach such ability, lies in the fundamental knowledge of all governing variables and processes of nanoparticle organization in a matrix. Another challenge is a fundamental understanding of mechanical and relaxation response of nanostructured composites. For example origin of mechanical reinforcement of polymer nanocomposites is still not fully understood and there is a lack of suitable models concerning processes on nanoscale. Nanoparticle can alter chain dynamics and molecular packing of polymer matrix on various time and length scales. Fundamental knowledge of such effects for relatively simple systems can help to understand more complicated structures and allow to tailor desired properties.

2. Theoretical part

2.1 Nanoparticle organization in a polymer matrix

A key to full utilization of the potential of polymer nanocomposites (PNCs) lies in the ability to control spatial organization of nanoparticles (NPs) in polymer matrix over multiple length scales. Despite the large volume of literature published on control of NP dispersion in polymer matricies[16-49], no generally accepted model quantitatively describing all the aspects of NP organization in polymer liquids has been proposed. The state of NP spatial organization critically affects the PNC properties. Since any given property requires a specific NP organization, no single length scale NP spatial organization can optimize all macroscopic properties simultaneously.

Nanoparticles can self-assemble into three limiting structures in polymer liquids. They can be organized into contact aggregates, chain bound clusters, or can be individually dispersed in polymer matrix. Particles in aggregates interact directly with each other by weak interparticle Van der Waals forces. Therefore, the whole aggregate seems like one big fragile particle. This reduces specific surface area that determines nanocomposite properties such as relaxation and mechanical response. Therefore, polymer nanocomposites with aggregates are undesirable. In the case of dispersion of individual nanoparticles in polymer matrix, maximum surface area can interact with surrounding chains and specific surface area equals to effective interface area. This is ideal state for a fundamental study, because interface area, on which interactions occur, is known, and also maximal possible amount of modified matrix is achieved in such system. Polymer nanocomposites with good dispersion of nanoparticles are characterized be significantly enhanced mechanical properties[15-17]. In the case of clusters, particles don't interact directly with each other, but through chains between them. Clusters can be considered independent entities dispersed in a polymer matrix. Thereby hierarchical system with two levels is formed.

Hooper and Schweizer[50, 51] published detailed computational study focused on the potential of mean force between hard spherical particles dissolved in an absorbing polymer melt using microscopic polymer reference interaction site mode (PRISM) integral equation theory. The model considers all reasonable variables such as particle-to-monomer size ratio, strength and spatial range of polymer–particle attractions, direct Van der Waals particle–particle attraction, and degree of polymerization. At weak interfacial attraction, all systems undergo direct nanoparticle aggregation due to extremely large depletion attraction between the particles independently on another variables. The enthalpy gain of polymer segments adsorbing onto the particle surface leads to good dispersion of NPs as the strength of interfacial polymer–particle attractions increases. In general, all systems exhibits attractive potential minima at some threshold value of the strength of the polymer–particle interactions beyond which particles tend to localize at system-specific separations. For high values of the strength and spatial range of

polymer–particle interactions, bridging-type attractions emerges in top of the already established steric stabilization layer. The latter behavior is called a tele-bridging which is similar to bridging but bridges larger distance. Direct interparticle Van der Waals interactions favor contact aggregation and hence compete with the attractive polymer–particle interactions. As they increase in strength, bridging configurations are eventually destabilized and replaced with contact aggregation as the most favored state. However, noncontact bridging minima often survive as metastable local minima, which could be significantly populated for either equilibrium or kinetic reasons due to the presence of barriers. Steric stabilization systems are much less perturbed by direct Van der Waals attractions due to the thermodynamic stability of two distinct bound layers, which resist interpenetration or desorption. These detail considerations lead to prediction of four fundamental types of pair nanoparticle organization in the matrix: contact aggregation, steric stabilization, bridging and tele-bridging. The predicted categories of the behavior of hard spheres in the polymer matrix are shown in Figure 3.

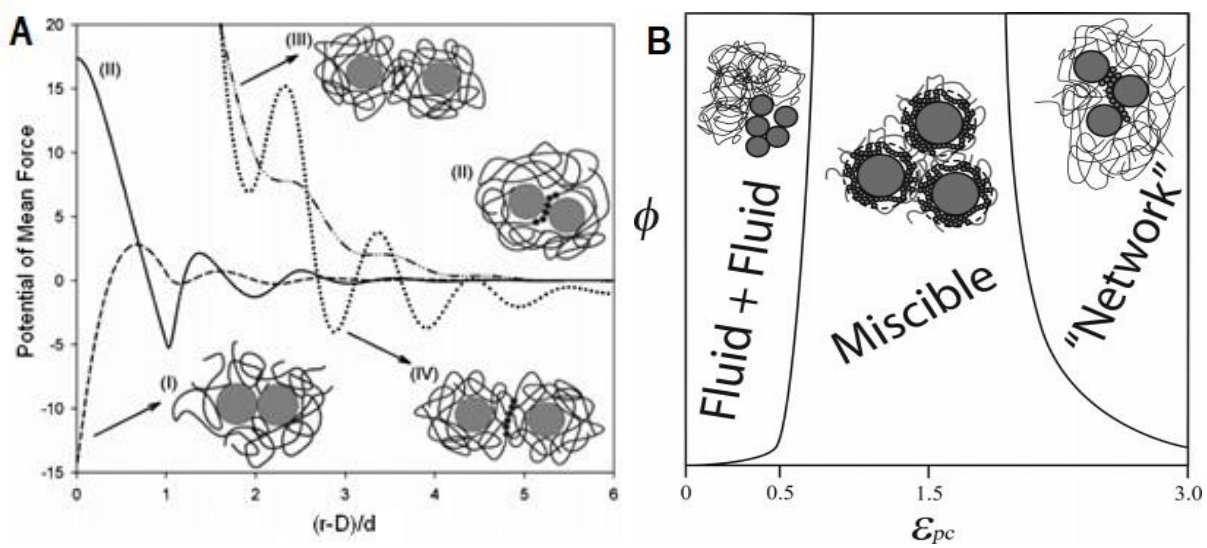

Figure 3: (A) Representative examples of the particle–particle potential of mean force for systems with particle diameter to monomer ratio of 16 and degree of polymerization of 100 which exhibit the four different types of organization: (I) dashed line, contact aggregation for low strength and spatial range of polymer–particle attractions; (II) solid line, bridging for high strength and low spatial range of polymer–particle attractions; (III) steric stabilization for medium strength and high spatial range of polymer–particle attractions; and (IV) tele-bridging for high strength and spatial range of polymer–particle attractions. Schematics of favored particle configurations are indicated. Reprinted with permission from[52]. Copyright 2018 American Chemical Society. (B) Schematic representation of generic polymer nanocomposite phase behavior. At low strength of polymer–particle attractions (units of k_BT) traditional fluid + fluid phase separation occurs, while at medium strength of polymer–particle attractions values adsorption of polymer onto the nanoparticle provides a thin bound layer that results in steric stabilization and miscibility. For high interfacial energies the adsorbed monomers

associate with multiple nanoparticles, leading to a bridging-induced "network"-like phase. Reprinted with permission from[53]. Copyright 2018 American Chemical Society.

The model was further exteded[52-54] from two particle issue to many body study in real space to find influence of filler volume fraction. Phase behavior was investigated and phase diagrams with filler volume fraction and strength of polymer–particle interaction as main variables presented on axis were constructed for various cases of particle-to-monomer size ratios, spatial ranges of polymer–particle attractions, direct Van der Waals particle–particle interactions, and degrees of polymerization. The schematic example is shown in Figure 3. It was found that the structure of the model polymer nanocomposites reflects a balance between two very different competition effects. One limit is entopically dominated athermal system, where oscillatory depletion attractions favor contact particle aggregation. The other limit is an enthapically dominated mixture, where addition of strong attractive interactions between the filler and monomers results in thin layers of polymer strongly associating with, or adsorbing onto, the particles. The resulting particle–particle potential of mean force favors well-defined, small interparticle separations, i.e., local bridging. Between these two extremes, third behavior, in which a polymer gains enough cohesive interaction energy to associate with a single filler, but not enough to give up the additional entrophy required for association with multiple particles. In this case, a nanoparticle is surrounded by a thermodynamically stable bound polymer layer, typically on the order a few monomer diameter thick, which sterically stabilizes the particles in the polymer matrix.

Another widely accepted study dealing with nanoparticle organization in polymer matrix was published by Mackay et al.[19]. Experimental approach in this study simplified complex situation of multiple parameters to just one, the particle radius to polymer gyration radius ratio. It should govern phase behavior, despite of PRISM theory described above that suggests just moderate dependence of nanoparticle dispersion state on the particle-to-polymer size ratio. Phase diagram suggesting that good dispersion is obtained when gyration radius is larger than particle radius was constructed based on the experimental data ant it is shown in Figure 4. In addition, authors suggest that dispersed nanoparticles swell the linear polymer chains, resulting in a polymer radius of gyration that grows with the nanoparticle volume fraction in non-expected manner with slope $1+\nu_f$ that overcome expected excluded volume prediction $(1+\nu_f)^{1/3}$, where ν_f is volume fraction (Figure 4). This behavior suggests significant conformation changes caused by presence of nanoparticles.

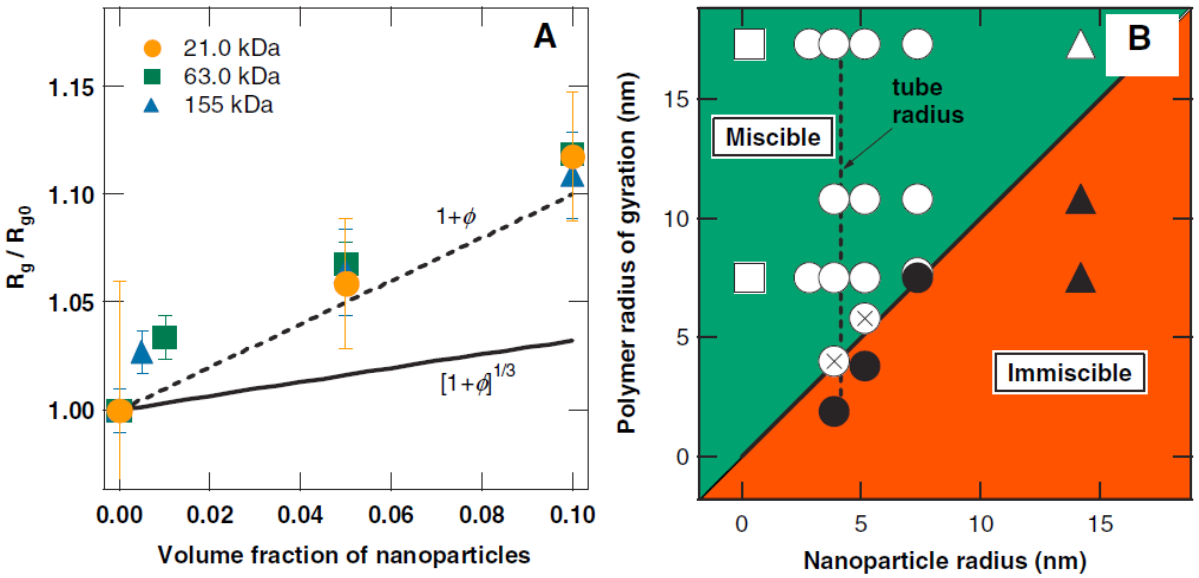

Figure 4: (A) The polymer radius of gyration (R_g) relative to that that without nanoparticles (R_{g0}) for three different molecular mass linear polystyrenes with 21, 63, and 155 kg·mol^{-1}, as function of volume fraction (Φ) of tightly cross-linked polystyrene nanoparticles with molar mass 52 kg·mol^{-1}. The nanoparticles stretch the polymer chains. The solid line represent the radius of gyration variation if the polymer density does not change upon mixing, and the behavior $(1+\Phi)^{1/3}$ is expected. Instead, the data obeyed $1+c\Phi$ with c about 1. From[19]. Reprinted with permission from AAAS. (B) A polymer radius of gyration–nanoparticle radius phase diagram, with the solid circles representing data where phase separation was detected and the open circles where miscibility occurs. Open circles with an × represent conditions where some agglomeration was detected by SANS yet large scale phase separation was not observed. Squares are the C60-polystyrene system; circles; the polystyrene nanoparticle-polystyrene system; and triangles, the dendritic polyethylene-polystyrene system. The dashed line represent the reptation tube radius, suggesting phase stability does not depend on entanglement structure. The nanoparticle fraction used to generate each data point was 2 wt. %. From[19]. Reprinted with permission from AAAS.

While significant progress has recently been made in the development of theories for predicting the equilibrium structure of the PNCs, there is a strong need to address the effects of processing and kinetic traps on their structure development. The NP spatial organization in an amorphous polymer results from a complicated interplay between thermodynamically controlled NP organization in the liquid phase, mixing kinetics in the liquid nanocomposite and the kinetics of the liquid nanocomposite vitrification. However, one has to keep in mind that the equilibrium NP dispersion may be inaccessible unless the correct preparation protocol is adopted, even when the dispersed state is thermodynamically favorable.

Jouault et al.[20, 21] prepared polymer nanocomposites with two different matrices, PMMA and PS. Silica NPs with three different radii were used. Surprisingly, NPs formed approximately the same aggregates in both cases independently on the composition (Figure 5). The NP–polymer interactions were expected to be weak in PS system due to weak dipole-dipole interactions, whereas they were considered to be strong in PMMA system due to polar interactions and possible hydrogen bonding[55], however no effect on the structure was found. The results suggested that preparation protocol, i.e. used solvent and shear forces intermediated by mixing, has key influence on final dispersion state. Therefore, Jouault et al.[23] investigated the influence of casting solvent on the final spatial nanoparticle dispersion in polymer nanocomposite films. Polymer nanocomposites of bare nanosilica and poly(2-vinylpyridine) (P2VP), system with strong attractions, were prepared. It was found that the final dispersion can be tuned from well-dispersed regime due to polymer adsorption to an aggregated state induced by depletion attraction and weakening of electrostatic repulsion simply by changing the solvent used. When methyl ethyl ketone (MEK) was used as the solvent, adsorbed polymer layer was formed already in diluted state and persist into the dry state, which led to good dispersion of NPs. In the case of pyridine, P2VP does not adsorb onto nanosilica surface and contact aggregation was found. The size of adsorbed polymer layer was determined to be close to the radius of gyration of the polymer used, R_g. Zhao et al.[24] provide support for this results and suggested that in solvent casting process, the primary factor determining the formation of a bound polymer layer is the relative interaction strength between the particle-solvent, and particle-polymer.

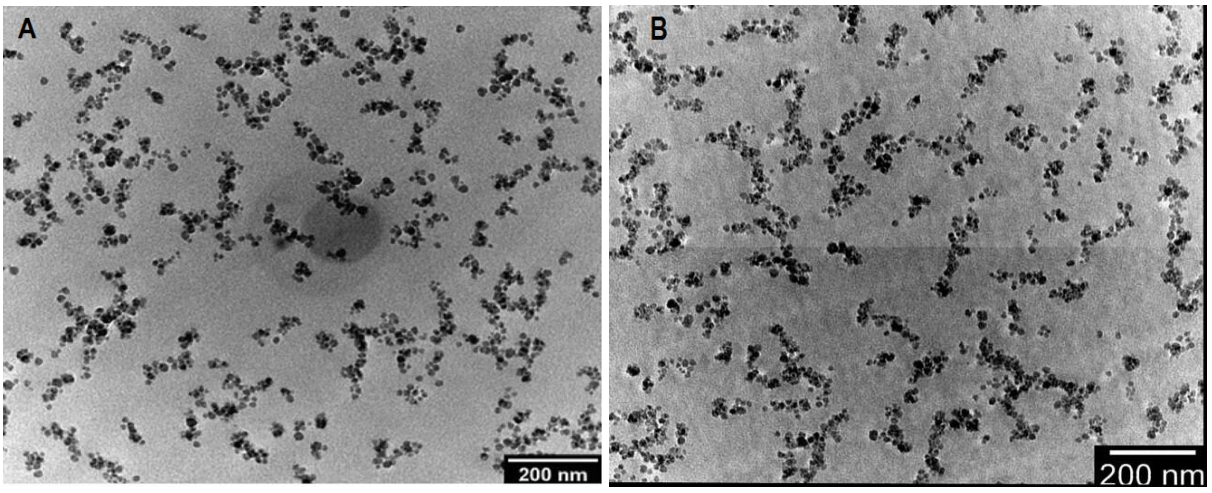

Figure 5: (A) PMMA and (B) PS filled with 5 and 6.6 vol. % of NPs, respectively, with same structure prepared at the same preparation protocol. Reprinted from[20], Copyright 2018, with permission from Elsevier. Reprinted with permission from[21]. Copyright 2018 American Chemical Society.

Kim and Zukoski[27] investigated the role of solvent on polymer segment–particle surface interactions in controlling nanoparticle dispersions in concentrated polymer solutions. Systems containing poly(ethylene glycol) as the matrix and silica nanoparticles prepared form water or

ethanol at two temperatures and various filler loadings were investigated. The results of this study were interpreted in the framework of the pseudo-two-component polymer reference interaction site model (PRISM) theory modified to account for solvent addition via effective contact strength of interfacial attraction, ε_{pc}, between polymer and particle surface. The results suggested that a complex interplay of solvent-solvent, solvent-polymer, solvent-particle, and polymer-particle interactions control the nanoparticle dispersion state. It was considered that the interfacial attraction strength represents the overall enthalpy gain of transferring a monomer unit from the continuous suspending phase to the particle surface during building of adsorbed polymer segment layer. Then, if the adsorbed monomer originates from a polymer–solvent mixture, the interfacial attraction strength losses from polymer-solvent, nanoparticle-solvent interaction and gain from solvent-solvent interactions. So, overall strength of the interactions between polymer segments and nanoparticle surface depends on above described interactions and on the volume ration of polymer in mixture. Based on these considerations and evaluation of the experimental results with aid of PRISM theory, dependence of the interfacial polymer-particle attraction strength on the volume ration for systems prepared from two different solution at two temperatures was constructed (Figure 6). Moreover, two different structures were created at theta conditions from different solvents and at different temperatures. It suggest only indirect influence of polymer-solvent interactions to the final NP dispersion.

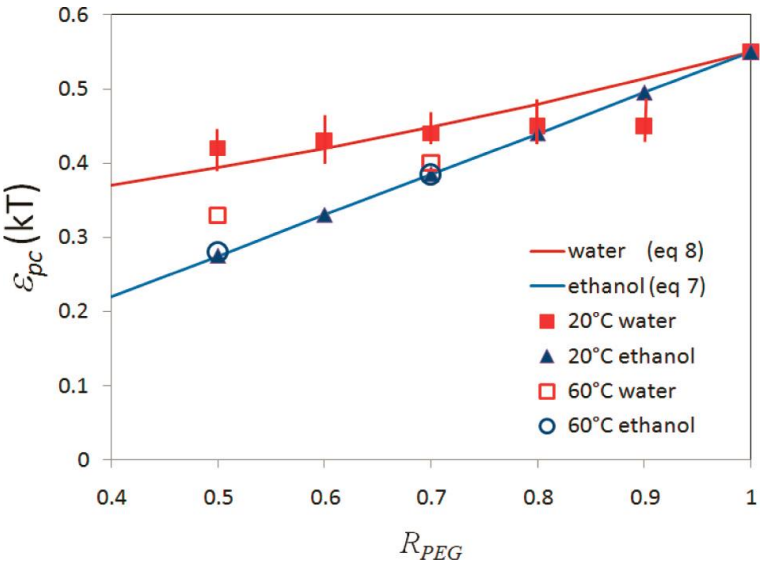

Figure 6: Dependence of the interfacial polymer-particle attraction strength on the polymer to polymer + solvent volume ratio for systems prepared from water and ethanol at 20 °C and 60 °C. Reprinted with permission from[27]. Copyright 2018 American Chemical Society.

Another strategy, how to tailor dispersion state, is nanoparticle surface modification[17, 34, 36, 37, 46, 49]. Hashemi et al.[17] controlled the interfacial interaction strength and spatial range by modifying nanoparticle surface. Nanosilica was grafted with tethers functionalized with 2-ureido-4-pyrimidinone (UPy) units, which caused significant enhancement of interfacial attraction due to strong H-bonding between UPy unit and acrylate group of poly(methyl

methacrylate) (PMMA) used as matrix. Spatial range of the attraction was tuned by length of linker between nanoparticle and UPy unit. Two types of linker was used. In the case of UPy 1 system short alkane with 10 carbons was used as linker with final length of 2 nm. UPy 2 system consisted of poly(butyl acrylate) with 60 monomer units with final length of 12 nm. Bare nanosilica, UPy 1, and UPy 2 systems were mixed with matrix using solvent casting process. There different dispersion states were obtained in dependence on surface modification. System with bare silica nanoparticles showed mixture individually dispersed NPs and small aggregates contained few NPs. UPy 1 system included bridged clusters due to enhanced strength of the interfacial attraction on the short spatial range. UPy 2 system was characteristic by well dispersed state with sporadic presence of tele-bridged clusters due to significant strength of the polymer–particle attraction on the large spatial range. TEM images and correlation function of described systems are shown in Figure 7. The results of this study corresponds well with above described polymer reference interaction site model (PRISM) theory[50-53].

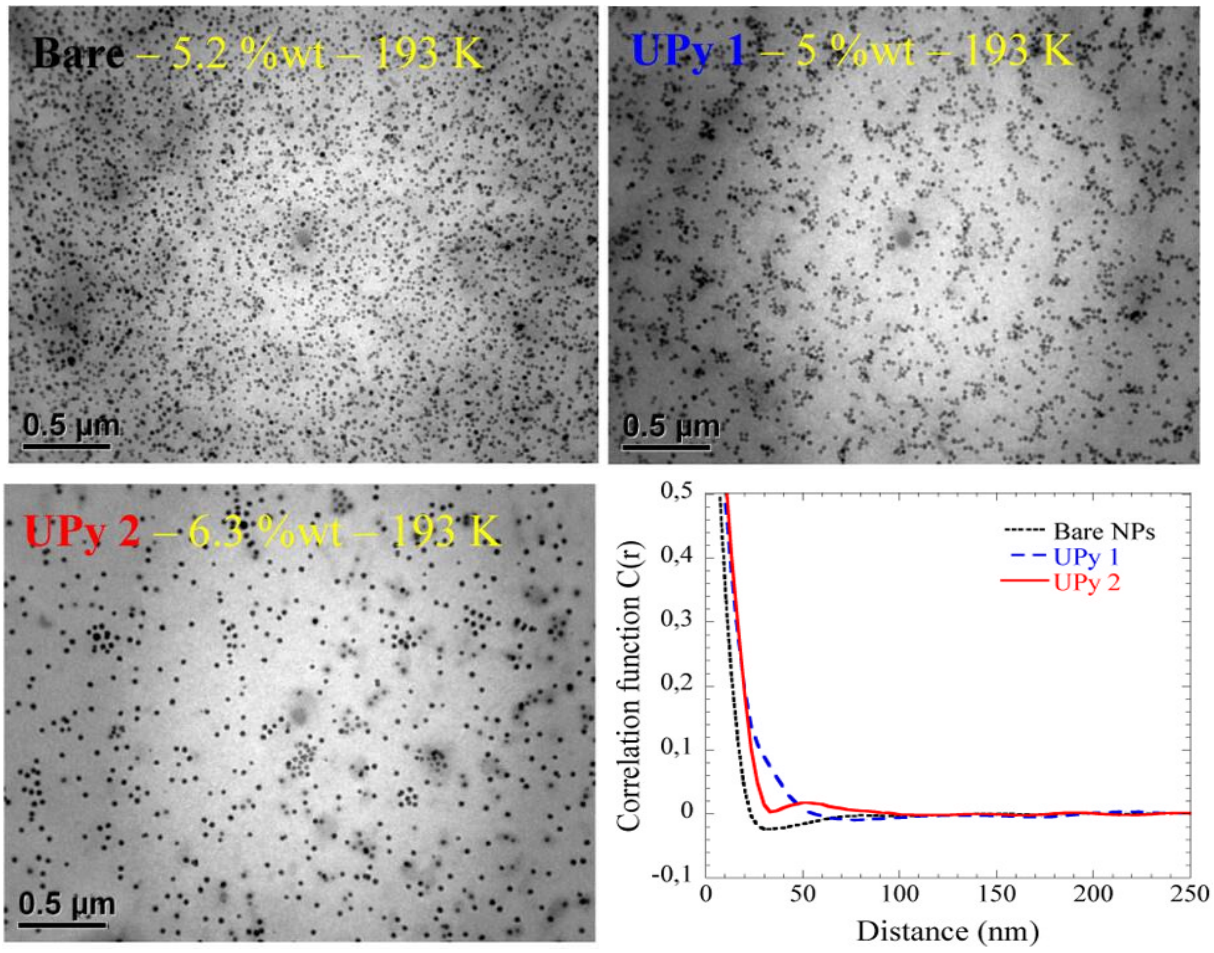

Figure 7: TEM images of polymer nanocomposites consist of silica nanoparticle as filler, PMMA as matrix with molecular weight of 193 kg·mol^{-1}, and with various surface modification marked as Bare, UPy1, UPy 2, respectively. Corresponding correlation function of distances from center of particle mass is shown down right. Reprinted with permission from[17]. Copyright 2018 American Chemical Society.

2.2 Nanoparticle–solvent interaction strength

Drago et.al.[56] proposed a semi-empirical model for calculating the interfacial interaction enthalpy in the donor–acceptor systems in the form of a four-parameter Equation 1:

$$-\Delta H = E_A E_B + C_A C_B, \quad (1)$$

where the subscripts A and B, respectively, belong to acid and base, respectively. Empirically determined parameters E and C were originally interpreted as susceptibility to undergo electrostatic interaction and to form covalent bonds. In his work, Drago et.al.[56] provided E and C parameters for many substances enabling prediction of over 1200 interaction enthalpies. Fowkes et.al.[57-61] extended the original acid–base interaction concept to polymers. They determined E and C parameters for a group of polymers and silanol groups of silica surface[61] and successfully applied the concept to analyze polymer adsorption onto filler surface from a solution [58]. It was found that a strong competition for acidic moieties on the filler surface exists between basic solvent and basic polymer while acidic solvent competes with the acidic filler surface for basic groups of the polymer. They also showed that acid-base interactions can govern dispersion of micro particles in polymer liquids[57]. The major limitation of their experimental results was small specific surface area of the fillers investigated making the observed effects relatively small.

2.3 Properties of polymer nanocomposites

Addition of nanoparticles with large specific surface area to polymer matrix leads to amplification of a number of molecular processes resulting from interactions between nanofiller surface and polymer chains. It results in significant changes of relaxation and mechanical response. Ability of nanoparticles to assemble into extended structures can bring extraordinary effects. Properties of polymer nanocomposites cannot be described by the common micromechanics models. Therefore, it is necessary to develop new approach to describe this class of materials connecting discrete nano scale molecular dynamics and micro scale continuum mechanics[16]. Schematic visualization of composite response through various length scales is shown in Figure 8.

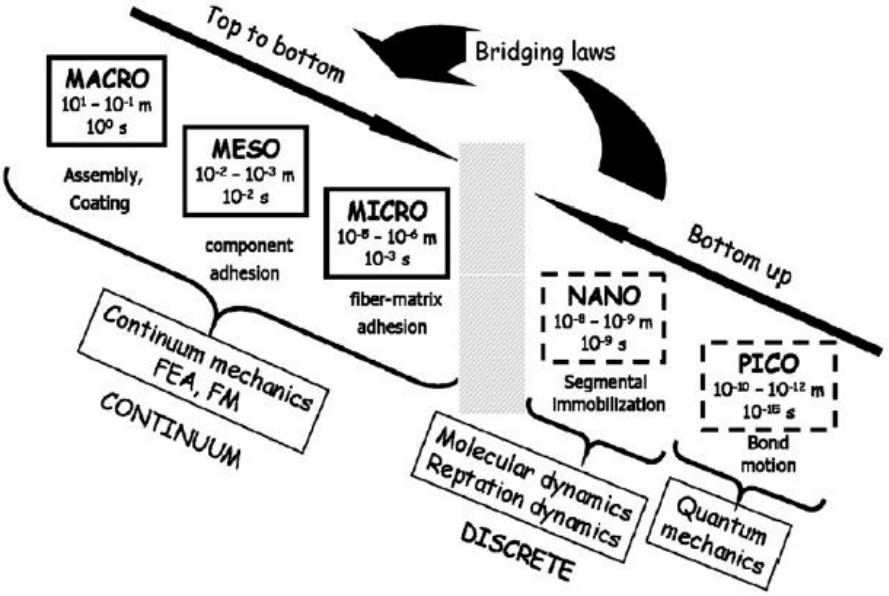

Figure 8: Schematic visualization of composite response through various length scales. Reprinted from[16], Copyright 2018 with permission from Elsevier.

2.3.1 Relaxation properties

Zidek et al.[62, 63] developed the model of random spatial packing of rigid spheres and found that inter-particle distance of randomly packed spheres equals to their diameter at ≈2.6 vol. %, Figure 9. At the filler volume fraction of 0.026, the inter-particle distance of particles with diameter of 1 μm equals 1 μm. This distance is much larger than the polymer radius of gyration (R_g). As a result, only negligible volume of macromolecules interacts with the filler surface, while majority remains unaffected in the bulk. On the other hand, inter-particle distance of particles with diameter of 10 nm equals to the polymer radius of gyration. Hence, almost all macromolecules are affected by the rigid particle surface. Therefore, specific surface area and strength of particle–chain interaction have to be considered in the microstructural interpretation of properties of polymer nanocomposite. Relative size of polymer coil against R_g is schematically shown in Figure 9.

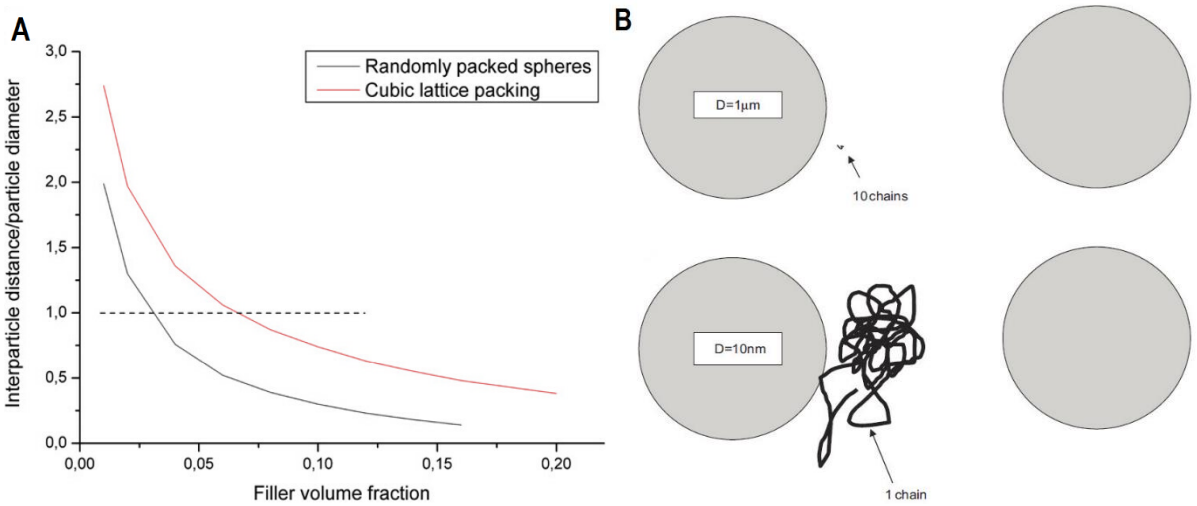

Figure 9: (A) Dependence of the ration of inter-particle distance to particle diameter on filler volume fraction calculated from the model for 1000 monodisperse spherical particles for randomly packed spheres (gray curve) and for cubic lattice packing (red curve) and (B) schematic representation of the size ratio of micro- and nanoparticles to chains. Reprinted from[16], Copyright 2018 with permission from Elsevier.

A three phase model considering nanoparticles, bulk matrix also "interface modified matrix" was developed[16, 64-67]. Volume and properties of the surface modified matrix depend on the specific interface area (i.e. filler loading and dispersion state) and strength of interactions, which are determined by chemical composition of polymer chains and functional groups on the surface of particles. Another variable not considered so far is the rigidity of the polymer chain. NP–polymer system with attractive interactions can form immobilized layer of chains around NPs with different molecular packing and dynamics from original matrix. The nanoparticle with the repulsive interactions can form layer of chains with enhanced mobility and chain packing differing from the bulk matrix. These assumptions suggest that besides particles and matrix, immobilized segment layer and frustrated packing layer exist in polymer nanocomposites. Schematic illustration of such system is shown in Figure 10.

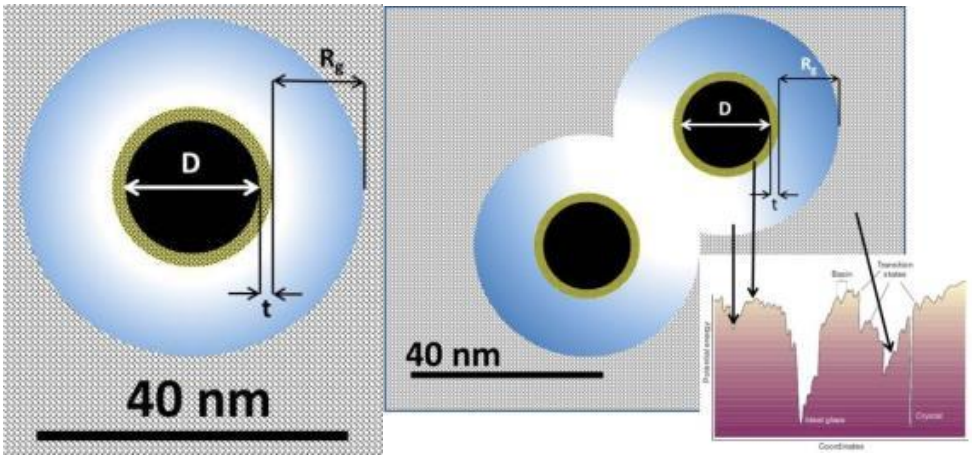

Figure 10: Simplified schema of single nanoparticle shown in black, immobilized segmental layer of thickness t in yellow and frustrated packing layer of thickness of approximately R_g in blue embedded in a glassy matrix shown in black textured background. Two nanoparticle situation showing possible structural polarization in the frustrated packing layer and schematic illustration of the position of segments with different distance from the nanoparticle on the potential energy landscape. In part adopted from[68] by permission of Nature, Copyright 2018.

Immobilization/repulsion of polymer segments and presence of frustrated polymer layer is reflected upon relaxation properties by changing molecular packing and dynamics. Influence of the nanoparticles on macroscopic properties is more significant near the glass transition, where interactions between polymer segments and nanoparticles surface have greater impact on polymer dynamics than on segments with "frozen" dynamics deeply in glassy state.

Vitrification occurs when relaxation time of molecular motions responsible for rearrangement of characteristic segments become longer than the experimental time frame. Local segmental motion freezes during the glass transition without any significant change of the structure of the glass forming liquid. Significant impact of nanoparticles on glass transition temperature was reported in literature[16, 20, 25, 31, 37, 65, 69-72]. The reason for nanoparticles altering vitrification is the immobilization/repulsion of polymer segments by nanoparticles. Different changes of glass transition temperature reported[69] for similar systems are caused by insufficient knowledge of all parameters influencing dynamics and molecular packing of polymer nanocomposites investigated.

It was suggested by molecular modeling[73] that nanoparticles should considerably affect primitive path of the surrounding chains. Increase of disentanglement time has not only origin in the increase of the primitive path contour length, where NPs act as sterical obstacles, but also because the chains must reptate through several domains of slower dynamics near the surface of the particles. This impact on reptation dynamic was significantly intensified by deformation. Figure 11 A and B shows impact of nanoparticle presence in polymer matrix on primitive paths in unstrained and deformed system, respectively. It suggests that large-deformation properties,

for example post-yield or creep behavior, should be more affected than variables measured at small deformations.

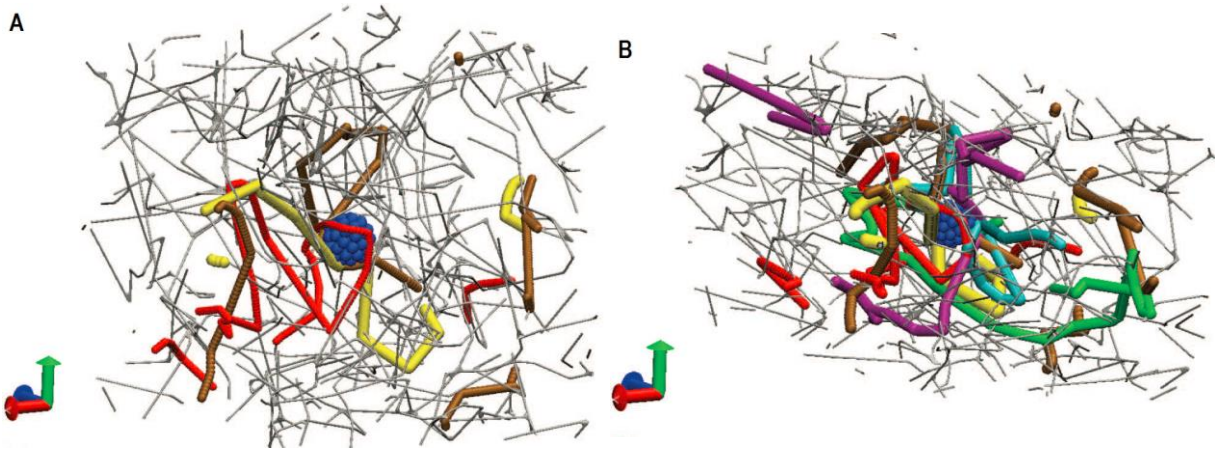

Figure 11: primitive path simulations in vicinity of NP of (A) unstrained and (B) strained system. Reprinted from[73] with the permission of AIP Publishing.

Transferring the knowledge to multi NP systems, Jouault et al.[20-22] investigated relaxation behavior of polymer nanocomposites to elucidate reinforcement origins in polymer nanocomposites. PMMA and PS were used as matrices and silica nanoparticles with three different radii were used as the nanofiller. Transition between isolated NP aggregates and interconnected NP network – percolation - was found at percolation threshold ≈ 10 vol. %. In the percolated regime, stronger reinforcement was found for the system with smaller particles, Figure 12A. Significant change of rheological behavior was found in both investigated systems, Figure 12B and C. Deviation of experimental data from the continuum mechanics volume replacement Guth-Smallwood model[74-76] was found Figure 12D. This suggests that there has to be an additional active reinforcing mechanism. The model that assume a presence of a physical network formed by chains interacting with more than one NP – the bridging chains [77-79] was considered as another possible reinforcing mechanism, schematically shown in Figure 13A. Assumption of bridging chains lead to significant amount of chains with highly retarded conformations – bridging chains would be extremely stretched. No evidences of such chains were obtained in the SANS study. Finally, it was found that chain immobilization can explain experimental data due to formation of immobilized layer around each nanoparticle that causes alternation of surrounding segmental packing and dynamics.

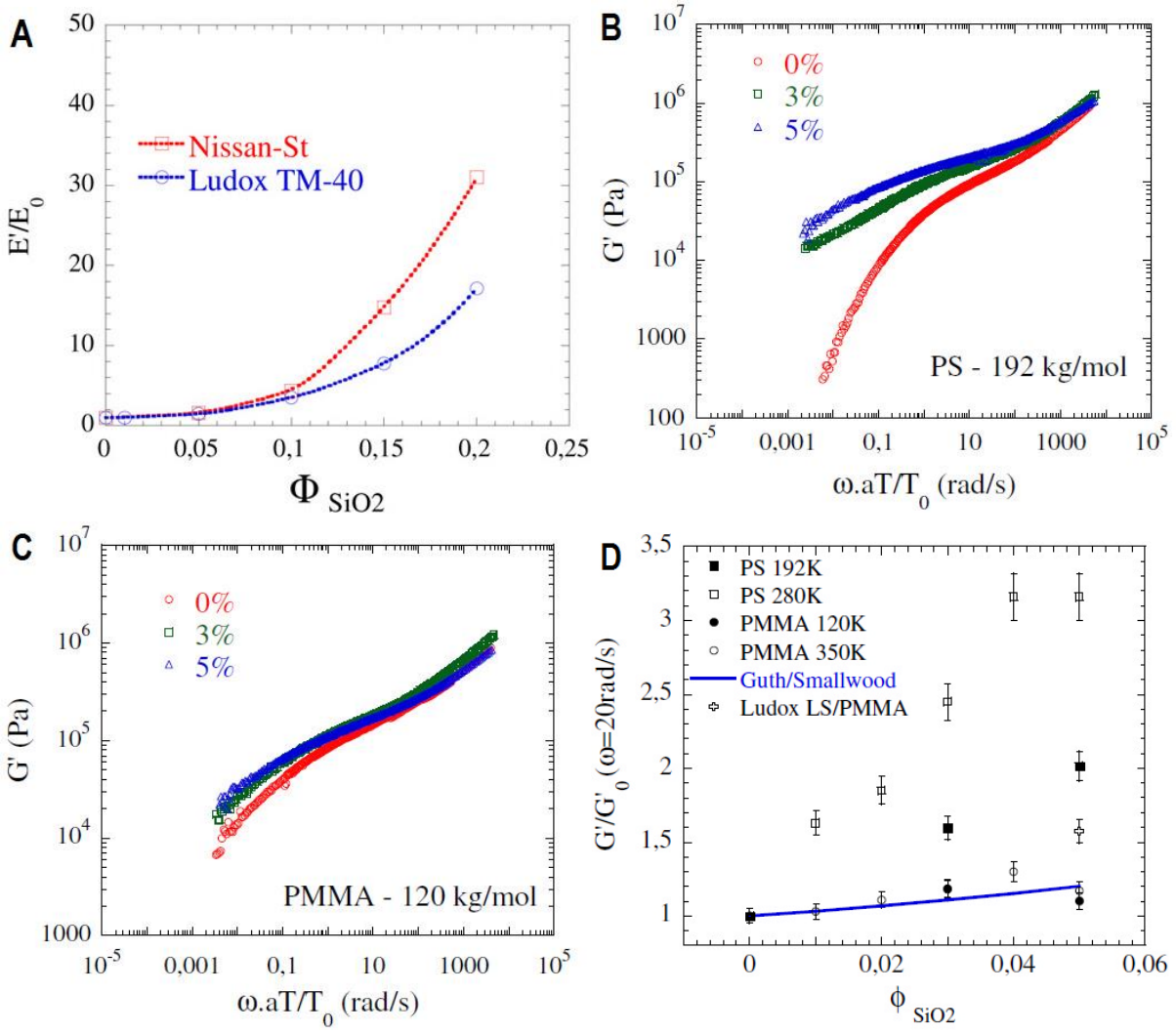

Figure 12: (A) Dependence of relative composite modulus on volume fraction of PMMA/SiO_2 nanocomposites with various NP diameter – Nissan-St (12 nm) and Ludox Tm-40 (28 nm). (B) Storage modulus master curve from oscillatory shear experiments of PS/SiO_2 PNCs with various volume fractions of NPs. (C) Storage modulus master curve from oscillatory shear experiments of PMMA/SiO_2 PNCs with various volume fractions of NPs. (D) Comparison of relative plateau moduli of PNCs with various composition, molecular weight, and nanoparticle diameter with theoretical volume replacement prediction of Guth-Smallwood. Reprinted with permission from[21]. Copyright 2018 American Chemical Society.

Stronger effect of NPs on the properties of the PS compared to the PMMA nanocomposites was in contrary with expectations made based on the interfacial attraction strength (Figure 12B, C, and D). The interactions were expected to be weak in the PS due to weak dipole-dipole interactions whereas they were considered to be strong in the PMMA due to a possible hydrogen bond formation. Possible explanation has its origin in the type of interfacial interaction. Tannenbaum and Ciprari et al.[80, 81] suggested that there are two possible scenarios for adsorption of polymer on a rigid attractive particle, Figure 13B. Weakly binding polymer prefers formation of short trains and long loops with long effective length, in which most of the segments reside

out of surface. Strongly binding polymer forms long trains and short loops with short effective length, in which most of the segments reside on the surface. Although, strongly binding chain adsorb strongly, surrounding chains are less affected due to small effective length. So in contrary with expectations, system with weaker interactions can have stronger change of properties due to the loops that can affect higher amount of surrounded chains. Based on this hypothesis, another variable, adsorption mode or effective length should be considered in interpretation of composition dependences of polymer nanocomposite properties.

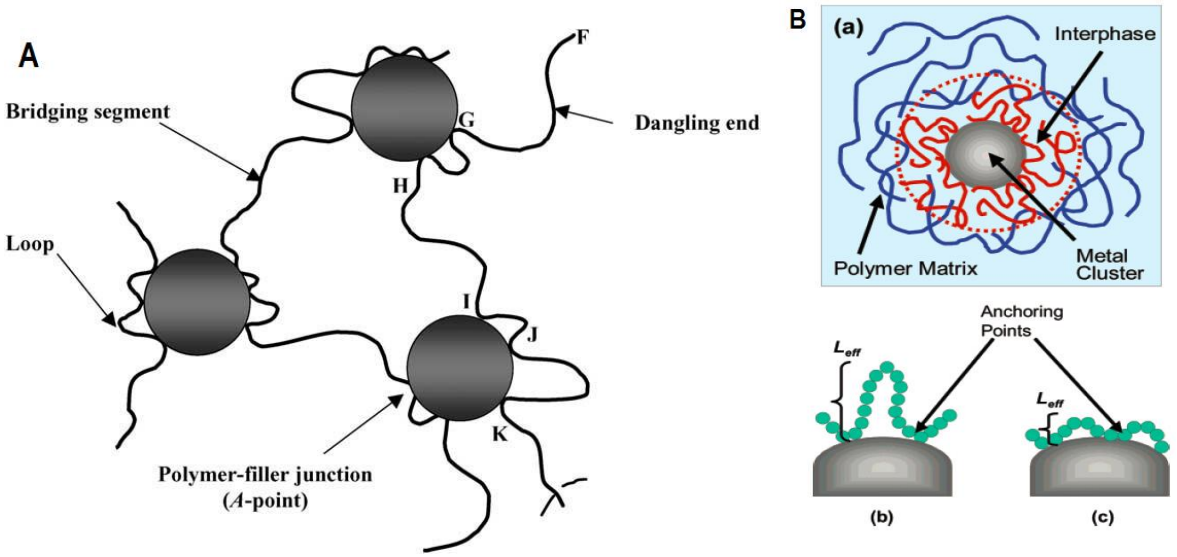

Figure 13: (A) Schematic representation of the molecular scale structure of the bridging chain model. Reprinted from[77] with permission from Elsevier. (B) Schematic representation of nanoparticle-polymer composite. (a) The various components in a nanoparticle-polymer composite. (b) A detailed schematic view of the adsorption characteristics on the surface of a nanoparticle of a weakly binding polymer, in which most of the segments reside in loops. (c) A detailed schematic view of adsorption characteristic on the surface of a nanoparticle of a strongly binding polymer, in which most of the segments reside on the surface. Reprinted with permission from[80]. Copyright 2018 American Chemical Society.

There are several ways how to estimate thickness of the adsorbed polymer layer. It was shown that the thickness depends on used experimental technique[82] and on the assumption that the layer thickness is uniform First method is based on the extraction of the non-adsorbed polymer. Amount of the adsorbed polymer is subsequently determined by thermogravimetric analysis[21, 82]. This method leads usually to underestimated values due to the severe extraction process. Second method is focused on the behavior of PNC in the dissolved state. Dynamic light scattering is utilized to determine NP hydrodynamic radius with and without presence of polymer in solution. Adsorbed polymer layer thickness is then calculated from the difference between these values[23, 24]. Third method is based on quantitative analysis of transmission electron microscopy images and simulation of correlation functions of NP dispersion in polymer matrix[82]. Fourth technique focuses on rheological behavior of PNC melt. Super Einstein

coefficient is determined by fitting volume fraction dependence of relative zero shear rate viscosity and subsequently utilized for calculation of effective hydrodynamic NP radius[83, 84]. Adsorbed polymer layer thickness is calculated from difference between determined effective hydrodynamic NP radius and real NP radius determined for example from image analysis. Small-angle neutron scattering[85] and small-angle X-ray scattering[86] were also utilized to measure scattering patterns of PNC. Adsorbed polymer layer thickness was determined by the core-shell model fitting of scattering patterns using the both methods.

2.3.2 Mechanical properties

Jancar and Recman[87] have shown that reducing the size of particles from micro- to nano-range, i.e., increasing the specific interface area, which is capable to interact with ambient matrix, leads to a pronounced enhancement of stiffness. It was found that this enhancement deviates positively from the classical continuum mechanics model (Figure 14). It suggests that there must exist another segmental scale reinforcement mechanism in addition to the volume replacement and stress transfer mechanisms. Strength of the segmental scale mechanism is related to the specific interface area and its contribution becomes dominating after reaching certain critical value of the particle surface area.

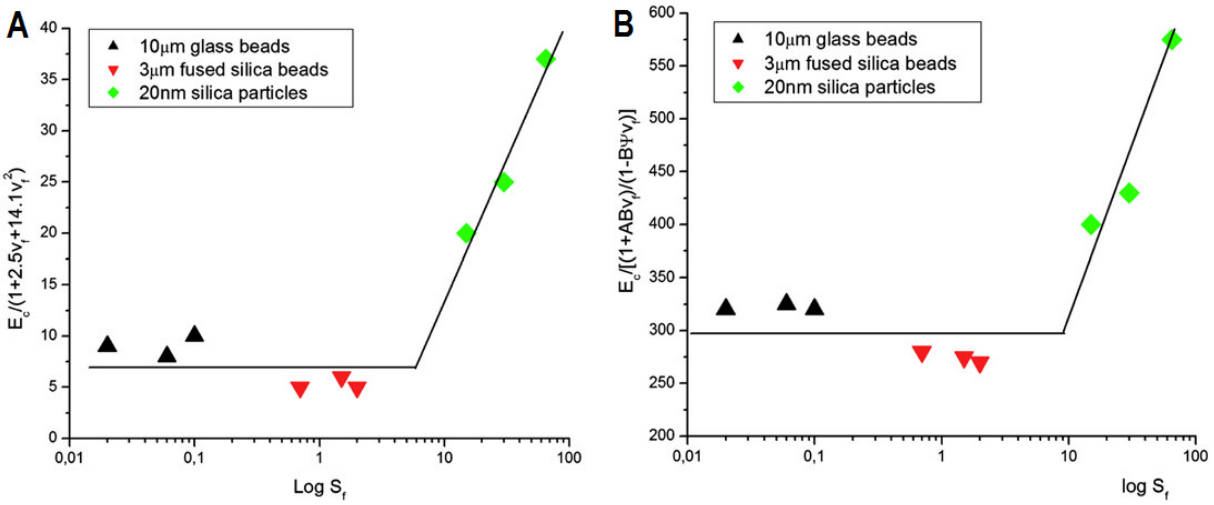

Figure 14: Dependence of the matrix modulus $M_m^* = E_c/f(v_f)$, on the logarithm of the specific interface area, S_f, (A) above T_g reduced to the Guth model and (B) below T_g reduced to the Kerner-Nielsen model. Reprinted from[87] Copyright 2018 with permission from Elsevier.

Jancar et al.[88, 89] published comprehensive studies on small and large strain mechanical response of SiO_2 microparticle (MP) and nanoparticle (NP) filled PMMA. Rigid particles were used as probes that alter local chain packing and dynamics. Effect of MPs and NPs on the elastic moduli, yield, strain softening, and strain hardening response for samples prepared with different thermal histories and deformed at range of strain rates and temperatures was investigated. It was found that MP-sized filler with small specific interface area did not disturb segmental packing and mobility in a significant volume of PMMA. Effect of MPs on the elastic modulus, yield stresses, and strain hardening modulus can be described by a simple volume replacement models. However, NPs modified the packing and dynamics on the segmental scale with behavior indescribable by any classical continuum model. Significant enhancement of elastic modulus was found in the NP-filled system, Figure 15A. The enhancement was less pronounced at T_g – 80 K deeply in the glassy state. The values of elastic modulus of NP-filled system at filler loading 5 vol. % corresponded to the values of elastic modulus of MP-filled system at filler loading 15 vol. %. PNC elastic modulus increased sharply with filler loading at T_g – 20 K resulting in the values at 5 vol. % unachievable by microcomposite up to 30 vol. %. Similar

results were found for strain hardening modulus behavior, Figure 15B. Kinetic analysis of both upper and lower yields, and strain hardening modulus showed that activation energies increase with specific interface area. These results led to consideration that attractive SiO_2–PMMA interactions increased the energy required to activate the segmental rearrangements associated with plastic flow and strain hardening. Moreover, the results pointed out that the effect of rigid particles is more pronounced for the α process involving the entire backbone chain compared to the β process presumably involving only few segments. Described results confirm the idea of immobilization as origin of reinforcement mechanism of PNCs.

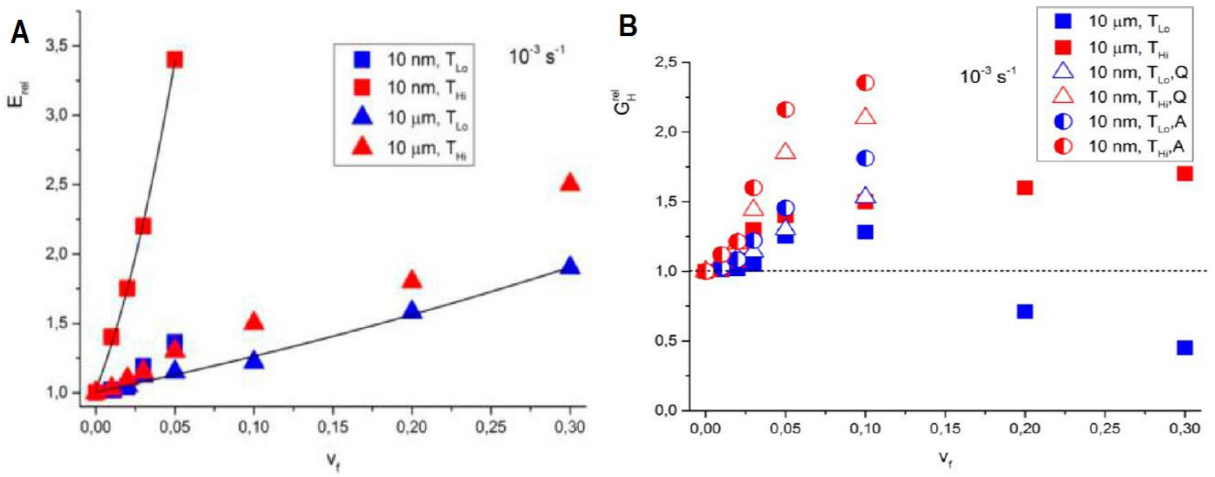

Figure 15: (A) Dependence of relative elastic modulus of SiO_2 NP and MP filled PMMA PNCs on filler volume fraction, v_f, at T_g – 80 K (blue) and T_g – 20 K (red). (B) Plot of relative strain hardening modulus of SiO_2 NP and MP filled PMMA PNCs as the function of filler volume fraction, v_f, at T_g – 80 K (blue) and T_g – 20 K (red) for different thermal histories – Q refer to quenched and A to annealed samples. Reprinted with permission from[88]. Copyright 2018 American Chemical Society.

Dorigato et.al[90] reported on mechanical properties of silica filled amorphous poly(lactic acid) (PLA) nanocomposites. Influence of the effective surface area, surface treatment, and volume fraction of nanofiller on tensile quasi-static, impact, and creep behavior was investigated. Slight increase of elastic modulus was found with increasing surface area of nanosilica at constant volume fraction with negligible influence of surface treatment. Elastic modulus increased with volume fraction more pronounced for bare hydrophilic nanosilica than hydrophobic nanosilica treated by octansilane (Figure 16A) due to better chain adsorption onto bare silica NPs. Yield stress enhancement was found for all investigated systems (Figure 16B). It suggested good filler–polymer interactions[91-95]. Increase of the yield stress with filler volume fraction was found at small volume fractions of approximately 0.01-0.02, followed by the stagnation at certain stress in the range of intermediate volume fractions between approximately 0.02-0.08, ended by yield stress decrease at higher loading for both untreated and treated NPs. Plateau on the composition dependence of the yield stress was explained by a gradual NP aggregation that reduced the effective interface area. Critical defects caused by extensive aggregation were

probably responsible for the observed sharp decrease of the yield stress and embrittlement above $v_f = 0.1$. Interestingly, strain at break increased in the case of PNC with organosilane treated NP (Figure 16C). Usually, increase of the yield stress caused by adding hard filler is connected to the decrease of ductility. This type of behavior was found for the PNC with untreated NPs (Figure 16C). Increase of yield stress and elongation at break of the PNCs with treated NPs was reflected upon increase of its specific tensile energy at break. It was hypothesized, that the surface treatment of NPs could have possible lubricating effect on the matrix. Other explanation could rest on the way, the treated NPs are spatially organized. It was found that organosilane treated NPs were organized into approximately 100 nm elements (Figure 16D). It could be chain bound clusters that have internal structure of interacting chains and particles. Then, whole system would gain one more hierarchical level. Hierarchical nature of the PNC with organosilane treated NPs could explain simultaneous improvement of stiffness, strength, and toughness. Fracture toughness was investigated under impact tensile conditions on the PNC with organosilane modified NPs. Significant increase of fracture toughness of the PNC with modified NPs was found compared to neat PLA with a maximum occurring at 6 and 8 vol. %. Significant improvement of creep resistance was found for investigated PNCs due to restriction of chain motion introduced by surface of NPs.

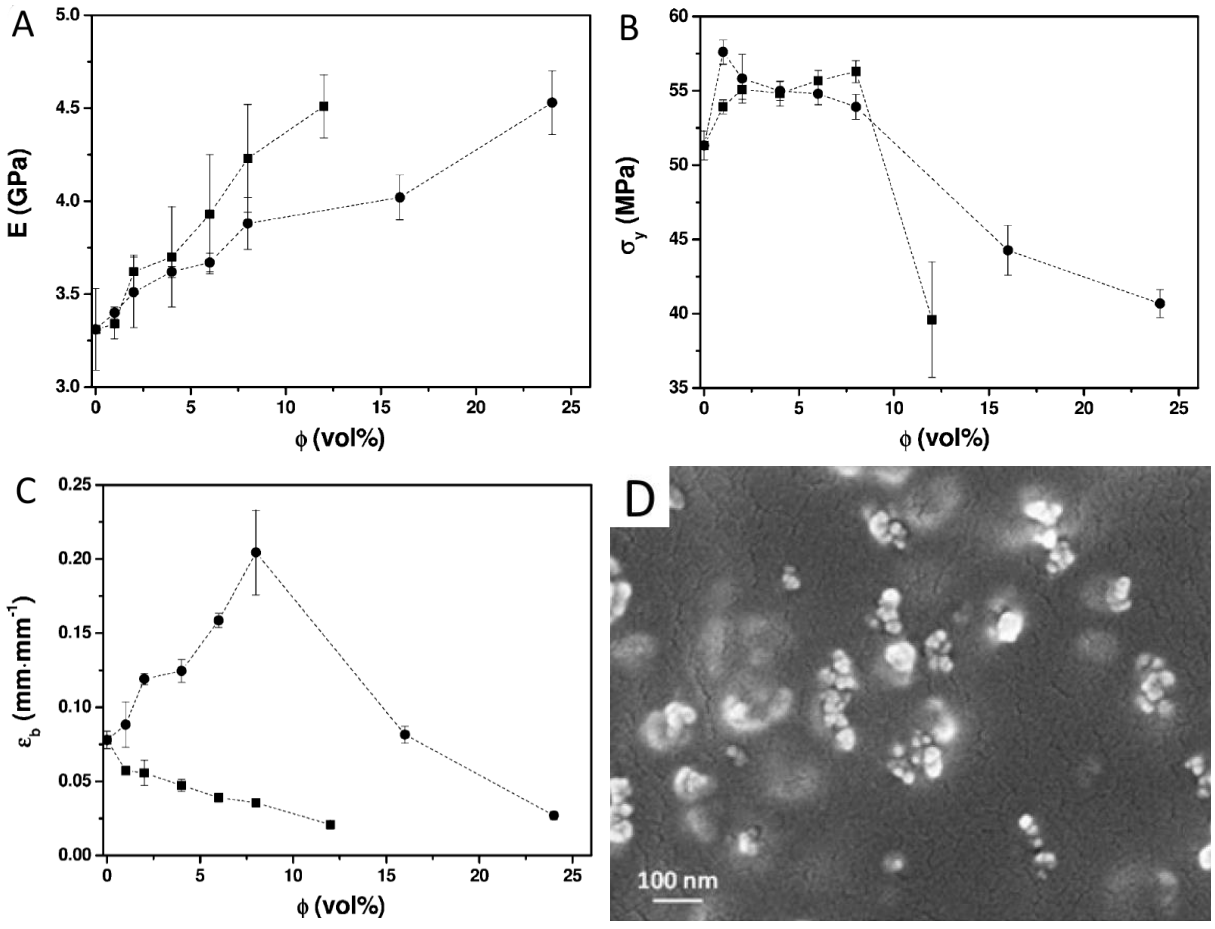

Figure 16: (A) Dependence of elastic modulus, (B) yield stress, and (C) elongation at break on volume fraction of PLA filled by fumed nanosilica with (squares) nontreated and (dots)

organotreated NPs. (D) SEM picture of organotreated NPs spatial organization in PLA/SiO_2 PNC with loading of 2 vol. %. Reprinted form[90] by permission of Springer Nature.

3. Goals of Thesis

The main goal of the Thesis is to determine relationships between thermodynamic parameters governing nanoparticle self-assembly in polymer matrix and kinetic parameters of various preparation protocols and the spatial organization of NPs. Further, the research under the Thesis aims at elucidating relationships between the NP spatial organization and the relaxation and thermo-mechanical properties of model PNCs. Specifically, methods enabling to prepare PNCs with controlled NPs spatial organization – individually dispersed, chain bound clusters, and contact aggregates are targeted. Dynamic mechanical properties of polymer nanocomposites with controlled nanostructures are investigated and multi length scale structural features are visualized utilizing SEM, TEM, and SAXS techniques. Attempt is made to link the measured relaxation and mechanical properties to elucidate molecular processes underpinning deformation response of polymer glasses and their nanocomposites.

4. Experimental part

In principle, there are three ways how to prepare a polymer nanocomposite: from melt, from solution, and by in situ polymerization. In general, it is hard to obtain good dispersion in the case of preparation protocol, where nanoparticle powder is added to a polymer melt. Nanoparticles are aggregated in a powder, and it is almost impossible to disperse them to individual particles, even when strong shear forces are expected in the melt state during mixing. Another route to PNCs is to polymerize monomer in which nanoparticles are dispersed. Good dispersion of nanoparticles is achievable by this technique. However, it is hard to govern polymerization without monomer–particle interactions, then undefined commonly "cross-linked" systems are formed. Also, significant amount of residual monomer usually remains in such composites. It is common, that PNCs prepared by this technique loose further processability. Main advantage of preparation protocol from solution is the ability to mix diluted nanoparticles and polymer on the molecular level. This technique brings multiple thermodynamic and kinetic variables which can be used to govern dispersion process yielding various nanostructures. Therefore, solvent blending technique was used in this study.

4.1 Materials

Used polymers and their physical parameters are listed in Table 1. PMMA with lower number average molecular weight, M_n, PC, and PS were of commercial grade – Plexiglas 8N, Makrolon 2407C, and Krasten 154, respectively. PMMA with greater M_n, and both PVAc were purchased from Sigma Aldrich. Glassy matrices were chosen in order to avoid influence of crystallization on the spatial organization of nanoparticles[96, 97] and the final properties[96-99].

Table 1: physical parameters of used polymers.

Polymer	M_w (kg·mol^{-1})	Polydispersity (-)	T_g (DSC) (°C)	Processing T (°C)	ρ (g·cm^3)
PMMA	100	2,1	113	190	1,19
PMMA	500	N/A	106	190	1,19
PVAc	500	2,2	47	80	1,19
PC	50	2,2	143	260	1,22
PS	200	3,6	88	190	1,05

The commercial grade PMMA Plexiglas 8N (Evonik, Germany), according to NMR analysis provided by the supplier, exhibited 5–7 % of isotactic sequences, 50–52 % of syndiotactic and 41–52 % of atactic sequences, all apparently randomly distributed along each chain. Tacticity of the other polymers used is not known, however, from the experimentally determined T_g, PMMA with 500 kg/mol differ in tacticity from the PMMA with 100 kg/mol. According to

Flory-Fox equation[100, 101] glass transition temperature should increase with increasing molecular weight, Equation 2:

$$T_g = T_{g,\infty} - \frac{K}{M_n}, \quad (2)$$

where the T_g is glass transition temperature, $T_{g\infty}$ is glass transition temperature at infinity molecular weight, K is empirical parameter, and M_n is number-averaged molecular weight. Glass transition temperature of PMMA can vary from approximately 60 to 140 °C because of tacticity[102, 103]. Glass transition temperature of isotactic PMMA is approximately 60 °C and of syndiotactic approximately 140 °C. Therefore, it is considered that used PMMA with 500 kg/mol has greater content of isotactic sequences compared to the PMMA with 100 kg/mol.

Only spherical nanoparticles were used to avoid effects of additional structural variables such as aspect ratio and orientation. Nanofillers used are listed in the Table 2. Colloidal bare silica nanoparticles dispersed in isopropanol with particle diameter of 20 ± 4 nm was supplied by Nissan Chemicals under commercial name IPA-ST. Advantage of this nanosilica grade is that particles are stabilized in colloidal solution without additional substances. Then, only short ultrasonication without another treatment is necessary to ensure presence of individual nanoparticles. Good dispersion of individual nanoparticles before use is critical because adding aggregated nanoparticles into polymer solution will obscure interpretation of experiments. Pyrolytic nanosilica from Sigma Aldrich with primary particles with diameter of 7 nm was also used. Due to the preparation process, pyrolytic silica usually contains primary particles sintered into bigger objects. Approximately 70 nm chains of sintered nanoparticles considered as primary elements were prepared by rigorous ultrasonication of pyrolytic nanosilica in a solvent. Additionally, zinc oxide nanoparticles doped with 2 wt. % aluminium oxide nanoparticles (AZO) with diameter of approximately 15 nm were purchased from US Research Nanomaterials. Magnetite nanoparticles also from US Research Nanomaterials with diameter of approximately 15-20 nm were also used. Dispergation of magnetite nanoparticles in a solvent was quite problematic due to strong interparticle attractive forces. Also, relatively high density of magnetite and AZO particles made their dispersion more complicated and the resulting dispersions exhibited reduced stability.

Table 2: physical properties of used nanoparticles.

Nanoparticles	Physical form	Diameter (nm)	Density ($g \cdot cm^3$)
Colloidal silica	colloidal solution	20	2,2
Fumed silica	powder	7 (70)	2,2
AZO particles	powder	15	5,6
Fe_2O_3 particles	powder	15-20	5,2

Acetone (p.a. grade, 99.98 %), toluene (p.a. grade, 99.24 %), tetrahydrofurane (p.a. grade, 99.8 %), ethyl acetate (p.a. grade, 99.7 %), 1.4-dioxane (p.a. grade, 99 %), and dichlormethane (p.a. grade, 99.5 %) were purchased from Lachner (Czech Republic).

4.2 Methods

Nanofillers were ultrasonicated in a solvent employing an ultrasonic tip (Bandelin Sonopuls, SRN). Firstly, resonance frequency was found and then ultrasonication was performed. Ultrasonication was divided into t_{on} of 0.1 s and t_{off} of 2.5 s time intervals with overall time of 5 minutes. Subsequently, solution of nanoparticles was added to a polymer solution with concentration of 66.7 mg of a polymer per one milliliter of a solvent (about 5.3 vol. %) which corresponds to semi-dilute region. Nanoparticle loading of final composites was 0.1, 0.5, 1, 2.5, 5, 7.5, and 10 vol. %. Various solvents were used: acetone, acetone-toluene 1:1 mixture (volumetric ratio), toluene, ethyl acetate, tetrahydrofurane, and dichlormethane. Dissolved PNCs were rigorously mixed at 1200 RPM using a magnetic stirrer for 1 hour. Then, PNC mixture was cast onto a flat sheet, dried at 140 °C for PMMA, 150 °C for PC and PS, and 80 °C for PVAc for 12 hours at atmospheric pressure. Dried PNCs were mechanically grinded using IKA A11 basic analytic mill (|IKA, GE). Powdered PNCs were dried for 6 days in a vacuum oven to ensure removal of solvent residues. Drying efficiency was checked utilizing thermogravimetric analysis. Dried samples were compression molded at 190 °C for PMMA and PS, 260 °C for PC, and 80 °C for PVAc and at 300 kN into 1 and/or 0.5 mm thick sheets by means of the LabEcon 300 Press. (Fontijne, NL). The samples were cooled down under pressure to the laboratory temperature at a cooling rate of approximately 30 $K \cdot min^{-1}$. Specimens with the desired geometry were cut from these sheets.

Radius of gyration, R_g, of matrices investigated was determined in the respective solvents used in this study. Rg was measured employing DynaPro NanoStar dynamic light scattering device (WYATT, USA) using concentration of 10 $mg \cdot ml^{-1}$. Viscosities of polymer solutions at various temperatures were obtained utilizing Ares-G2 rheometer (TA Instruments, USA) using concentric cylinder geometry.

Morphology of the PNCs was determined by means of the transmission electron microscopy (TEM) and ultra-small-angle X-ray scattering (USAXS). TEM (FEI, CZ) provides a direct view of silica spatial arrangement in polymer matrix. Ultratomed slides of PNCs with constant thickness of approximately 50 nm were prepared (Leica Microsystems, GE). TEM observations were performed using Morgagni 268D 100 kV transmission electron microscope (FEI, CZ), STEM MIRA3 (TESCAN, CZ) and STEM Verios 460L (FEI, CZ). TEM snapshots were analyzed with the help of image analysis software – size of elements and interparticle distances were determined. USAXS provides the average shape and internal structure information of nanoparticles arrangement in the polymer matrix. USAXS was performed using X-ray diffractometer Smartlab (Rigaku, JPN) with copper rotating anode, 2 × 220 germanium

monochromator and 2 × 220 germanium USAXS analyzer. USAXS patterns were analyzed by means of the Guinier and Porod laws.

Oscillatory shear small deformation tests and dynamic mechanical analysis (DMA) were carried out to provide thermomechanical properties of prepared polymer nanocomposites. Shear test corresponding to low deformation levels (0.5 %) were performed in the dynamic mode under the strain controlled conditions with the plate-plate geometry employing ARES G2 rheometer (TA Instruments, USA). Thermal environment equipped with an air oven ensures a temperature control within 0.1 °C. Weak axial force was used in order to gently compensate gap position with respect to thermal expansion and retraction occurred during a test. Frequency sweeps from 0.01 to 20 Hz in a temperature ramp 10 °C were performed for the temperature ranging from 200 to 150 °C. Dynamic mechanical analysis was carried out using DMA RSA G2 (TA Instruments, USA). Measurements were performed in linear viscoelastic regime at deformation amplitude of 0.05 %, and frequency of 1 Hz. DMA analysis was used to characterize relaxation behavior in the transition regime and to determine glass transition temperature.

Mechanical properties were measured utilizing Zwick Roell Z010 (Zwick-Roel, CH). Mechanical measurements were conducted using dog-bone shaped specimens in tension and cylindrical specimens were utilized for compression tests at true strain – true stress conditions. The experiments were carried for strain rates ranging from 10^{-5} to 10^{-1} s^{-1} at various temperatures. Long-term tensile creep measurements were performed at 80 °C and various constant loading.

5. Results and discussion

5.1 Controlling nanoparticle spatial organization in polymer matrix

The control of NP spatial organization in polymer matrix is a prerequisite for transforming PNCs from scientifically interesting materials to technologically viable engineering materials.

By varying the solvent strength, different nanoparticle (NP) organizations were prepared in the model PMMA/colloidal SiO_2 PNC. Mixture of individually dispersed NPs and contact aggregates were identified for tetrahydrofuran (THF) (Figure 17), individually dispersed NPs for acetone and ethyl acetate (Figure 18 and 19), chain bound clusters for acetone–toluene 1:1 mixture (Figure 20), and contact aggregates for toluene (Figure 21), respectively. TEM results were confirmed by USAXS analysis (Figure22). The size of individual NPs, clusters, and aggregates determined by imager analyses and by fitting of USAXS data is shown in Figure 23.

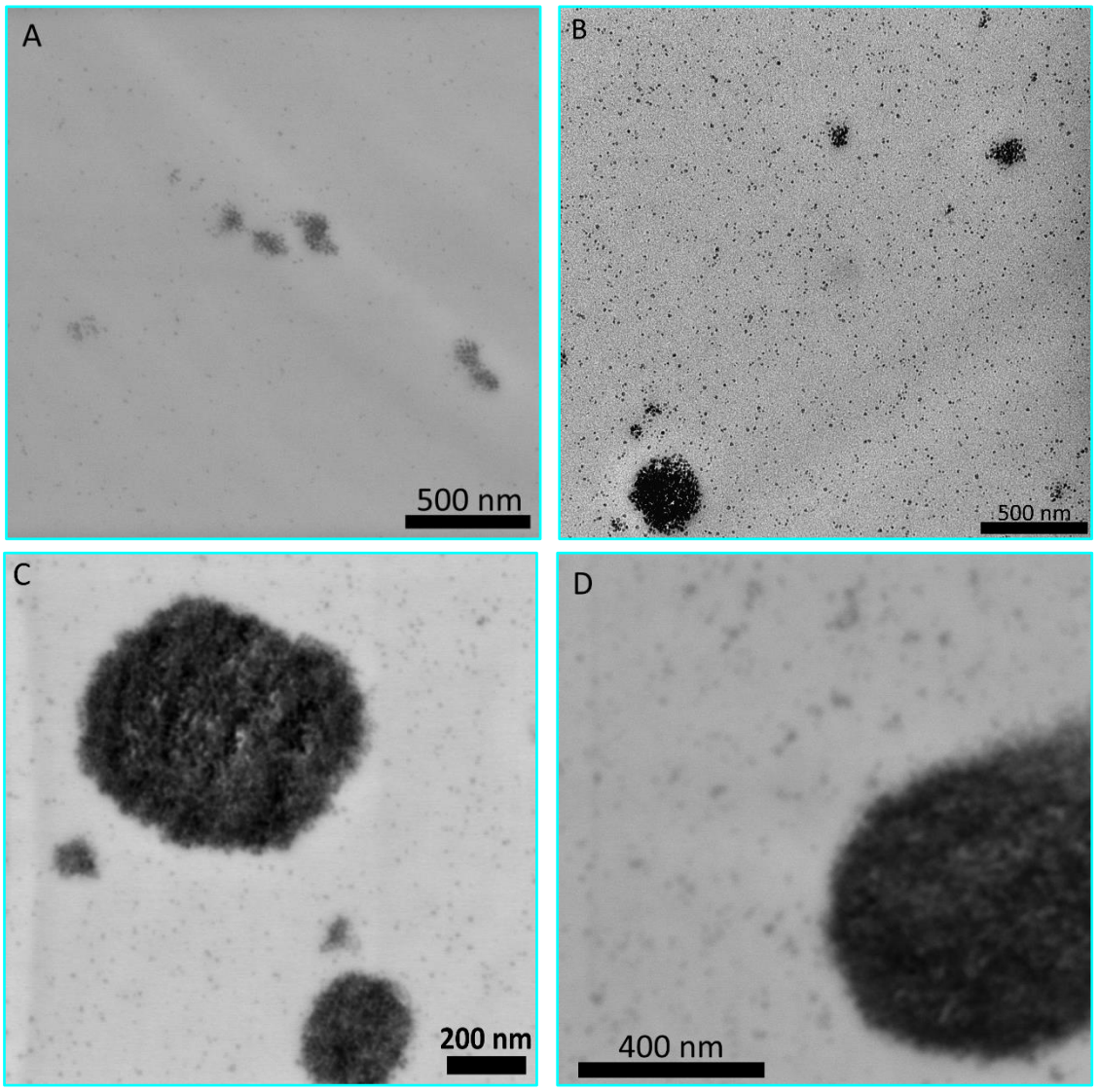

Figure 17: TEM images of THF series PMMA/colloidal SiO_2 PNC with loadings of 0.5, 1, 2.5, and 5 vol. %, respectively.

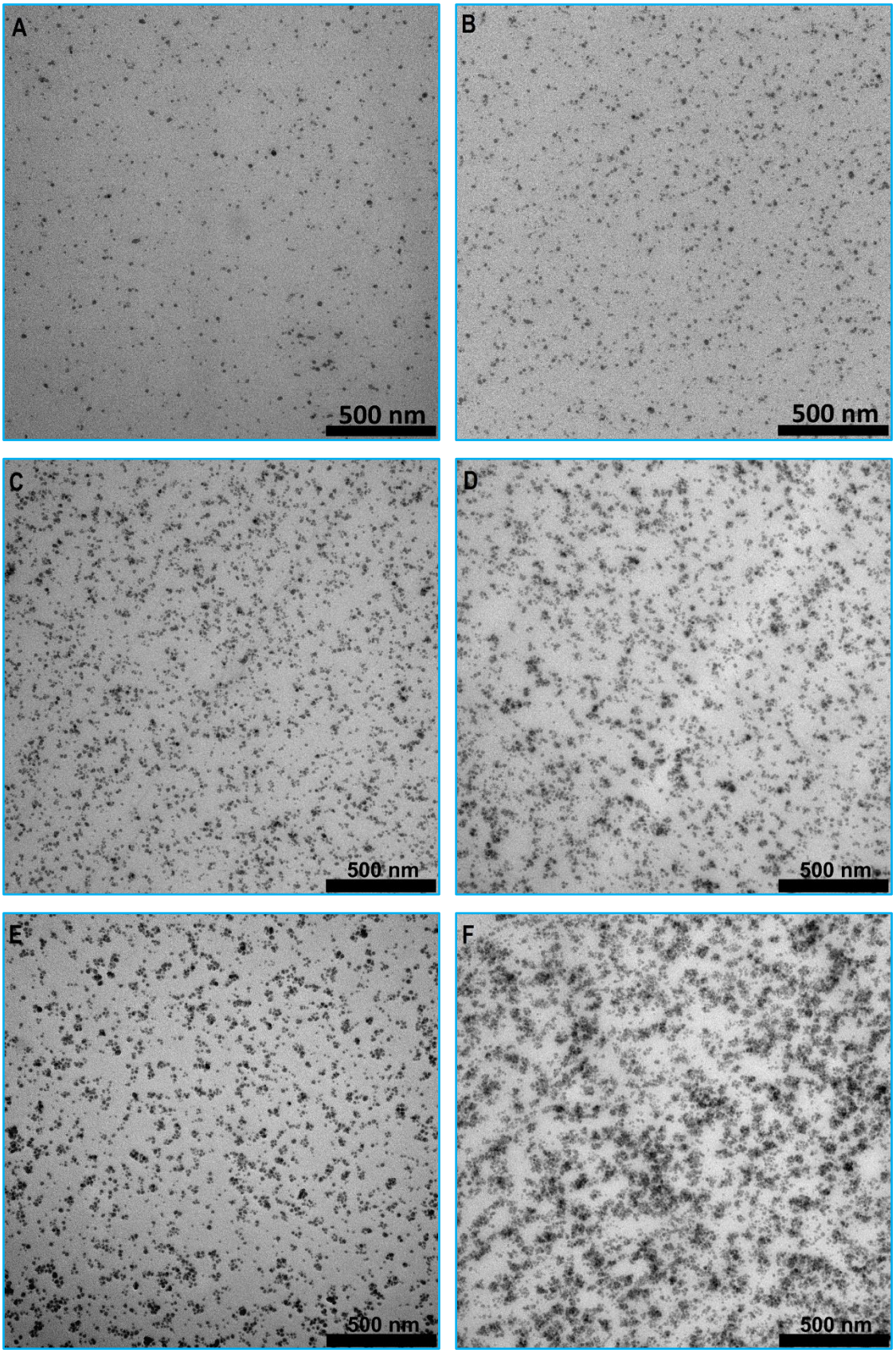

Figure 18: TEM images of acetone series PMMA/colloidal SiO_2 PNC with loadings 0.5, 1, 2.5, 5, 7.5, and 10 vol. % for A, B, C, D, E, and F, respectively.

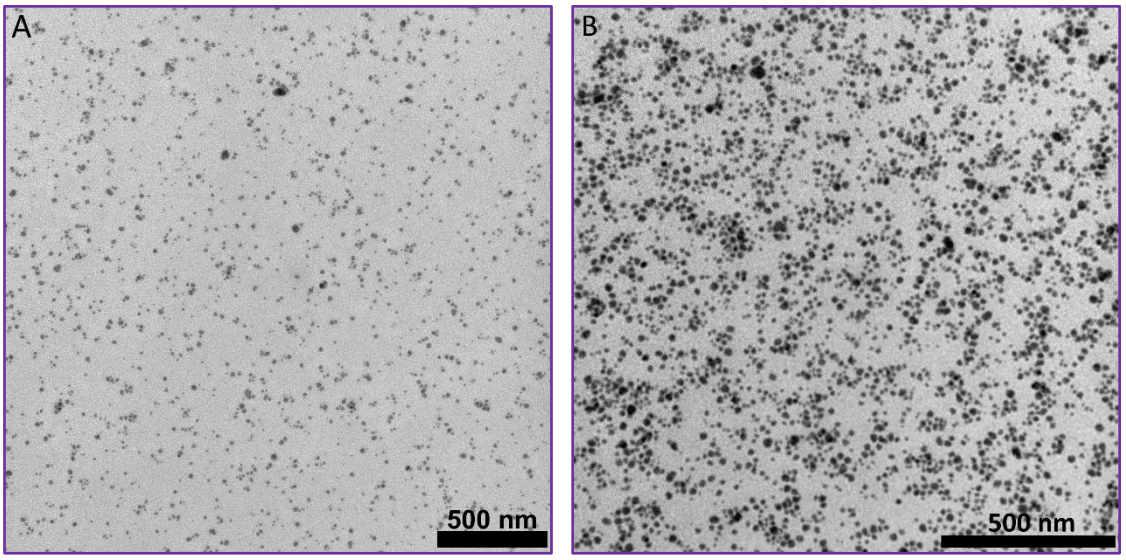

Figure 19: TEM images of ethyl aceteta series PMMA/colloidal SiO_2 PNC with loadings of 1 and 5 vol. %, respectively.

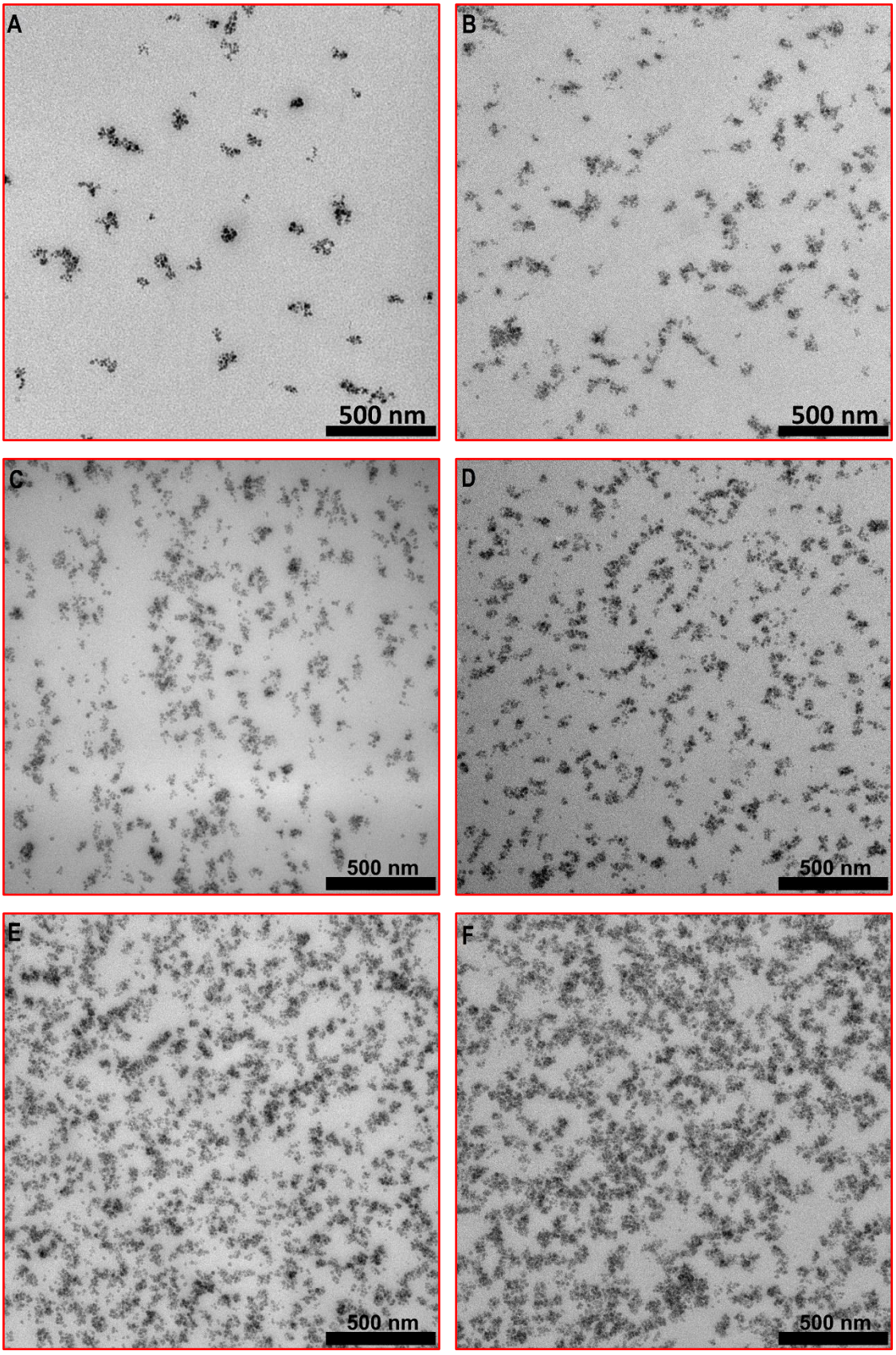

Figure 20: TEM images of acetone-toluene 1:1 mixture series PMMA/colloidal SiO_2 PNC with loadings 0.5, 1, 2.5, 5, 7.5, and 10 vol. % for A, B, C, D, E, and F, respectively.

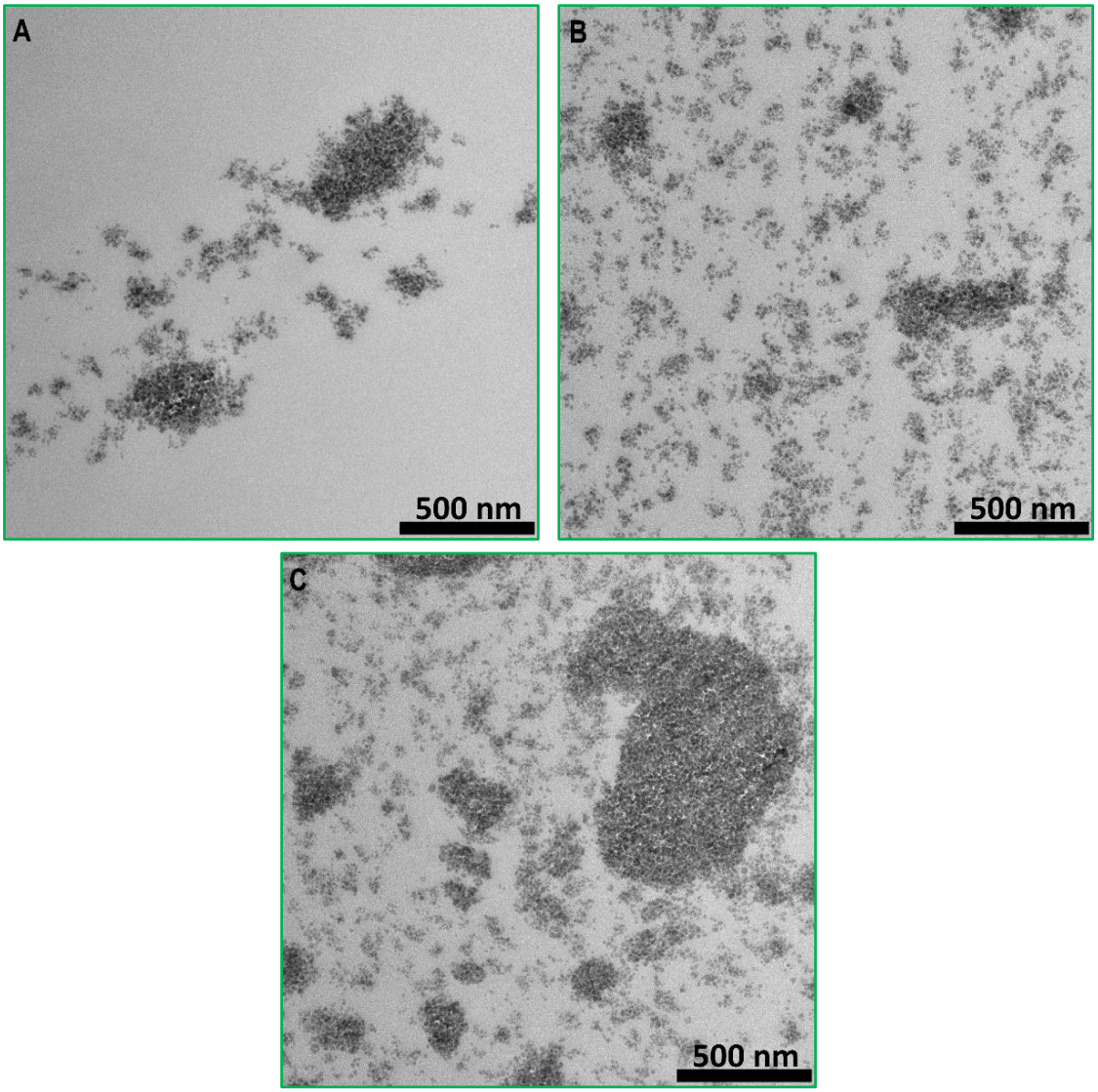

Figure 21: TEM images of toluene series PMMA/colloidal SiO_2 PNC with loadings 1, 5, and 10 vol. % for A, B, and C, respectively.

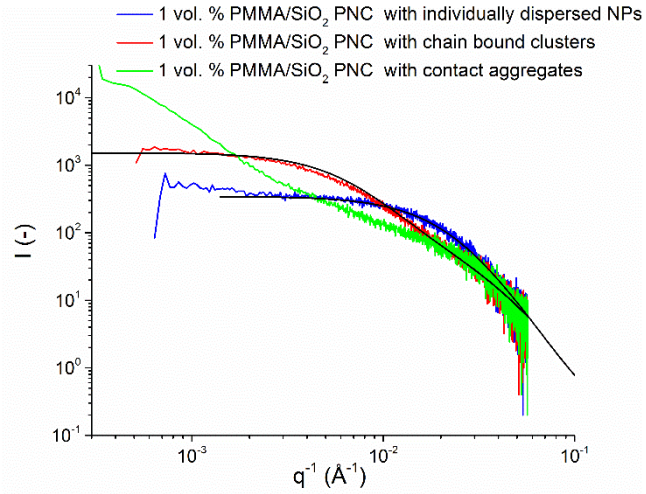

Figure 22: USAXS dependence of intensity, I, on length of scattering vector, q, of PNCs with various nanostructures with 1 vol. % of NPs.

Individual NPs dispersion in the PMMA/1 vol. % colloidal SiO_2 prepared from acetone (Figure 18B) was verified by the USAXS analysis. Flat low q region and smoothly decreasing intermediate q region of USAXS pattern confirmed the TEM results (Figure 22). The interparticle distance in the PMMA/1 vol. % colloidal SiO_2 prepared from acetone (Figure 18B) and ethyl acetate (Figure 19A) was determined by image analysis to be approximately 33 and 40 nm (Figure 24), respectively. Note that the determined interparticle distances tends to be undervaluated because of the 3D reality projected into a 2D TEM image of approximately 50 nm thick ultramicrotome slides. The results showed that the dispersion of isolated NPs in the PNCs prepared from acetone is only achieved at low filler loadings of 0.5 and 1 vol. % (Figure 18A, B) while above 2.5 vol.%, silica NPs tend to aggregate (Figure 18C, D, E, F). It is probably a consequence of shortened interparticle distance which promoted the short range Van der Waals interaction always acting against good dispersion. The aggregate size was relatively small (about 26–34 nm) and grew gradually with filler content, Figure 23. Dispersion of individual NPs in PNCs prepared from ethyl acetate were also attained only below 1 vol. % (Figure 19A). In the ethyl acetate prepared PNCs, the TEM micrographs suggest (Figure 19B), that NPs begun to form clusters with diameter of approximately 32 nm (Figure 23) above 1 vol. %.

Chain bound clusters (Figure 20) were formed in the PMMA using the 1:1 acetone-toluene solvent mixture. Three populations of cluster sizes were found with few individually dispersed NPs. The smallest clusters contained 2 to 3 NPs (the least frequent occurrence), the intermediate clusters contained 5 to 9 NPs, and the large clusters consisted of 16 to 26 particles (the most frequent occurrence). Theoretical models[104] suggest gradual increase of cluster size with time assuming that individual particles form small clusters consisting of two to three nanoparticles and once formed, these elementary clusters connect building up larger clusters. The USAXS results showed complex behavior in low and intermediate q regions (Figure 22), indicating the presence of two scattering populations which confirms that the PNC contained inclusions with an internal structure consisting of clusters with size of approximately 45 nm and their primary building blocks with the diameter of 20 nm. Clusters were observed in all samples of acetone-toluene series and the cluster size of approximately 43 nm was preserved throughout the whole concentration range investigated Figure 23. Good agreement was found between the TEM image analysis and the USAXS data for both acetone and acetone-toluene series. NPs in chain bound clusters are closely packed into bundles – clusters where the NP-NP contact is mediated through the adsorbed polymer chains[50-54]. These so-called bridging chains[77-79], which interact with multiple NPs at once, differ from the chains at the NP–bulk matrix interface as they are tightly confined between several NPs and their dynamics is greatly retarded. Clusters behave as independent entities or elements dispersed in a polymer matrix and could be considered as a hierarchical structure with a two-level hierarchy – NPs and clusters.

Finally, preparing the PNC utilizing THF (Figure 17) or toluene (Figure 21) resulted in the presence of contact NP aggregates with the average size of approximately 400 and 500 nm,

respectively. The USAXS pattern of PMMA/1 vol. % colloidal SiO_2 prepared in toluene also showed the presence of big and small populations of multi NP agglomerates with size larger than 100 nm. However, aggregates in THF and toluene PNCs have different origin. Aggregates in PNCs prepared from THF are formed due to depletion attraction arising from high affinity between silica NPs and THF molecules. Aggregates in PNCs prepared from toluene have their origin in low interaction strength between toluene and silica NPs leading to separation of NPs. Mixture of individually dispersed NPs and contact aggregates was found for all NP volume fractions investigated in PNCs prepared from THF as shown in Figure 17. Both populations of aggregates presented in PNCs of toluene series grew with increasing silica content.

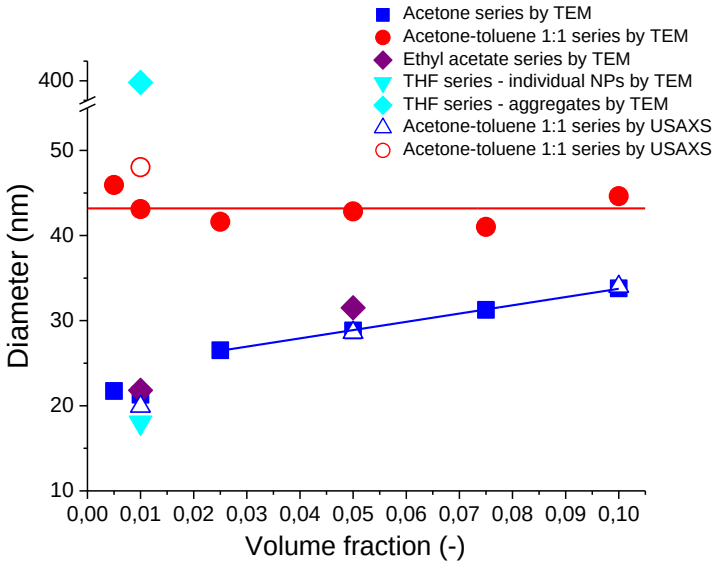

Figure 23: Dependence of element diameter on volume fraction of 50 kg/mol PMMA/colloidal SiO_2 PNCs prepared from acetone, acetone-toluene, ethyl acetate, and THF, respectively.

Interelement distance (Figure 24) was determined as the most frequently occurring value, which was established from the maximum of the distribution function of the 5 nearest neighbors of each element. NPs, clusters, and aggregates were considered as independent elements. The internal structure of clusters was neglected for the purpose of the calculations. Dependence of interelement distance and interelement distance divided by element diameter on volume fraction is shown in Figure 24. A fair agreement between the experimental results and theoretical study of random distribution of monodisperse spheres[62, 63] was found. A deviation from the model was found at low and high volume fractions, especially in the case of PNCs prepared from acetone. Significant underestimation of interparticle distance at small volume fractions could be caused by evaluation of 2D projection of 3D situation as already mentioned above. By closer inspection of TEM pictures, it is possible to find particle rich and particle poor areas throughout the specimens of acetone PNC series. Interelement distance is calculated from the distribution function of 5 nearest neighbors which can lead then to slight underestimation of interelement distance at small concentrations. It could be a fingerprint of complex morphogenetic processes occuring during solvent evaporation. Another deviation from the theoretical model was found

at high concentrations, where the determined values had larger interelement distance than predicted. The van der Waals interactions are more pronounced at such small distances. Another important variable is the ratio of the radius of gyration to the interelement distance. Radius of gyration of the PMMA used is approximately 5 nm. Interparticle distance should reach 10 nm at filler volume content of approximately 6.5 vol. % at idealized NP diameter of 20 nm. Smaller interparticle distance would lead to significant distortion of the chain conformation. Therefore system prevents this undesired state by aggregation.

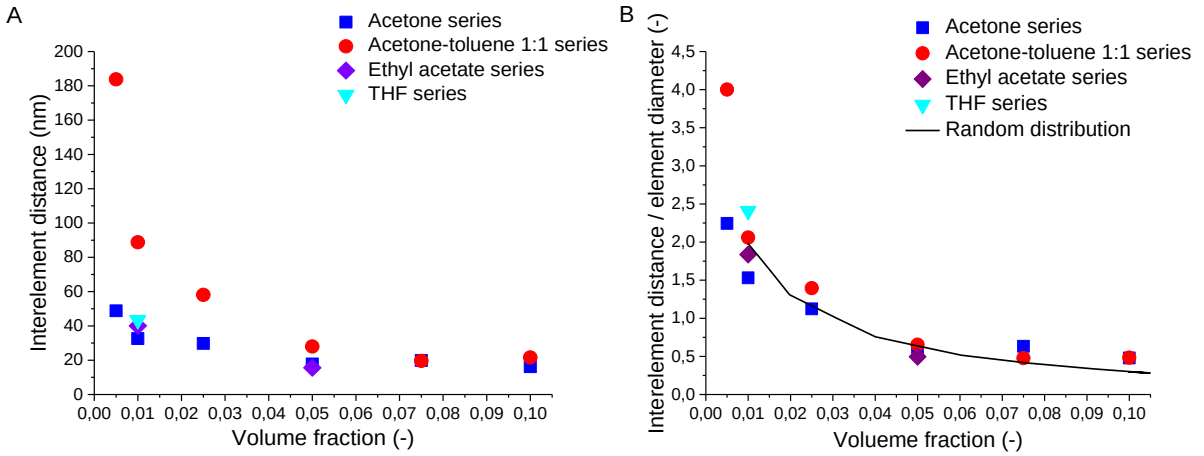

Figure 24: Dependence of (A) interelement distance and (B) interelement distance reduced to element diameter on volume fraction of acetone, acetone-toluene, ethyl acetate, and THF PNC series, respectively.

Taking into consideration experimental results discussed above, we propose a general approach to analyze structural variables affecting stable NP dispersion in glass forming polymer liquids. For silica NPs in the PMMA solution, the interfacial interactions are dominated by the acid–base interactions between acidic silanol groups on the silica surface and the basic groups of the PMMA and the solvent[57-61]. Interaction enthalpies were calculated using Equation 1 from the E and C constants reported in the literature[56, 61]. Values for the toluene were taken as a mean average of benzene and xylene, since the data for toluene was not available. This uncertainty has no significant effect on the interpretation of experimental data due to the close E and C values for benzene and xylene, both being significantly smaller than the E and C for acetone. The E and C for the 1:1 acetone-toluene mixture were obtained by averaging the values for acetone and toluene.

The calculated donor–acceptor interaction enthalpies of for prepared model PNCs are shown in the Figure 25A. The highest value of the negative interaction enthalpy, $-\Delta H = 8.9$ kcal·mol^{-1}, in this study is found between the THF and silanol groups on the silica surface, which is significantly stronger than the attraction between PMMA and silica ($-\Delta H = 4.0$ kcal·mol^{-1}). In combination with the large excess of solvent in the mixture, it suggests that the adsorption onto silica is dominated by the THF molecules and a strong solvation shell is formed around NPs,

which, in turn, repels the polymer chains from the vicinity of NPs and causes NP aggregation due to depletion attraction.

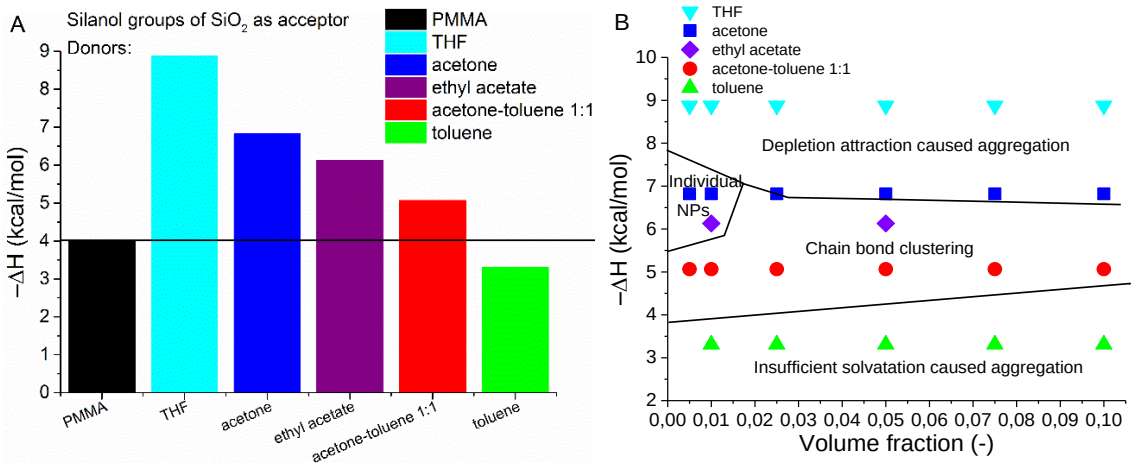

Figure 25: (A) Bar diagram of donor-acceptor enthalpies of adducts of silanol groups of SiO_2 nanoparticles with PMMA and various solvents. (B) Volume fraction dependence of silica–solvent interaction enthalpy phase diagram of PMMA/SiO_2 PNCs.

The interaction enthalpies of silica-acetone ($-\Delta H = 6.8$ kcal·mol^{-1}) and ethyl-acetate-silica ($-\Delta H = 6.1$ kcal·mol^{-1}) are smaller than the THF-silica, but still stronger that of the silica-PMMA couple. Since the solvent molecules are the favorably adsorbed onto silica, the stabilization of the experimentally observed dispersion of individual NPs is likely caused by the solvation effect in addition to the previously suggested[23] repulsion of adsorbed polymer layer induced by polymer-NP attraction . Unlike in the previous studies using extremely slow solvent removal[23], the dispersion of isolated NPs obtained in our experiments is maintained through relatively fast solvent removal upon the PNC solidification. Viscosity of the liquid PNC progressively increases significantly slowing down the NP diffusion and, thus, reducing their ability to aggregate. This explains the previously reported experimental results[19] claiming that the fast solvent evaporation often leads to improved NP dispersion.

The strength of attraction between the 1:1 acetone-toluene mixture and silica ($-\Delta H = 5.1$ kcal·mol^{-1}) prevented the contact aggregation. However, it was not sufficient to stabilize the dispersion of individual NPs. Since the PMMA-silica attraction is only slightly weaker than that between silica and mixed solvent, the PMMA chains may locally replace the solvent and adsorb onto the NP surface. This competition between the polymer and solvent adsorption is proposed as the mechanism by which the chain bound NP clusters are formed.

The low enthalpy of attraction between toluene and silica ($-\Delta H = 3.3$ kcal·mol^{-1}) is reflected by the inability of the solvent to stabilize the dispersed NPs leading to contact aggregation. The strength of attraction between PMMA and silica ($-\Delta H = 4.0$ kcal·mol^{-1}) is greater than that for the toluene-silica interaction, which suggests that polymer adsorption onto the NP surface takes

place as a competitive process to contact aggregation, as manifested by the presence of two populations of NP ensembles.

The dependence of the NP–solvent acid–base interaction enthalpy on the filler volume fraction was used to construct phase diagram of the PMMA/SiO_2 PNCs investigated (Figure 25). Only a narrow window was found of conditions suitable for spatial organization of individually dispersed NPs for the medium strong NP–solvent attraction enthalpy at relatively low NP volume content (≈ 1 vol. %). Strengthening the NPs-solvent attraction led to aggregation caused by the depletion attraction. Slight lowering of the interaction enthalpy led to chain bound clusters in the entire range of the filler volume fractions investigated. Further decrease of the interaction enthalpy led to aggregation caused by insufficient solvation of NPs by the solvent.

The surface of elements in PNC (total interfacial area) and specific surface area were calculated from the TEM image analyses data considering NPs, clusters, and aggregates as independent elements. Both surfaces are compared with values calculated for idealized NP diameter of 20 nm (Figure 26). Significant deviation from the idealized values was found. The observed trends reflect the peculiarities described above. Only acetone and ethyl acetate prepared PNC containing 0.5 and 1 vol. % of NPs almost approach the idealized values, respectively. Systems with higher NP content of the same PNCs tend to gradually decrease their specific surface and deviate from the idealized surface area of the real elements. Clusters observed for the acetone-toluene prepared PNCs exhibit constant specific surface area of roughly 65 m^2/g. The specific interface area of clusters was always smaller that in acetone and/or ethyl acetate prepared PNCs and never approached the idealized values. It is important to mention that internal structure of clusters and the surface morphology of nanoparticles were not taken into account in the calculations. These calculations were not performed for the THF and toluene prepared PNCs because of their complex character.

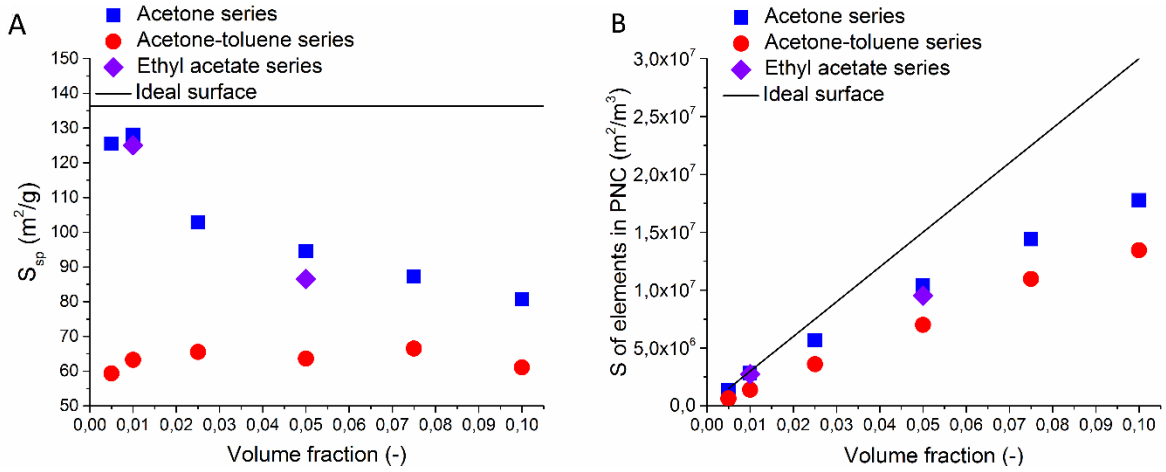

Figure 26: Dependence of specific surface and surface of elements in PNC on volume fraction of 50 kg/mol PMMA/colloidal SiO_2 acetone, acetone-toluene, and ethyl acetate PNC series, respectively.

Influence of molecular weight and tacticity was investigated by comparison of two PMMAs with molecular weight, M_w, of 100 and 500 Kg/mol. Colloidal nanosilica was used as nanofiller. As mentioned in experimental part, used 500 Kg/PMMA had different tacticity with greater isotactic content. Improvement of dispersion is expected with increasing molecular weight because longer polymer chains with adsorbed segments are more effective at pushing particle apart[51]. TEM pictures of 1, 2.5, and 5 vol. % 500 kg/mol PMMA/colloidal SiO_2 are shown in Figure 27.

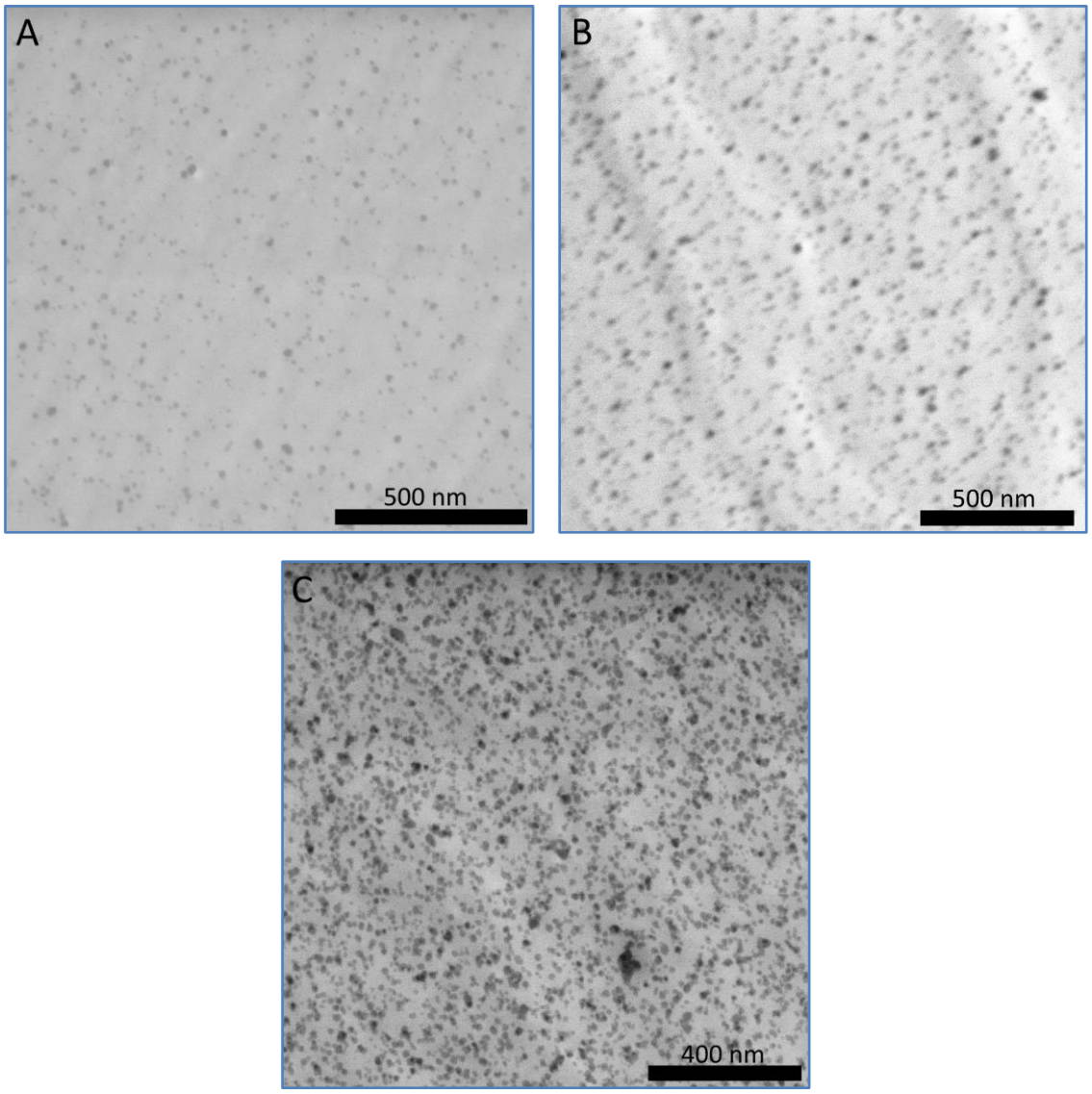

Figure 27: TEM images of 500 kg/mol PMMA/colloidal SiO_2 prepared from acetone with loadings of 1, 2.5, and 5 vol. %, respectively.

Dispersion of individual NPs was found for both molecular weights of PMMA matrices at volume fraction of 1 vol. % of colloidal nanosilica. Increase of molecular weight of the PMMA matrix led to improvement of dispersion of individual NPs at 2.5 vol. %. PNCs with lower molecular weight matrix showed gradual aggregation from 2.5 vol. % loading. Image analysis of 5 vol. % PNC with higher molecular weight revealed that NPs organize into bigger structures

with average diameter of 26 nm, Figure 28A. Interelement distance of PNCs with higher molecular weight matrix was significantly larger than for PNCs with matrix of lower molecular weight, Figure 28B. It means that NPs distribution and dispersion state is much more homogeneous in the case of higher molecular weight. It seems that increase of molecular weight leads to broadening of good dispersion of individual NPs and leads to transformation from aggregation to clustering at higher filler content due to enhanced polymer–mediated repulsion between particles[51]. Although results interpretation fits well with the theoretical PRISM model[51], it is important to keep in mind that the PMMA tacticity varied significantly with molecular weight. It was reported that isotactic PMMA interacts with silanol groups stronger than syndiotactic or atactic PMMA because iso-PMMA undergoes more interfacial conformational changes than the other isomers which allows more functional groups to be involved in the interfacial interactions with silica surface[105, 106].

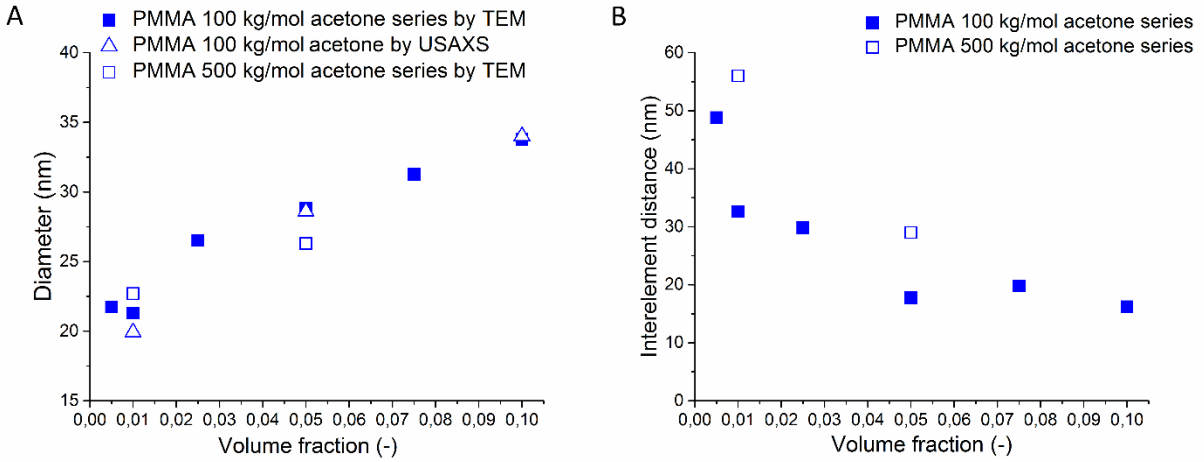

Figure 28: Comparison of (A) NP diameter and (B) interelement distance of PMMA/colloidal SiO_2 PNCs with different molecular weights.

PMMA/colloidal SiO_2 system, extensively described in the previous chapters, was taken as a model system. Other PNCs were compared with this model system. PMMA acts as a Lewis base due to the ester side groups. Silica acts as a Lewis acid due to the silanol groups onto its surface. Therefore, it was assumed that a good dispersion or chain bridging should occur due to the possible NP-PMMA polar interactions and hydrogen bonding[55].

Fumed nanosilica has also silanol groups on its surface but with structural character different from the colloidal nanosilica. Fumed silica is formed at elevated temperatures, therefore primary particles are usually fumed together into bigger particles with a string-like shape and high specific surface area. Therefore, 70 nm secondary particles were found in the acetone prepared PNCs containing fumed nanosilica instead of the dispersion of individual primary particles with diameter of 14 nm found in the case of colloidal nanosilica, Figure 29A and Figure 18B, respectively. Smaller objects were assumed impossible to obtain without breaking the fused strings of primary NPs which would require large imput energy and harsh conditions. At 1 vol. %, fumed silica formed in the PMMS matrix 3D strings in the PMMA matrix in the

case of PNC prepared from acetone-toluene rather than separated clusters, Figure 29B and Figure 20B. This behavior can be utilized for lowering the percolation threshold to obtain enhanced mechanical properties at very low NP content.

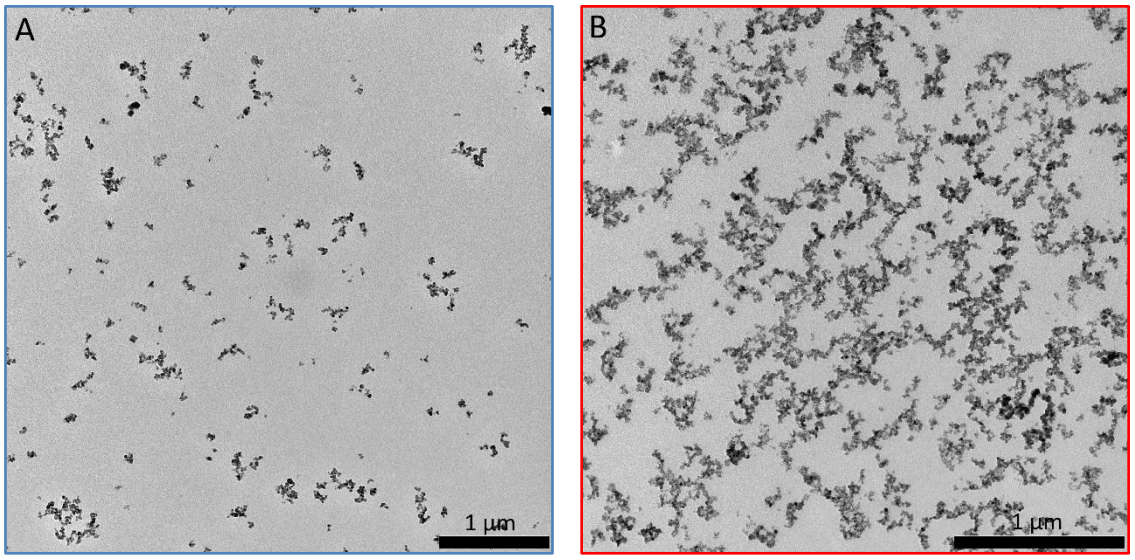

Figure 29: TEM images of 1 vol. % PMMA/fumed SiO_2 PNC prepared from acetone (A) and acetone-toluene (B), respectively.

A difference was found between the NP spatial organization of AZO nanoparticles and colloidal silica NPs for the same solvent used. Worsening of the dispersion state of AZO NPs (Figure D30) compared to the colloidal SiO_2 NPs (Figure 18B and 20B) was observed. This effect was attributed to the different character of the ZnO surface chemistry and stronger particle–particle interactions. ZnO has amphoteric character[107], therefore, it can act as both Lewis acid or base. Hence, weaker polymer–particle interactions compared to SiO_2 NPs were assumed. Also, stronger Van der Waals interactions between the AZO NPs were expected. NPs in PMMA/1 vol. % AZO PNC prepared from acetone formed pairs and trios (Figure D30A). Formation of pairs and trios is expected as the early stage of aggregation[104]. NPs were self-assembled into larger organizations in the PNCs prepared from acetone–toluene solvent mixture (Figure D30B). Several hundred nanometers large objects were created when toluene was used as the solvent (Figure D30C). The dispersion state was worsened as basicity of used solvent decreased. Acid-base attraction enthalpy could not be calculated because E and C parameters of AZO particles were not known.

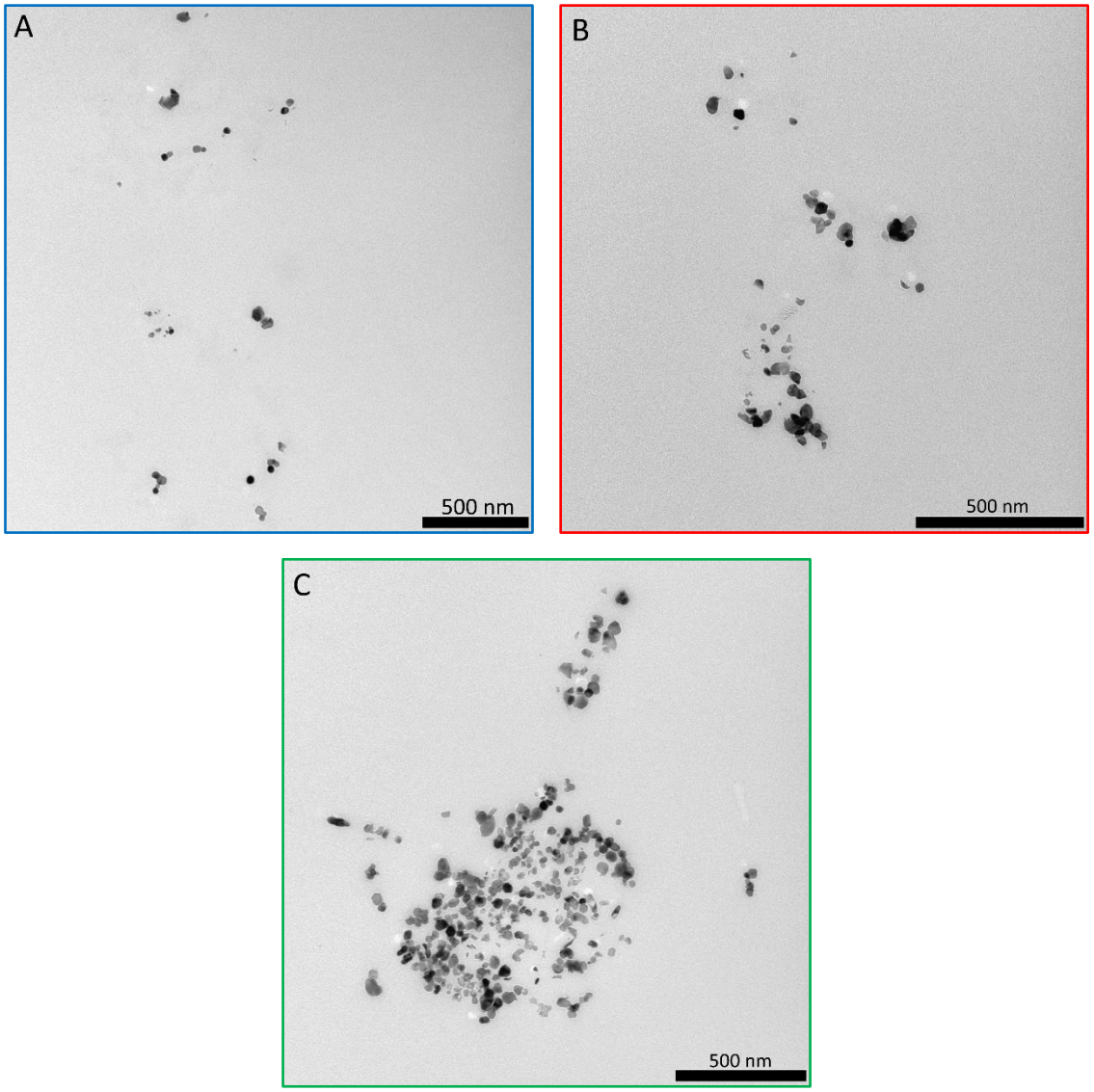

Figure 30: TEM images of 1 vol. % PMMA/AZO PNCs prepared from acetone (A), acetone-toluene 1:1 mixture (B), and toluene (C), respectively.

The Fe_2O_3 nanoparticles were also used in the PMMA matrix. The PMMA/Fe_2O_3 PNC containing 0.5 vol. % of NPs was prepared using acetone as a solvent. NPs spatial organization is shown in the Figure D31. Several hundred nanometers large aggregates were observed. Use of SiO_2 led to individually dispersed NPs for the same matrix and preparation conditions. Similarly to AZO, the Fe_2O_3 is amphoteric, therefore, it can act as both Lewis acid or base[60, 108]. The acidic character of the surface Fe-OH functional groups of hematite is weaker than the Si-OH groups of silica[60, 108]. Moreover, it is assumed that the attractive van der Waals particle–particle interactions of the Fe_2O_3 are stronger than those for the SiO_2.

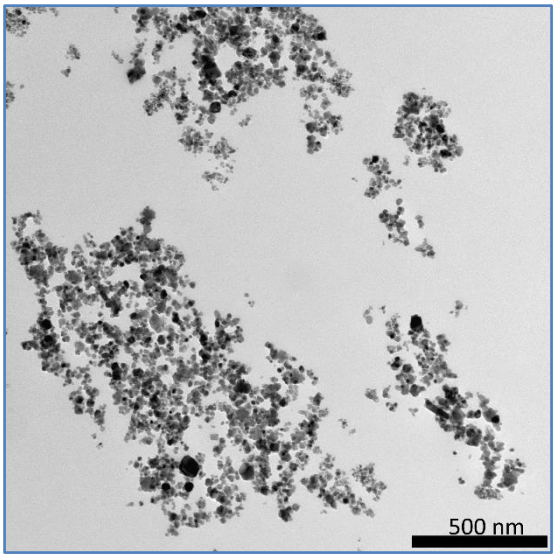

Figure 31: TEM image of 0.5 vol. % PMMA/Fe_2O_3 PNC prepared from acetone.

PC can act as a Lewis base due to its carbonate groups in the backbone. Since silica acts as a Lewis acid due to the silanol groups onto its surface, attractive NP–polymer interactions are expected. PC/1 vol. % colloidal SiO_2 PNCs was prepared from dichloromethane (DCM) and tetrahydrofuran (THF). Dichloromethane is a Lewis acid and tetrahydrofuran is Lewis base with high donor–acceptor interaction enthalpy (8.9 kcal·mol^{-1}) to acid silanol groups of nanosilica. Contact aggregates with a diameter of approximately 200 nm were found in PC/1 vol. % colloidal SiO_2 PNC prepared from DCM (Figure 32A). A mixture of small aggregates with average diameter of 62 nm and individual NPs was found for PC/1 vol. % colloidal SiO_2 PNC prepared from THF (Figure 32B). The dispersion state of this nanocomposite had very similar NPs spatial organization like the PMMA/1 vol. % colloidal SiO_2 PNC prepared from the same solvent (Figure 17B). We believe that both NP spatial organizations have their origin in the depletion attraction caused by the very strong donor-acceptor enthalpy between the silica and THF. Similar NP spatial organization of PC/1 vol. % colloidal SiO_2 PNC prepared from DCM (Figure D32A) and PMMA/1 vol. % colloidal SiO_2 from toluene (Figure 21A) have their origin in the insufficient solvation of silica nanoparticles by the used solvent, leading to an extensive aggregation of NPs. The results strongly support the hypothesis put forward above, stressing out the key role of the solvent–particle interactions for the final equilibrium dispersion state.

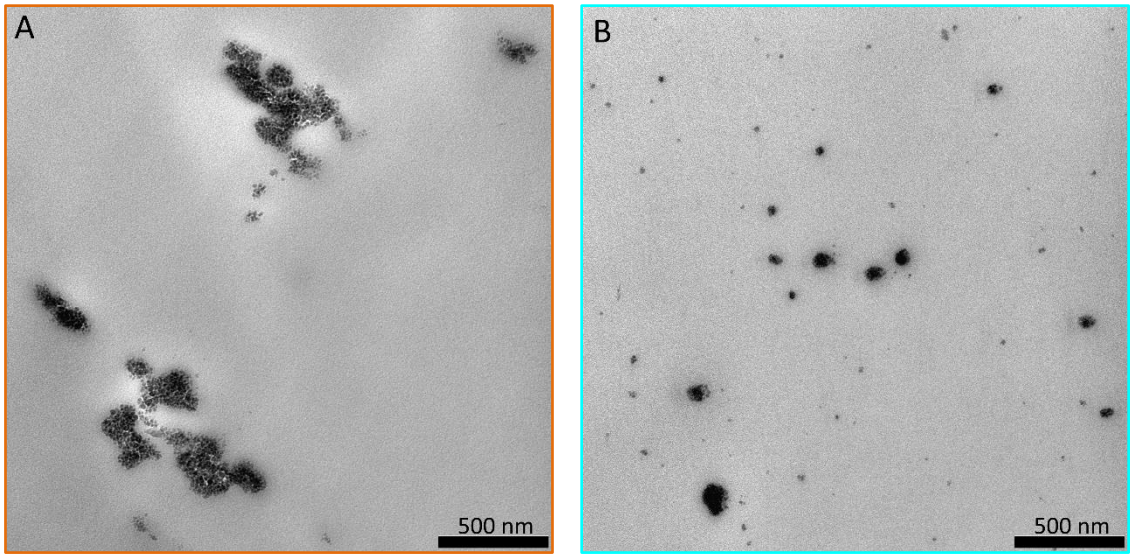

Figure D32: TEM images of 1 vol. % PC/colloidal SiO_2 PNC prepared from (A) DCM and (B) THF, respectively.

PS has no polar heteroatoms and; therefore, only weak dipole–dipole interactions between the polymer and SiO_2 are expected. PS/1 vol. % colloidal SiO_2 PNC was prepared from THF. TEM image of the 1 vol. % PS/colloidal SiO_2 PNC sample is shown in Figure 33. Micrometer sized aggregates were created probably due to a massive depletion attraction. It seems that the PS is more prone to the depletion attraction than PMMA, PC, and PVAc due to weak NP-polymer interaction strength.

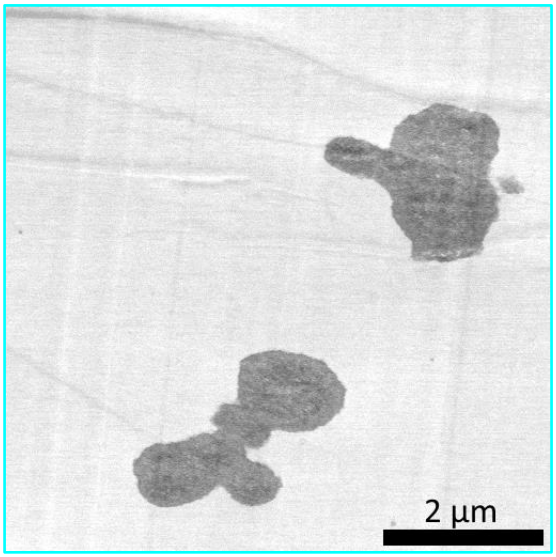

Figure 33: TEM image of 1 vol. % PS/colloidal SiO2 PNC prepared from THF.

PVAc acts as a Lewis base due to its ester groups. Therefore, attractive interactions with the acidic surface of SiO_2 were assumed. PVAc/colloidal SiO_2 PNCs containing 1 and 5 vol. % of NPs were prepared from acetone. Individual particles and 4-10 particle clusters were found in the PVAc containing 1 vol. % of NPs, Figure D34A while clustered NPs were found in the

PVAc/5 vol. % colloidal SiO_2, Figure 34B. Both diameter of elements and interelement length were found to be greater for the PVAc based PNCs compared to the PMMA PNCs (Figure D35). The reason was gradual NP clustering in the PVAc/colloidal SiO_2 PNCs. The difference between NPs spatial organization in PMMA and PVAc could be caused by the different preparation protocol. Acetone was removed from PVAc at 80 °C instead of 140 °C as in the case of PMMA because of the different T_g andthe degradation of PVAc matrix observed near 140 °C.

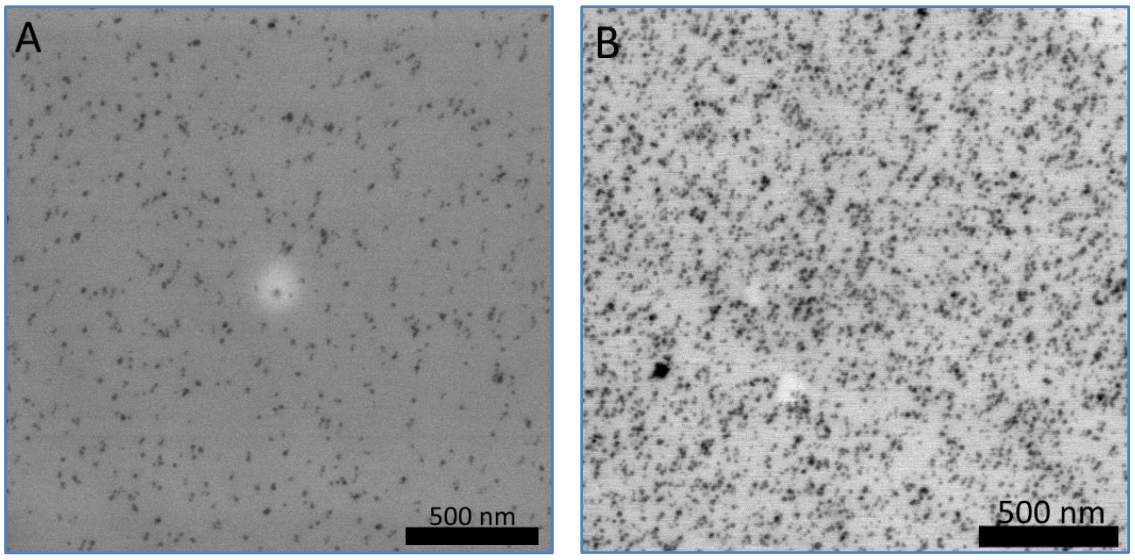

Figure 34: TEM images of 1 (A) and 5 (B) vol. % PVAc/colloidal SiO_2 PNCs, respectively.

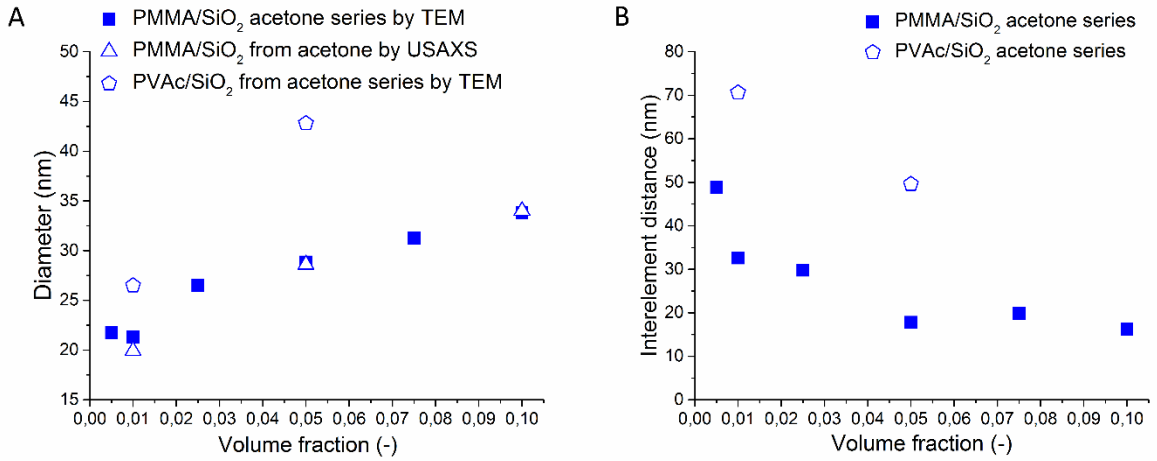

Figure 35: Comparison of (A) diameter and (B) interelement length of PMMA and PVAc filled by colloidal SiO_2 NPs.

In order to quantitatively analyze the state of NP dispersion in polymer liquids, Mackay et al[19] proposed a hypothesis suggesting the decisive role of the ratio between the NP radius (R) and the polymer radius of gyration (R_g). To test this hypothesis, coil diameter was plotted against NP diameter (D). Because it is assumed that final structure originates from NP–polymer–solvent system, coil diameter varies in different solvents. Therefore, the coil diameters of the

matrices investigated were determined employing DLS in various solvents (Table 3). The solvent specific coil diameters were utilized further in this chapter.

Table 3: coil diameters of investigated matrices in used solvents.

Polymer	Acetone	Acetone-toluene 1:1	Toluene	THF	Ethyl acetate	DCM
100 kg/mol PMMA	10.5	11.4	10.8	13.7	14.8	
500 kg/mol PMMA	32.6					
PVAc	26.6					
PC				12.8		4.6
PS				19		

According to the Mackay et al[19] hypothesis, the R larger than R_g should result in a poor NP dispersion and, the NP aggregation should occur. This prediction fundamentally contradicts our experimental observations. Dependence of polymer coil on NP diameter of the PNC systems prepared from various solvents is shown in Figure 36. Considering Mackay model for our systems, individually dispersed NPs should only occur for 500 kg/mol PMMA and PVAc/colloidal SiO_2 PNCs. In contrary to the predictions, these systems tend to form chain bound clusters. Dispersion state of PC/colloidal SiO_2 and 100 kg/mol PMMA/SiO_2 and AZO systems can be tailored from contact aggregates to individually dispersed NPs by control of preparation conditions as was comprehensively described in previous chapters. Only PMMA/Fe_2O_3 and PS/colloidal SiO_2 fulfilled Mackay prediction, but it is believed that the origin of aggregation in these systems is linked to weaker polymer–particle interaction, stronger particle–particle interactions, and extensive depletion attraction are expected in PMMA/Fe_2O_3 and PS/colloidal SiO_2 PNCs, respectively. The results suggest that the problem requires to take into consideration additional variables than just the size ratio. It seems necessary to consider the enthalpies of interaction between all the components. However, needless to say, that Mackay, et al.[19] investigated PNCs consisting of fullerenes in polyolefin or tightly cross-linked polystyrene nanoparticles in linear polystyrene with almost "no specific interfacial interactions". In these specific cases, the proposed hypothesis can be valid, however, it not generally applicable. Moreover, the ability to tune the structure while keeping a constant composition provides a direct evidence that not only polymer-particle and particle-particle interaction, but rather a complex interplay of solvent-solvent, solvent-polymer, solvent-particle, polymer-particle, and particle-particle interactions controls the equilibrium nanoparticle dispersion state in polymer liquids.

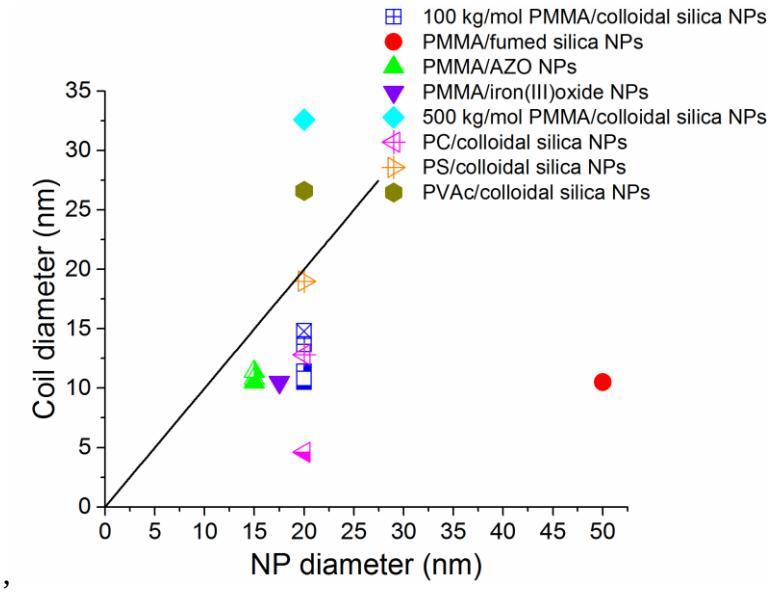

Figure 36: Dependence of polymer coil diameter on NP diameter. Colors designate various composition. Solvents from which were the PNCs prepared and in which coil diameters were measured are marked by various symbols: acetone (full symbol), acetone-toluene 1:1 mixture (half right symbol), toluene (open symbol), THF (+ center symbol), ethyl acetate (x center symbol), and DCM (half down symbol).

5.2 Relaxation properties

Relaxation properties were measured in order to provide information about chain dynamics and molecular packing in the presence of NPs with varying spatial organization. Presence of nanoparticles can significantly alter chain motion especially in glass transition, plateau, and terminal regions. Dynamical mechanical analysis (DMA) and rheological measurements were employed to investigate PNC behavior in these temperature regions.

Temperature dependences of the storage modulus, loss modulus, and tan(δ) are shown in Figure 37 for the 100 kg/mol PMMA. Glass transition temperature, T_g, was determined from the maximum of the loss modulus. The results are listed in Table 4.

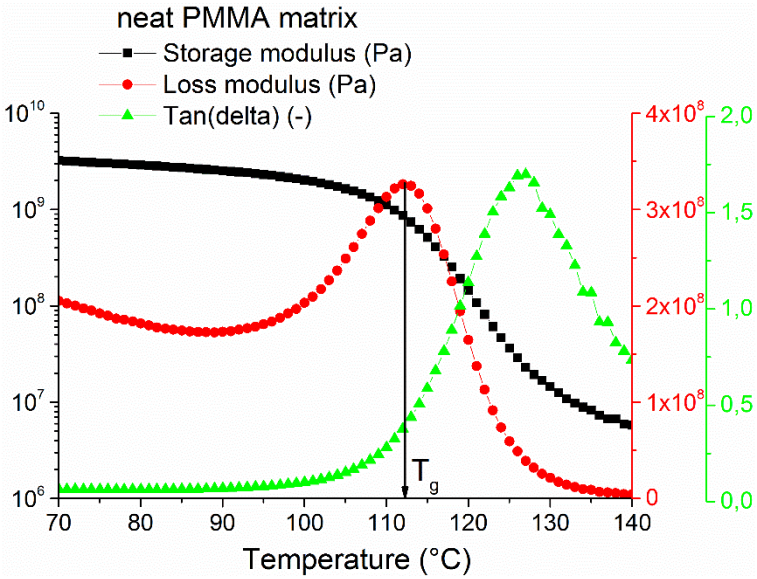

Figure 37: Dependence of storage modulus, loss modulus, and tan(δ) on temperature of 100 kg/mol PMMA matrix.

Small amplitude oscillation shear tests were performed to investigate relaxation behavior in the rubbery plateau and terminal zone regions. Master curves of storage modulus, loss modulus and tan(δ) were constructed over a wide range of frequency utilizing time-temperature superposition[109-111] of frequency sweep data measured at various temperatures. The master curves of 100 kg/mol PMMA are shown in Figure 38A. Reptation time was determined as reciprocal value of frequency in the crossover of storage and loss modulus in the terminal zone[112]. Plateau modulus was determined as the storage modulus at minimum of tanδ[112–114].

Molecular weight between entanglements was calculated by means of Equation 3[112-116]:

$$M_e = \frac{\rho RT}{G_0^N}, \tag{3}$$

where M_e is molecular weight between entanglements, R is universal gas constant, T is temperature, and ρ is density. The number of entanglements per one chain was calculated as a

ratio of number average molecular weight of polymer and molecular weight between entanglements (Table 4).

Steady state shear measurements were performed in order to investigate flow behavior close to the processing conditions and use zero shear rate viscosity for further investigation of the NP–polymer interactions. The dependence of the viscosity on shear rate of 100 kg/mol PMMA is shown in Figure 38B. Zero shear rate viscosity was determined by fitting the flow data by the Cross model[117]:

$$\frac{\eta-\eta_\infty}{\eta_0-\eta_\infty}=\frac{1}{1+(k\dot{\gamma})^h}, \tag{4}$$

where η is viscosity, η_0 zero shear rate viscosity, η_∞ infinity shear rate viscosity, $\dot{\gamma}$ shear rate, k consistency and h the power law index. The zero shear rate viscosities of investigated matrices are listed in Table 4.

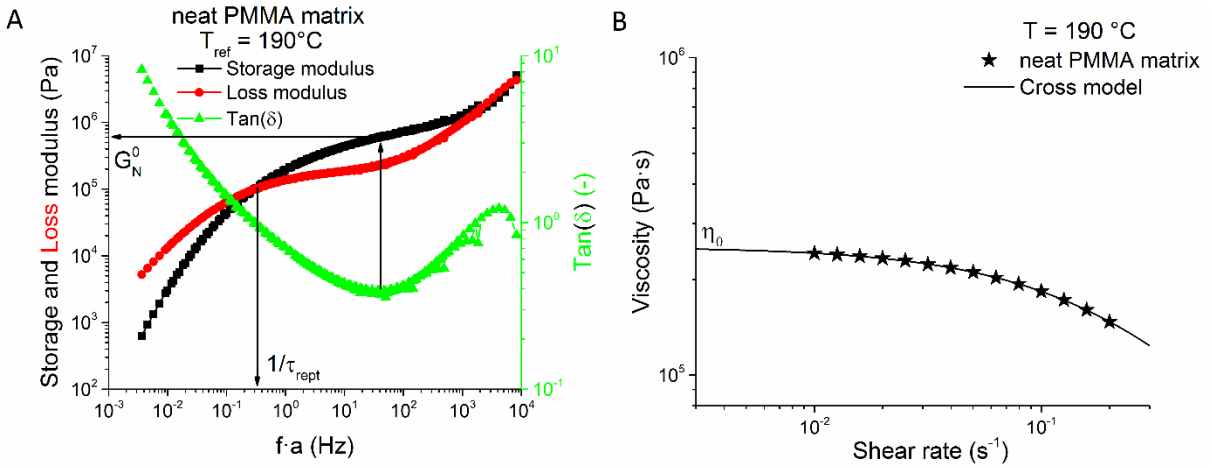

Figure 38: (A) Dependence of storage modulus, loss modulus and tan(δ) master curves on frequency and (B) shear rate dependence of viscosity of neat 100 kg/mol PMMA matrix.

The observed increase of the T_g and the reptation time with increasing molecular weight of the PMMA were expected. Unexpectedly, significant decrease of plateau modulus was found due to different tacticity. Molecular weight between entanglements calculated from plateau modulus increased from approximately 8 kg/mol for 100 kg/mol PMMA to 51 kg/mol for 500 kg/mol PMMA. Molecular weight between entanglements of atactic PMMA was reported to be approximately 13 kg/mol [118-120]. Increase of the molecular weight between entanglements was reflected upon decrease of the number of entanglements per one chain that should be 5 times greater for 500 kg/mol PMMA than 100 kg/mol PMMA. This discrepancy was caused by different tacticity of the investigated PMMAs. It is assumed that 500 kg/mol PMMA has significantly higher content of isotactic sequences.

Table 4: Glass transition temperature, T_g, reptation time, τ_{rept}, plateau modulus, G_0^N, number of entanglements per one chain, N_{ent}, and zero shear rate viscosity, η_0, of investigated matrices.

Matrix	T_g (°C)	τ_{rept} (s)	G_0^N (MPa)	N_{ent} (-)	η_0 (MPa·s)
100 kg/mol PMMA	112.1	3.4	0.58	6.2	0.25
500 kg/mol PMMA	122.2	34.7	0.09	4.9	
PS	93.9				

Relaxational properties of PMMA/SiO_2, exhibiting three different NP spatial organizations: (i) dispersion of individual nanoparticles, (ii) chain bound clusters, and (iii) contact aggregates, were investigated.

Although, there is not a generally accepted theory of glass transition phenomena[121-126], the glass transition temperature can still be very useful material parameter restricting the applicability of the PNCs. Glass transition temperatures of PNCs with various NP spatial organizations are listed in Table 5. The dependence of the difference between the glass transition temperature of PNCs and the neat PMMA, ΔT_g, on volume fraction for various dispersion states is shown in Figure 39A. Increase of T_g was found for all the PNCs investigated. Attractive PMMA-SiO_2 interactions were expected due to the hydrogen bonding between ester groups of PMMA and surface silanol groups of silica[55]. The greatest increase of T_g was recorded for PNCs with individually dispersed NPs. The greatest increase of T_g was recorded for PNCs with individually dispersed NPs. The NP content dependence of ΔT_g exhibits an initial rapid increase compared to the neat PMMA followed by a weak growth at higher concentrations which suggests that the dynamics of almost all polymer chains was already frustrated at the loading as low as 0.5 vol. %. The additional increase of ΔT_g would then be caused by the increasing volume of the immobilized segmental layers onto NP surface. Hamieh et.al[127] found that T_g increase for syndiotactic PMMA induced by silica equals approximately to 5 °C, which supports the hypothesis suggested. Clustered system showed a gradual rise of T_g with increasing NP volume fraction. The lowest ΔT_g was found in PNCs with aggregated. The results fall onto one curve when related to the specific interface area (Figure 39B) or reciprocal value of interelement distance (Figure 39C). NP organization independent increase of T_g with the surface of elements in PNC and the reciprocal value of interelement distance suggests slower dynamics in vicinity of NPs caused by immobilization. Apparently, these two structural variables are more appropriate for interpretation of T_g changes than the volume fraction alone. This approach could shed more light onto the discrepancy found in literature dealing with the volume fraction dependence of T_g of PNCs[16, 34, 69, 70].

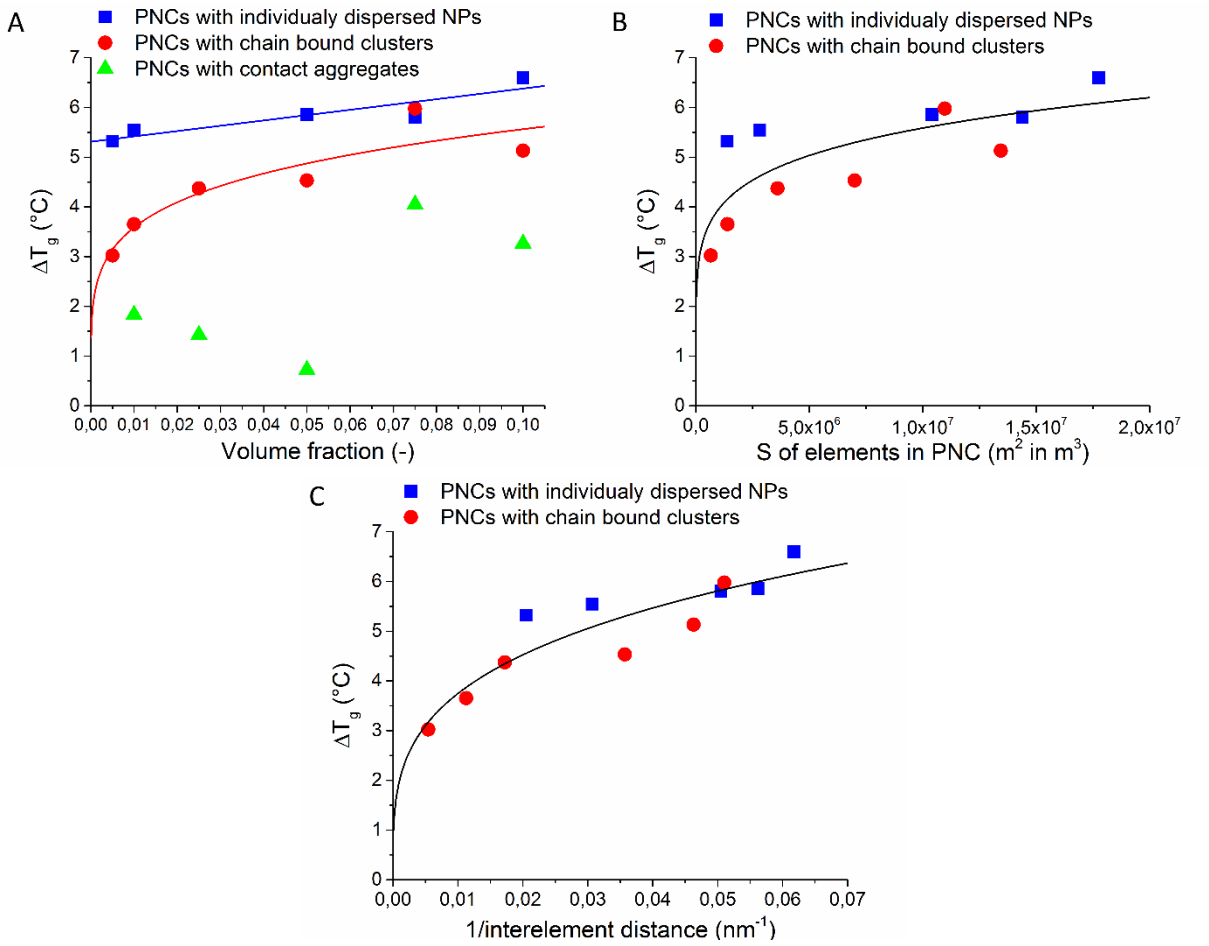

Figure 39: dependence of ΔT_g on (A) volume fraction, (B) surface area of elements in PNC, and (C) reciprocal value of interelement distance of various PNCs.

The melt rheology of a glassy polymer in the range of its typical processing temperature is greatly altered by the presence of NPs determining the PNC processability and practical applicability and brings the rheological evaluation into the light of interest with practical consequences. Storage modulus master curves spanning over a wide range of frequencies were constructed using the time–temperature superposition[109-111]. The master curves reflect behavior in plateau and terminal region for PNCs with various NP spatial organizations and volume fractions (Figure 40). Reptation time, modulus of the rubbery plateau and the thermal dependence of zero shear rate viscosity were evaluated as representative rheological parameters.

Reptation times of the PNCs with various NP spatial organizations are listed in Table 5, respectively. The dependence of reptation time on the filler volume fraction showed differences between various nanostructures (Figure 41A). However, the reptation time of various nanostructures fell onto one curve when plotted against interface area (Figure 41B). The obtained increase of reptation time has not only origin in the increase in the primitive path contour length, but also because chains must reptate through several domains of slower dynamics near the surface of the NPs. These experimental results are in good agreement with molecular modeling reports[73]. The internal structure of clusters was neglected in the calculation

of the interfacial surface and they were treated as compact entities. Since the data collapsed onto the same curve as the dispersion of individual NPs, it seems that the bridged chains inside the clusters were unable to contribute significantly to the determined macroscopic response within the investigated volume fraction, temperature and frequency range.

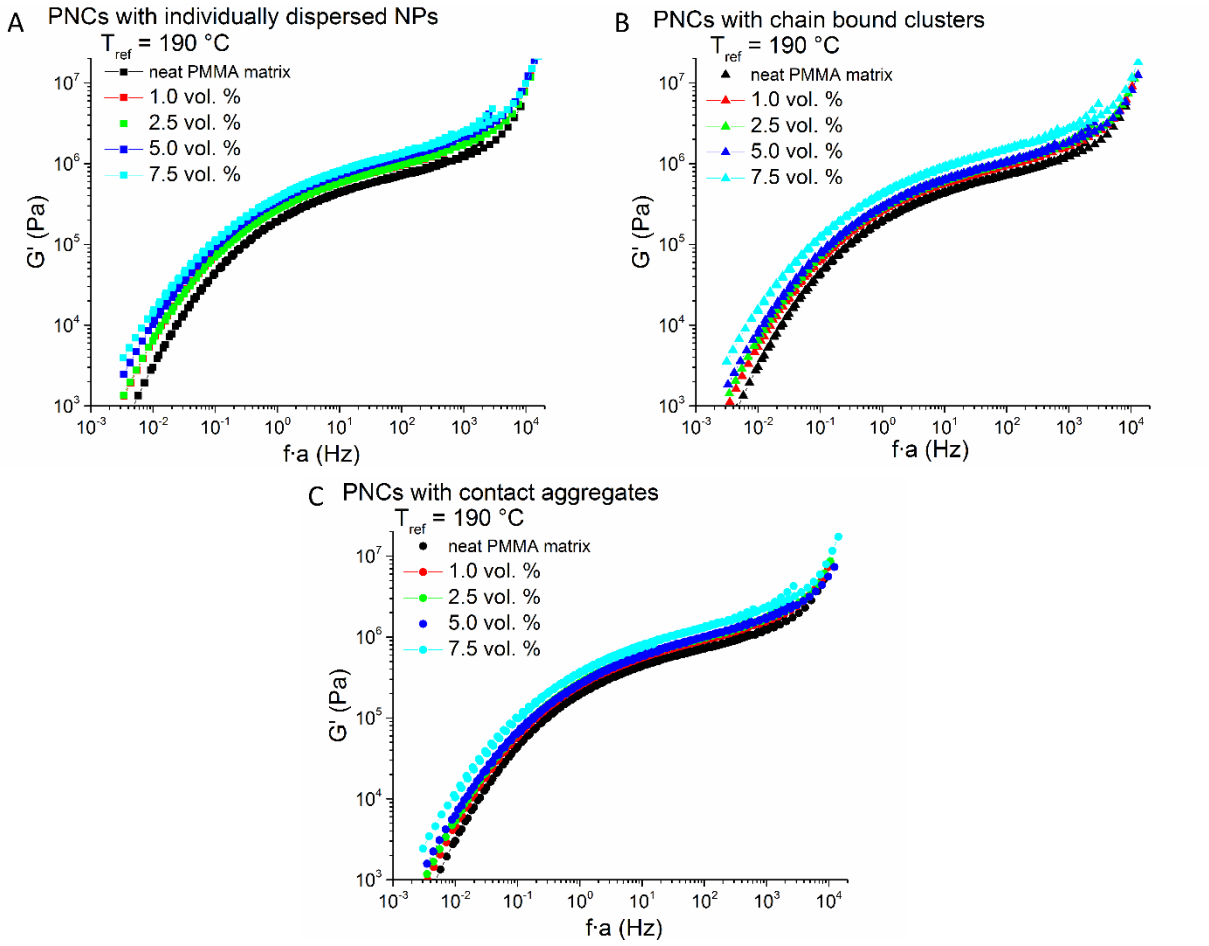

Figure 40: Storage modulus master curves of PNCs with various NP spatial organizations and volume fractions.

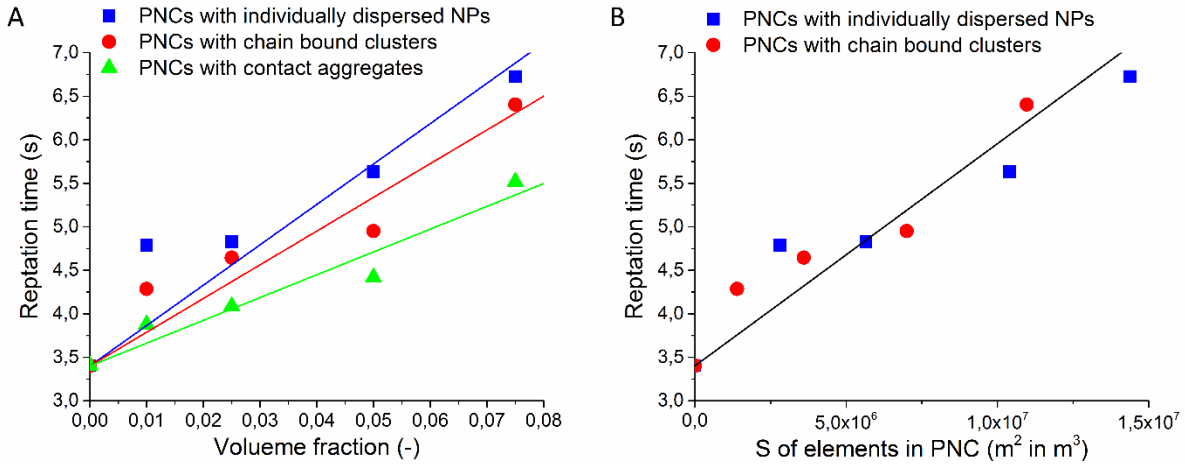

Figure 41: Dependence of reptation time at 190 °C on (A) volume fraction and (B) effective surface area of elements in PNC.

Chain dynamics of the rubbery plateau was retarded by the attractive NP-polymer interaction. Immobilized segments reached relaxation times similar to glassy segments while unaffected bulk dynamics exhibited unchanged dynamics with several orders magnitude longer relaxation times[16, 128-130]. The existing volume replacement continuum mechanics models[74-76] for the composition dependence of the plateau modulus were not able to describe the dependence of the relative modulus on the NP volume fraction (Figure 42A). An additional segmental scale reinforcing mechanism characterized by the composite modulus reduced to the matrix modulus and appropriate continuum micromechanics model were proposed to be directly related to the interfacial area[87]. An important structural difference arisen when this reinforcing mechanism was related to the total interfacial area (Figure 42B). Plateau modulus of individually dispersed NPs tend to slightly decrease or stagnate with the increasing interfacial surface (volume fraction) up to about $5 \cdot 10^6$ m^2/m^3 (2.5 vol. %), where it becomes overwhelmed by a rapid growth. Clusters exhibited modulus stagnation up to $3 \cdot 10^6$ m^2/m^3 (2.5 vol. %) followed by gradual modulus increase which was more pronounced than the corresponding dispersion of individual NPs. As suggested by the simulation of Long, et al.[131, 132], the strong increase might be caused by the percolation of the immobilized domains around the NPs due to the weakly worsening dispersion state and filler morphology. This overpowered dependence on the interfacial surface lead to a conclusion that NPs assembled into close-packed clusters experience a significant contribution of the internal structure to macroscopic properties originating from the highly affected bridging chains inside the clusters and also from the inter-cluster percolation at higher volume fractions. Plateau moduli of the PNCs were reduced to the Guth-Smallwood model[74-76] and matrix moduli were calculated by Equation 5:

$$G^N_{0\,matrix} = \frac{G^N_{0\,c}}{G_{G-S}} = \frac{G^N_{0\,c}}{1+2.5v_f+14.1v_f^2}, \tag{5}$$

where $G^N_{0\,matrix}$ is matrix plateau modulus, $G^N_{0\,c}$ nanocomposite plateau modulus, G_{G-S} modulus calculated by the Guth–Smallwood model, and v_f volume fraction (Table 5). Modified matrix moduli were used for calculation of the number of entanglements per one chain in the PNCs (Equation 5). Dependence of the number of NP induced entanglements per one chain on the volume fraction is shown in Figure 42C and the data are listed in Table 5. The number of entanglements per one chain increased in all PNCs investigated suggesting that NPs act as entanglements attractors. The greatest increase was found in clustered PNCs and the lowest in aggregated PNCs.

Table 5: Glass transition temperature, T_g, reptation time, τ_{rept}, plateau modulus, G_0^N, modified matrix plateau modulus, $G_{0\,matrix}^N$, number of entanglements per one chain, N_{ent}, and zero shear rate viscosity, η_0, of PMMA/SiO_2 PNCs with various NP spatial organizations.

Sample	T_g (°C)	τ_{rept} (s)	G_0^N (MPa)	$G_{0\,matrix}^N$ (MPa)	N_{ent} (-)	η_0 (MPa·s)
PMMA/colloidal SiO_2 with individually dispersed NPs						
0.5 vol. %	117.5					
1 vol. %	117.7	4.8	0.78	0.76	8.3	0.45
2.5 vol. %	117.2	4.8	0.79	0.74	8.0	0.48
5 vol. %	118.0	5.6	0.99	0.85	9.2	0.72
7.5 vol. %	118.0	6.7	1.12	0.88	9.6	1.03
10 vol. %	118.7					
PMMA/colloidal SiO_2 with chain bound clusters						
0.5 vol. %	115.2					
1 vol. %	115.8	4.2	0.77	0.76	8.2	0.41
2.5 vol. %	116.5	4.6	0.82	0.77	8.3	0.48
5 vol. %	116.7	4.9	0.97	0.84	9.1	0.60
7.5 vol. %	118.1	6.4	1.2	1	10.8	1.49
10 vol. %	117.3					
PMMA/colloidal SiO_2 with contact aggregates						
1 vol. %	114.0	3.9	0.74	0.72	7.8	0.36
2.5 vol. %	113.6	4.1	0.79	0.74	8.0	0.43
5 vol. %	112.9	4.4	0.81	0.70	7.6	0.50
7.5 vol. %	116.2	5.5	1.09	0.86	9.4	0.92
10 vol. %	115.4					

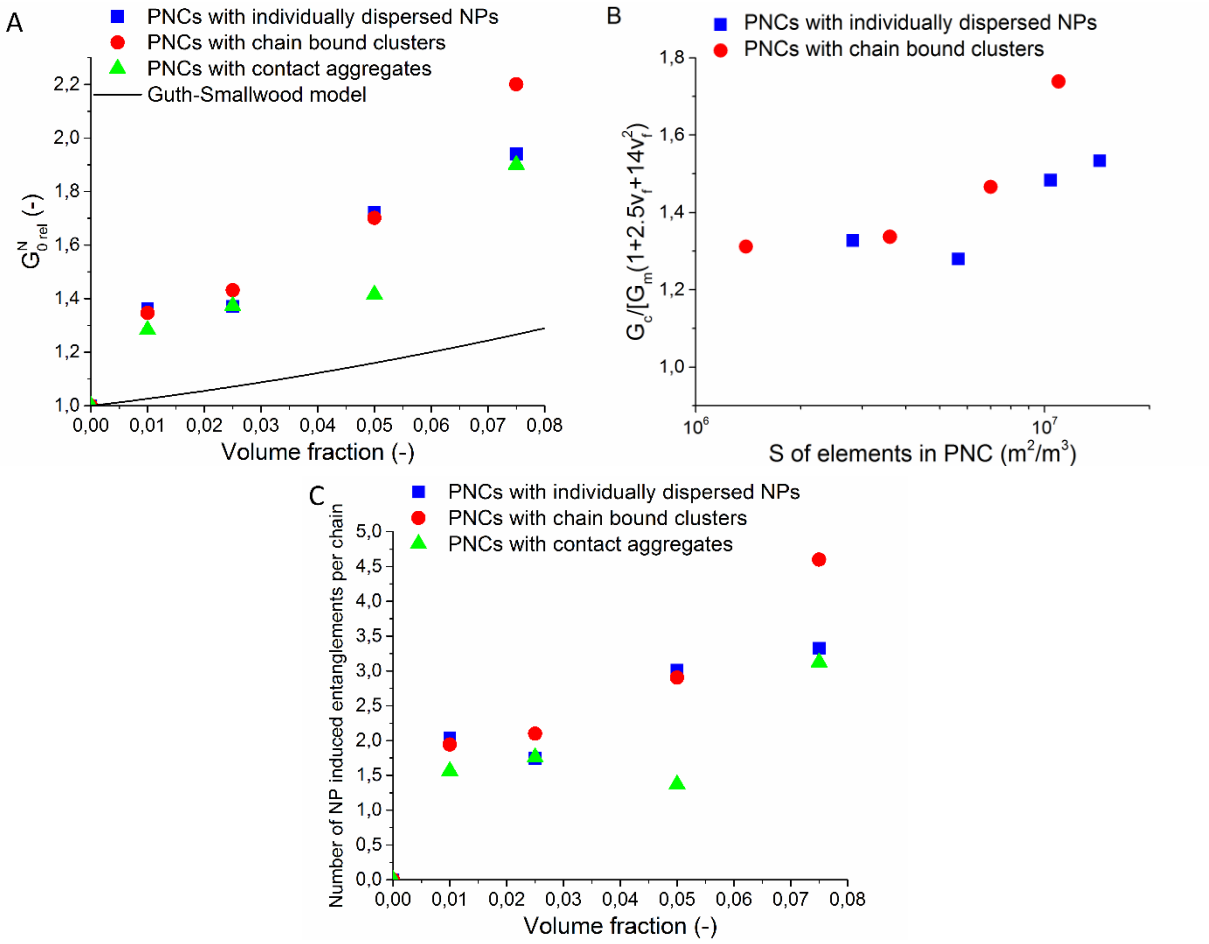

Figure 42: Dependence of plateau modulus on (A) volume fraction, (B) plateau composite modulus reduced to the matrix modulus and appropriate continuum micromechanics model on surface of elements in PNC, and (C) dependence of number of entanglements per one chain on volume fraction of PNCs with various NP spatial organization.

Dependence of the viscosity on shear rate for PNCs with various NP spatial organizations and volume fractions is shown in Figure 43. The experimental data were fitted with the Cross model to evaluate the zero shear rate viscosity (Table 5). Dependence of the relative zero shear rate viscosity on the filler volume fraction is also shown in Figure 43. For the purpose of further analysis, PNCs investigated are assumed to be suspensions of particles in a high-viscosity continuum of polymer segments. Under this assumption, dependence of the relative zero shear rate viscosity on the filler volume fraction can be described by the Equation 6[29, 83, 84, 133, 134]:

$$\eta_{r\,0} = 1 + 2.5k\phi + P\phi, \tag{6}$$

where $\eta_{r\,0}$ is relative zero shear rate viscosity, 2.5 is Einstein coefficient, k is the parameter that characterize influence of polymer adsorption on intrinsic viscosity[29, 83, 84, 133, 134], and P is the particle interaction coefficient that characterize effect of particle interactions on the suspension viscosity[29, 83, 84, 133, 134] (Table6).

Adsorption of polymer segments onto surface of particles increases their hydrodynamic size. This effect is more pronounced with decreasing particle size. Therefore, significant discrepancy characterized by the *k* parameter was found from Einstein coefficient of 2.5 derived for non-interacting particles. The highest *k* value exhibited PNCs with individually dispersed NPs due to the highest effective interface area. The *k* value of PNCs with chain bound clusters was close to the value of PNCs with individually dispersed NPs. The lowest *k* value was found for PNCs with contact aggregates, but their *k* value still differed significantly from the Einstein coefficient. This effect was ascribed to the adsorption of polymer segments onto smaller aggregates that have still relatively large surface area. Adsorbed polymer layer thickness was calculated by means of Equation 7:

$$h = \sqrt[3]{\frac{3Vk}{4\pi}} - r, \tag{7}$$

where *h* is the thickness of the affected polymer layer, *V* is the element volume, *k* is the above mentioned parameter, and *r* is the element radius. Radii determined by image analysis of TEM snapshots were used (average radius of 15 nm for series of individually dispersed NPs and 20 nm for series with chain bound clusters as their internal structure was neglected) (Table 6). The thickness of affected polymer layer was approximately the same for the various NPs spatial organizations. The obtained affected layer thickness suggests that every NP influences dynamics of approximately 2 coils in the direction perpendicular to the NP surface. It means that chain dynamics of all polymer chains is affected by NPs below the interparticle distance of approximately 40 nm. It corresponds to about 1 vol. % filler loading for individually dispersed NPs and 5 vol. % for chain bound NP clusters. The PNCs with chain bound clusters had the highest particle interaction coefficient due to strong adsorbed chains mediated interactions of particles in closely packed clusters. The lowest *P* value was found for PNCs with individually dispersed NPs because of their largest interelement distances and absence of clusters.

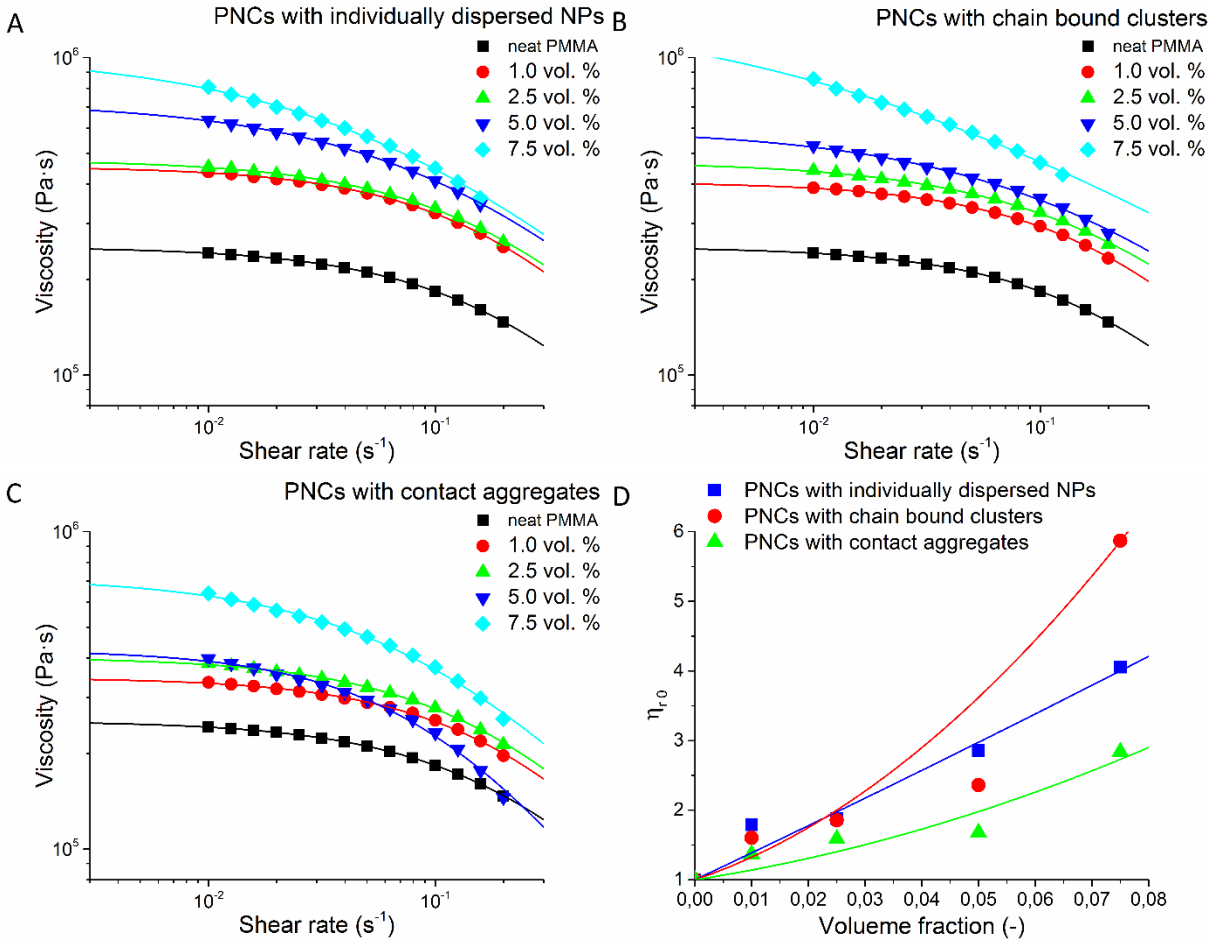

Figure 43: (A, B, C) Dependence of viscosity on shear rate of PNCs with various spatial organization and volume fractions fitted by the Cross model (Equation 4). (D) Dependence of zero shear rate viscosity on volume fraction fitted with Equation 6.

Table 6: Fitting parameters of Equation 6 and length of affected polymer layer determined by Equation 7.

PNCs	*k*	*P*	*h* (nm)
With individually dispersed NPs	15	21	22
With chain bound clusters	11	497	24
With contact agreggates	5	139	

Dependence of the ΔT_g on the SiO_2 volume fraction in the PMMA with various matrix molecular weight and tacticity is shown in Figure 44. The T_g increase in the PMMA with higher molecular weight matrix was about one order of magnitude smaller than for the matrix with smaller molecular weight. This difference cannot be attributed to the effective surface area

because both samples have similar dispersion state. Inverse results were expected. Further experiments will be performed to elucidate this peculiar results.

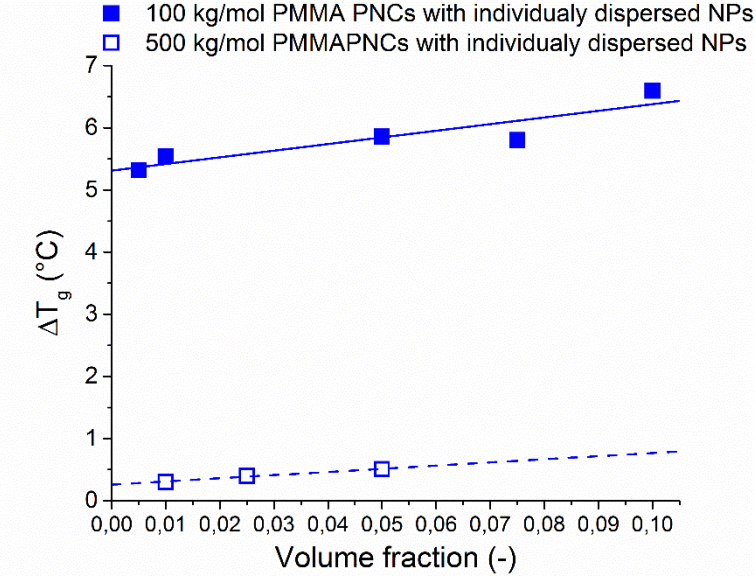

Figure 44: dependence of ΔT_g on volume fraction of PMMA/SiO_2 PNCs with various molecular weight.

Figure 45 shows dependence of reptation time and number of entanglements per one chain on the filler volume fraction in the PMMA/SiO_2 with various matrix molecular weight and tacticity. Much greater increase of these properties was found in the case of higher molecular weight matrix. One possible reason is the stronger NP–polymer interaction of isotactic PMMA chains[105, 106] contained in greater amount in the 500 kg/mol PMMA matrix. Another possible explanation could lie in the presence of bridging chains. This effect is more probable for the 500 kg/mol PMMA matrix due to smaller interparticle distance to R_g ratio.

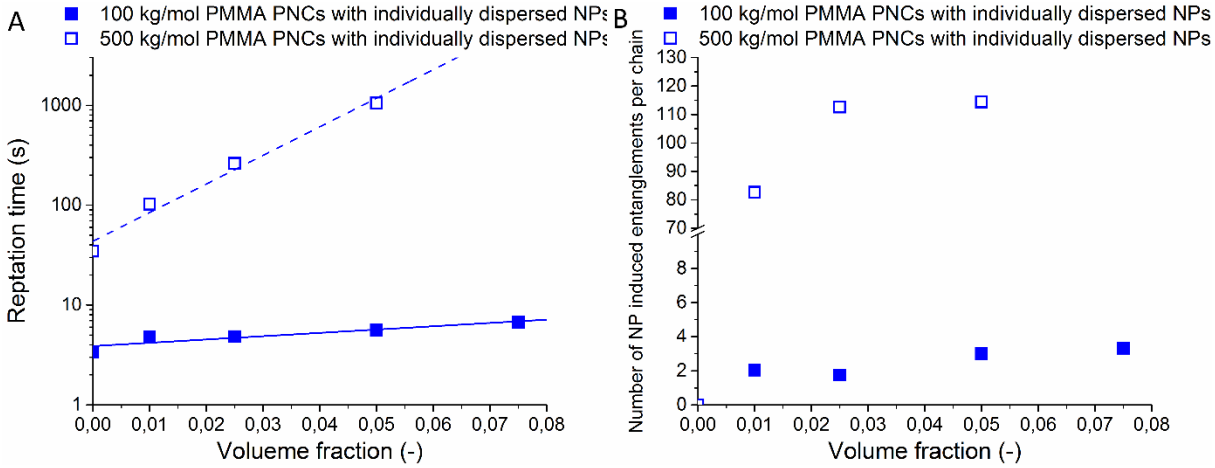

Figure 45: (A) Dependence of reptation time and (B) number of NP induced entanglements per one chain on volume fraction of PMMA/SiO_2 PNCs with various molecular weight and tacticity.

Table 7: Glass transition temperature, T_g, reptation time, τ_{rept}, plateau modulus, G_0^N, modified matrix plateau modulus, $G_{0\,matrix}^N$, and number of entanglements per one chain, N_{ent}, of 500 kg/mol PMMA/colloidal SiO_2 PNC with individually dispersed NPs.

Sample	T_g (°C)	τ_{rept} (s)	G_0^N (MPa)	$G_{0\,matrix}^N$ (MPa)	N_{ent} (-)
PMMA/colloidal SiO_2 with 500 kg/mol matrix					
1 vol. %	122.5	102.0	1.66	1.61	87.5
2.5 vol. %	122.6	261.8	2.328	2.17	117.6
5 vol. %	122.7	1052.6	2,56	2.21	119.4

PMMA/colloidal SiO_2 was taken as the model system. This system was fully described in previous chapters. Strong interactions were expected due to possible polar interactions and hydrogen bonding[55]. Enhancement of the relaxation properties was ascribed to the immobilization of NP surrounding segments. Fumed silica has the same functional groups as colloidal silica. Only difference is the effective surface because PMMA/fumed SiO_2 PNCs included 70 nm fused strings of primary particles. This reduced their effective surface significantly. The PMMA/1 vol. % fumed SiO_2 with of NPs fitted nicely into dependence of ΔT_g on the interface surface area (Figure 46A, Table 8). It confirmed the key role of immobilization.

Gradual decrease of the ΔT_g with dispersion state worsening was found in PMMA/1 vol. % AZO (Figure 46B, Table 8). The T_g decreased in the same manner as in PMMA/ SiO_2, but overall increase of T_g was smaller. It confirmed weaker particle–polymer interactions between the AZO NPs and the PMMA chains compared to the SiO_2 NPs and PMMA chains. As discussed in previous chapters, AZO particles have amphoteric character, therefore, they are less acid and interact weaker with basic PMMA chains.

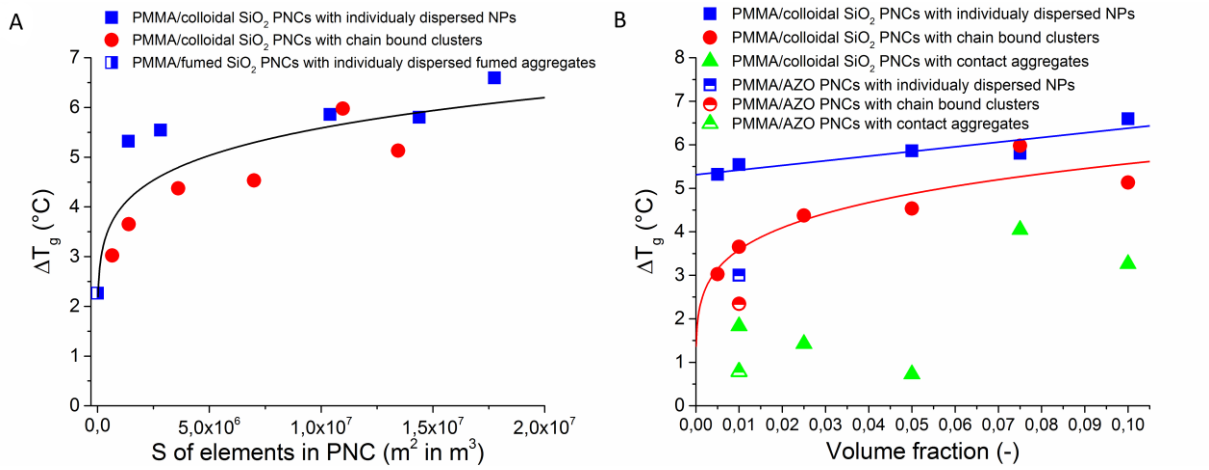

Figure 46: (A) Dependence of the ΔT_g on surface area of elements in PMMA filled with colloidal and/or fumed SiO_2. (B) Dependence of ΔT_g on volume fraction of PMMA colloidal SiO_2 and PMMA/AZO PNCs.

Table 8: Glass transition temperature, T_g, of PMMA/fumed SiO_2 with individually dispersed fumed aggregates of primary particles and PMMA/AZO PNCs with 1 vol. % of NPs and various NP spatial organization.

Sample	T_g (°C)
PMMA/fumed SiO_2 PNC with individually dispersed fumed aggregates of primary particles	
1 vol. %	114.4
PMMA/AZO PNC with individually dispersed NPs	
1 vol. %	115.2
PMMA/AZO PNC with chain bond clusters	
1 vol. %	114.5
PMMA/AZO PNC with contact aggregates	
1 vol. %	112.9

Weak increase of T_g was found for the PS/1 vol. % SiO_2 (Figure 47, Table 9). The ΔT_g of the PS/SiO_2 PNC was compared with ΔT_g of PMMA/SiO_2 PNCs prepared from the same solvent (THF). Both composites consist of contact NP aggregates formed by depletion attraction, but the PMMA/SiO_2 contained also individually dispersed NPs. Greater increase of the T_g for the PMMA/SiO_2 was caused by both higher effective interface area and stronger interactions between PMMA–SiO_2. Only weak dipole–dipole interactions are expected in PS/SiO_2.

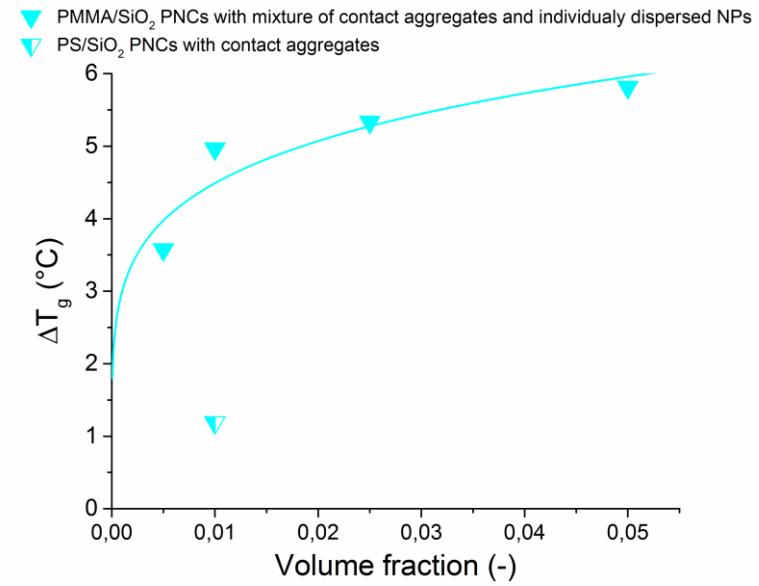

Figure 47: Dependence of ΔT_g on volume fraction of PMMA and PS colloidal SiO_2 PNCs.

Table 9: Glass transition temperature, T_g, of PMMA/colloidal SiO_2 with mixture of contact aggregates and individually dispersed NPs and PS/colloidal SiO_2 with contact aggregates.

Sample	T_g (°C)
PMMA/colloidal SiO_2 with mixture of contact aggregates and individually dispersed NPs	
0.5 vol. %	115.7
1 vol. %	117.1
2.5 vol. %	117.5
5 vol. %	118.0
PS/colloidal SiO_2 PNC with contact aggregates	
1 vol. %	95.1

5.3 Mechanical properties of polymer nanocomposites

Added NPs alter the dynamics of the surrounding polymer matrix as described above. It can lead to change of stiffness, yield and post-yield behavior.

Mechanical properties of neat matrices were measured first. Figure 48 shows tensile results of neat PMMA matrix measured at three temperatures of 60, 70, and 80 °C and in a range of strain rates spanning four orders of magnitude. The PMMA matrix showed brittle response at 60 °C. Mechanical response of the neat PMMA at 70 °C was characteristic by presence of two brittle regions at high and low strain rates. Ductile response was found in the whole strain rate range of the PMMA results measured at 80 °C. Yield stresses were extracted from the data and plotted against logarithm of strain rate. Dependence of yield stress on logarithm of strain rate showed that pure PMMA followed ductile flow deformation mode even when some results were macroscopically brittle. The dependence of yield stress on strain rate could be fitted by two lines with a crossover around strain rate of 10^{-3} s^{-1}. PMMA is rheological complex liquid, therefore the two regions were obtained. Pronounced β relaxation is very close to α relaxation in PMMA influencing its relaxation and mechanical behavior in large experimental range [135-144]. The lower strain rate line belongs to α response and the high strain rate line is assigned to $\alpha + \beta$ response. Polycarbonate is rheological simple liquid because α and β relaxation are well separated and β relaxation is weak and located far below room temperature (≈ –100 °C)[143, 145-147]. It is possible to obtain contribution of β relaxation in PC mechanical results but only at low temperatures and high strain rates[147]. Performed experiments on PC were far from this region, therefore no influence of β relaxation on PC data is assumed. Results of Young modulus and yield stress of investigated matrices measured in tension at temperature of T_g – 35 °C and strain rate of 10^{-2} s^{-1} are shown in Table 10.

Table 10: Young modulus and yield stress of investigated matrices measured in tension at temperature of T_g – 35 °C and strain rate 10^{-2} s^{-1}.

Matrix	E (GPa)	σ_y (MPa)
100 kg/mol PMMA	1.4	31.0
500 kg/mol PMMA	1.5	31.5
PC	2.1	41.1

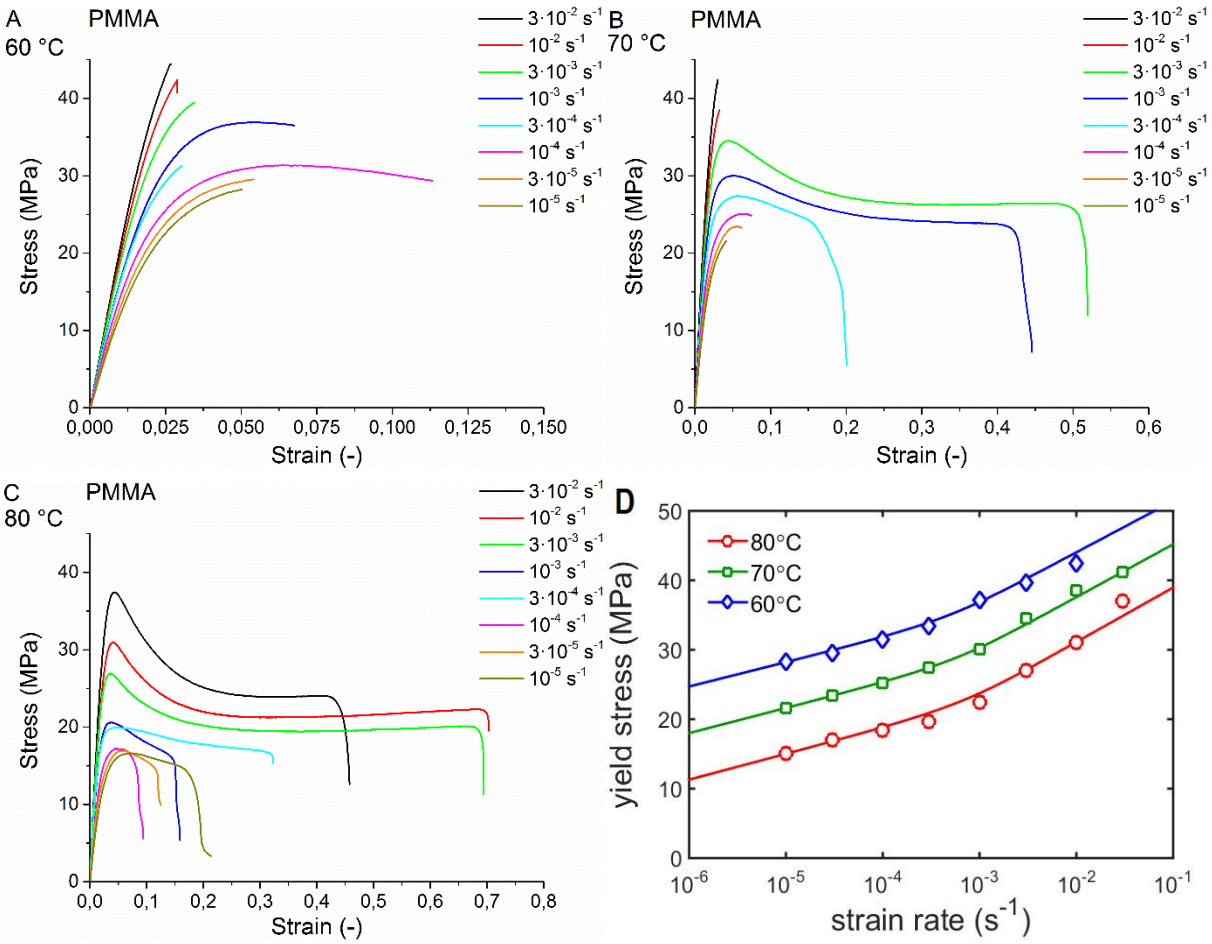

Figure 48: Tensile curves of 100 kg/mol PMMA measured at (A) 60 °C, (B) 70 °C, (C) 80 °C and various strain rates, respectively. (D) Dependence of yield stress on strain rate for various temperatures fitted by Ree-Eyring equation[142, 148-150].

Long term mechanical behavior of the neat PMMA matrix was investigated by creep measurements. Creep curves and dependence of stress on time to failure the PMMA matrix are displayed in Figure 49. Creep curves with presence of all three regimes of creep response and Linear dependence of stress on time to failure indicate ductile flow deformation mode at measured conditions.

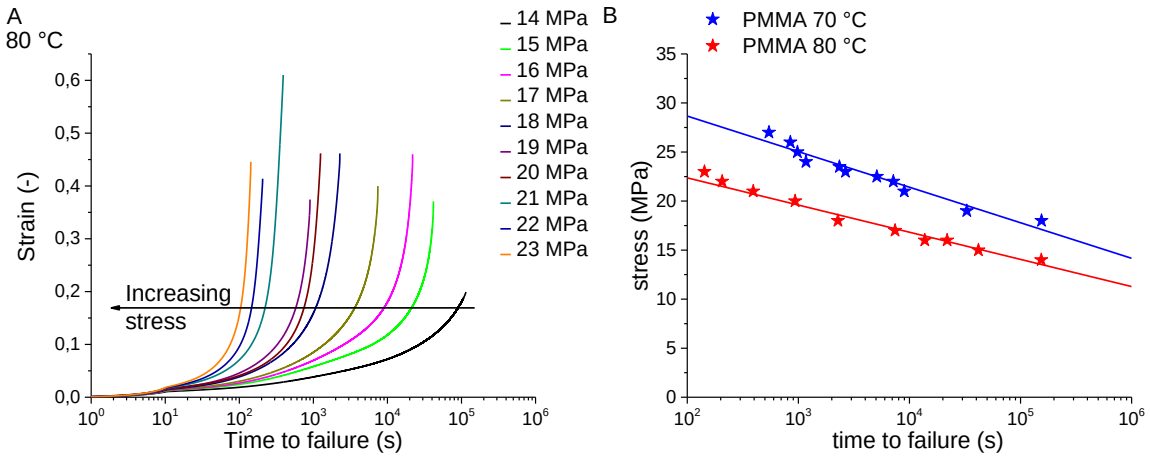

Figure 49: (A) Creep curves of 100 kg/mol PMMA measured at 80°C and various stresses and (B) dependence of stress on time to failure of 100 kg/mol PMMA at 70 and 80 °C.

Considering a different deformation of the polymer chains in bulk matrix, in the vicinity of NPs, and in the inner structure of clusters, PNCs can exhibit a complex macroscopic response consisting of these contributions. Mechanical properties of PMMA/SiO_2, exhibiting the three different nanostructures were investigated (Figure 50). All samples showed ductile deformation response at 80 °C. The crossover between α and $\alpha + \beta$ regime remained localized near the strain rate of 10^{-3} s^{-1}. PNCs with individual NPs exhibited the most pronounced increase of the yield stress, aggregates the lowest, and clusters lied between them. Moreover, slopes of yield stress-strain rate dependence and related activation volumes did not change compared to the neat PMMA. Quite different situation was found at 60°C, Figure 51. While the neat PMMA was macroscopically brittle, it still followed the ductile yielding regime whereas embrittlement of PNCs with aggregates was so extensive that they did not follow ductile yielding regime. PNCs with clusters followed ductile yielding with different slope of yield stress–strain rate dependence compared to the neat PMMA. Moreover, the response was macroscopically ductile at certain strain rates, possibly due to the hierarchical nature of clusters. Clusters can represent structured inclusions yielding hierarchical composite endowing both intrinsic and extrinsic deformation processes to become active.

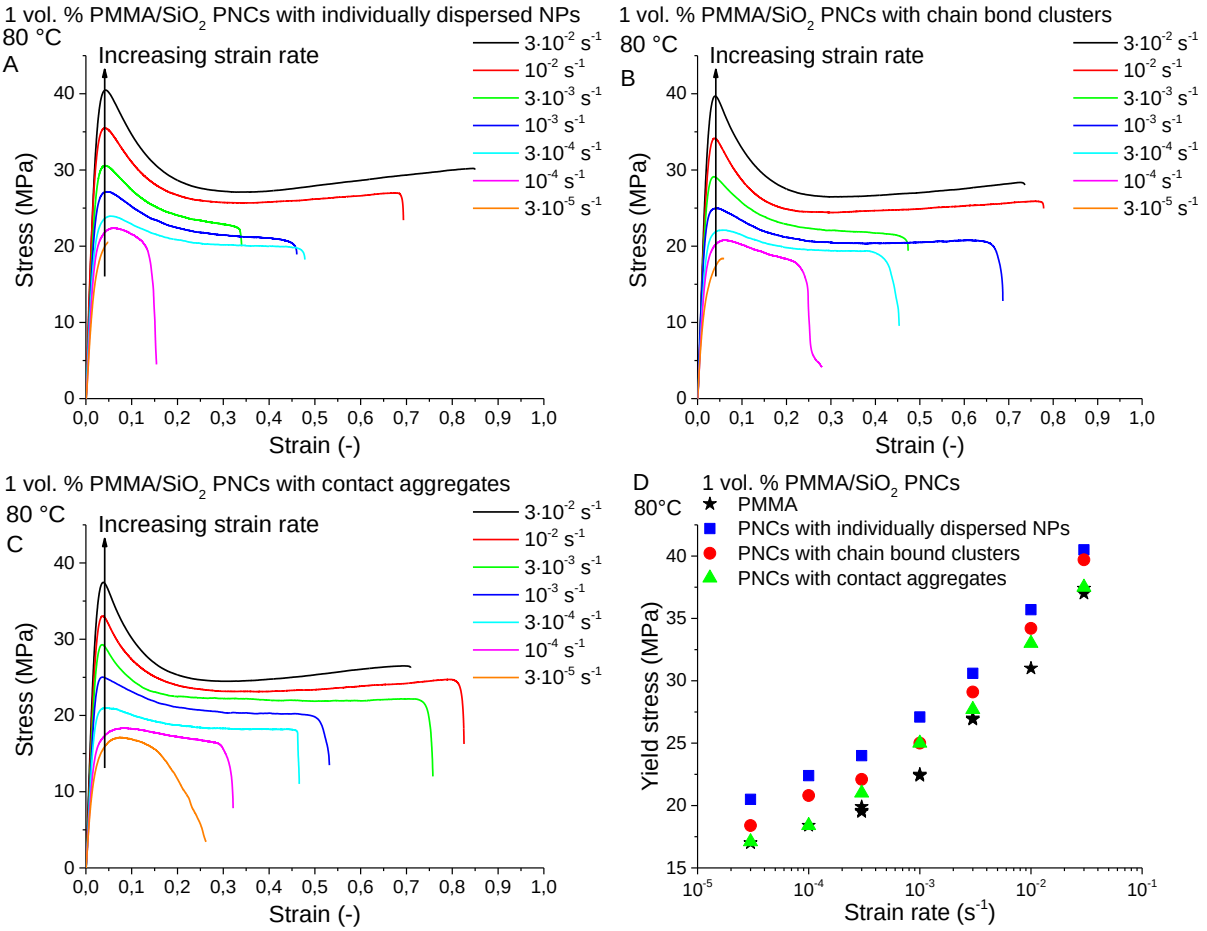

Figure 50: (A, B,C) Tensile curves of 1 vol. % PMMA/SiO_2 PNCs with various nanostructures at 80 °C and various strain rates and (D) their yield stress–strain rate dependence compared with neat PMMA matrix.

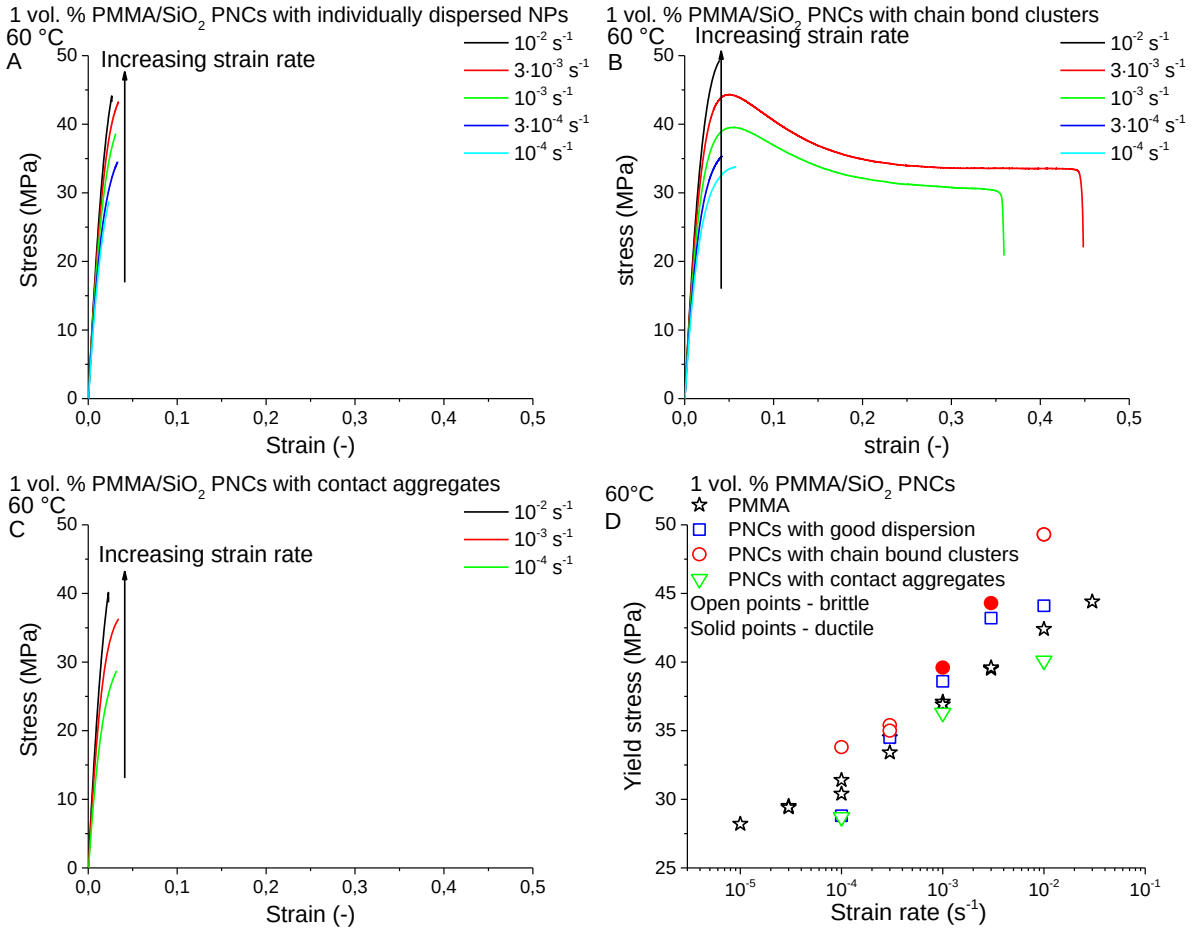

Figure 51: (A, B, C) Tensile curves of 1 vol. % PMMA/SiO_2 PNCs with various nanostructures at 60 °C and various strain rates and (D) their yield stress–strain rate dependence compared with neat PMMA matrix.

Dependence of the yield stress on the strain rate for the PMMA with 2.5 and 5 vol. % NPs is shown in Figure 52A and B, respectively. Differences between the various NP spatial organizations were less pronounced that at 1 vol. % and the position of the crossover between α and $\alpha + \beta$ regime has not changed. However, at 5 vol. % NPs, PNCs with contact NP aggregates became brittle at strain rates above 10^{-3} s^{-1} and strain rate dependence of yield stress failed to follow the ductile yielding regime at higher strain rates. Origin of this behavior lies probably in presence of sub-micro contact aggregates that could act as crack promoters due to weak particle-particle interactions. Strain rate dependence of the yield stress for PMMA/5 vol. % SiO_2 with individually dispersed NPs was locked in the a+β regime in the range of strain rates measured. It suggests range change of responsible chain dynamics.

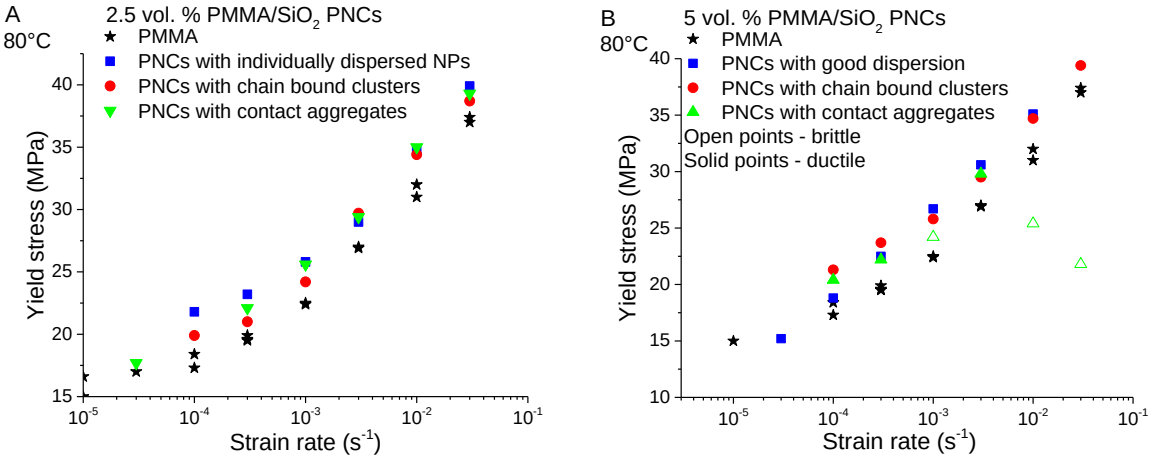

Figure 52: Dependence of yield stress on strain rate of PNCs with various NP spatial organizations and volume fraction of (A) 2.5 and (B) 5 vol. % measured in tension at 80 °C, respectively.

Dependence of the yield stress on the NP volume fraction for PNCs with various NP spatial organizations is shown in Figure 53. Basically, there are three types of the composition dependences of the yield stress for composites. Firstly, a decrease of yield stress was reported in systems with no adhesion due to the absent load transfer to the filler and the total load being carried only by the matrix. Yield stress then depends on the load bearing cross-section that is reduced by the filler particles. The yield stress of composite with no adhesion can be described by the modified[91] Nicolais–Narkis model[151, 152]:

$$\sigma_{yc} = \sigma_{ym} \frac{1-\varphi}{1+2.5\varphi}, \tag{8}$$

where σ_{yc} is the composite yield stress, σ_{ym} the matrix yield stress, φ the volume fraction, and 2.5 comes from geometric arrangement of spheres in the cross-section area[92]. Secondly, no change of the yield stress is expected for the composites with perfect adhesion and small surface area or no specific interaction that could change the matrix properties. Thirdly, the increase of the composite yield stress with increasing filler volume fraction was described by Pukanszky[91-94]. It was found that incorporation of fillers with large surface and good interaction with matrix can modify mechanical properties of the surrounding matrix. This effect is described by the *B* parameter in the Pukanszky model[91-94]:

$$\sigma_{yc} = \sigma_{ym} \frac{1-\varphi}{1+2.5\varphi} \exp(B\varphi), \tag{9}$$

The *B* parameter depends on the filler interfacial area, strength of particle–polymer interactions, and thickness of the influenced matrix. The nanocomposite yield stress was found to increase compared to the neat matrix in all PNCs investigated with the only exception of 5 vol. % PNC with contact aggregates which supports the presence of attractive interactions in nanosilica–PMMA assumed earlier. The strongest enhancement of the yield stress was found for PNCs with individually dispersed NPs due to the highest effective surface area. Yield stress stagnation

between 1 and 5 vol. % of NPs can be explained by gradual aggregation – a decrease of the effective surface area as suggested by Dorigato et.al[90]. However, similar situation was found for a clustered system, where no aggregation was observed. A possible explanation could be a saturation – majority of chains are influenced by NPs even at low filler volume fraction; therefore, no further increase of the yield stress was found. Quite different behavior was found for PNCs with contact aggregates. Dependence of the yield stress on the filler volume fraction of PNCs with contact aggregates can be fitted with the Pukanszky model up to 2.5 vol. % with interaction parameter B = 8. Further increase of volume fraction led to a sharp decrease of the yield stress. Extensive aggregation caused the presence of critical defects; therefore 5 vol. % PNC with contact aggregates had macroscopically brittle response and its yield stress fitted well to the modified Nicolais–Narkis model.

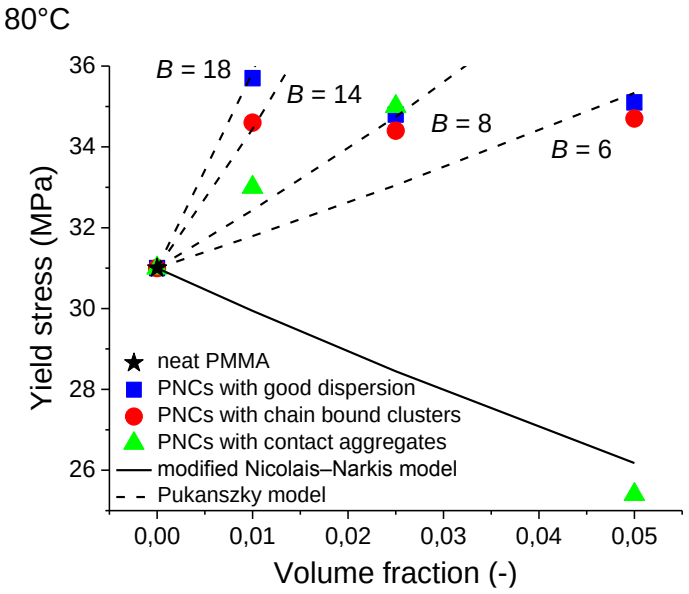

Figure 53: Dependence of yield stress on volume fraction of PNCs with various NP spatial organizations at 80°C and strain rate of 10^{-2} s^{-1}. Solid line shows the modified Nikolais Narkis model[92, 151]. Dash lines shows the Pukanszky model[92] with various values of interaction parameter B.

Significant enhancement of elastic modulus was found near the glass transition. In the glassy state, relaxation time difference between the affected and bulk chains is not as pronounced as in the rubbery state[16], but the affected chains could exhibit a different path through the vitrification process during cooling, resulting in a different position on the energy landscape[68]. The dependence of the elastic modulus behaved similarly to the above discussed plateau modulus. The existing volume replacement continuum mechanics models[153-155] for the composition dependence of the elastic modulus were not able to describe the dependence of the relative modulus on the NP volume fraction (Figure 54A). An additional segmental scale reinforcing mechanism characterized by the composite modulus reduced to the matrix modulus and appropriate continuum micromechanics model were proposed to be directly related to the

interfacial area[87]. An important structural difference was found when this reinforcing mechanism was related to the total interfacial area (Figure 54B). The initial increase of the elastic modulus at low concentrations was much more pronounced for individually dispersed NPs compared to chain bound clusters. The elastic modulus of individually dispersed NPs tend to slightly decrease or stagnate with the increasing interfacial surface (volume fraction) up to about 10^7 m^2/m^3 (5 vol. %), where it becomes overpowered by a rapid growth. Clusters exhibited modulus stagnation up to $3 \cdot 10^6$ m^2/m^3 (2.5 vol. %) followed by gradual modulus increase. As suggested by the simulation of Long, et al.[131, 132], the strong increase might be caused by the percolation of the immobilized domains around the NPs due to the weakly worsening dispersion state and filler morphology. This overwhelmed dependence on the interfacial surface lead to a conclusion that NPs assembled into close-packed clusters experience a significant contribution of the internal structure to macroscopic properties originating from the highly affected bridging chains inside the clusters and also from the inter-cluster percolation at higher volume fractions.

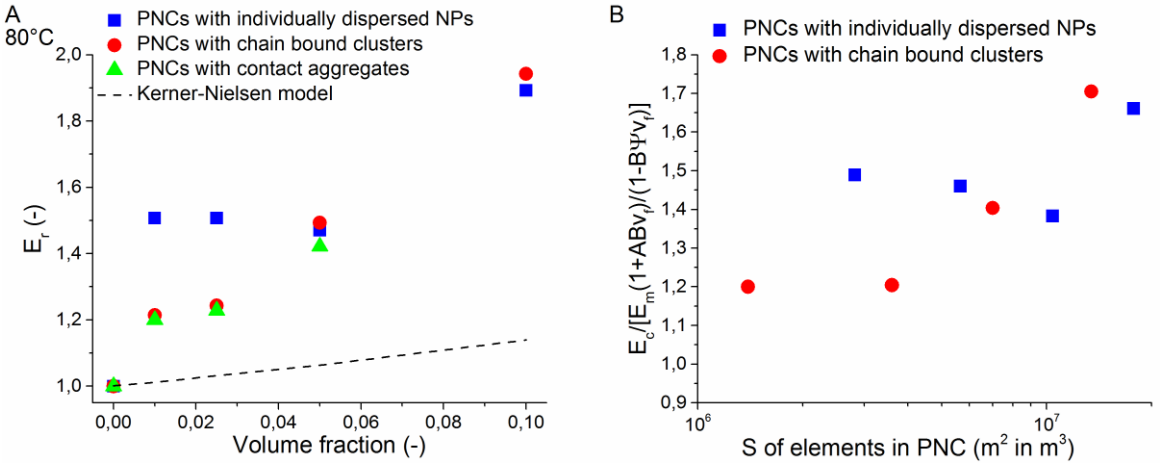

Figure 54: Dependence of relative elastic modulus on (A) volume fraction and (B) elastic composite modulus reduced to the matrix modulus and appropriate continuum micromechanics model on surface of elements in PNC with various NP spatial organization measured in tension at temperature of 80 °C and strain rate of 10^{-2} s^{-1}.

Good durability performance is a critical parameter of a high-end material design. Long-term mechanical response was investigated on various nanocomposites[156-159]; nevertheless, the fundamental effect of the NP organization has still been missing. Therefore, long-term creep behavior of 1 vol. % PNCs were compared with neat PMMA matrix, Figure 55. Different long-term response was found for different NP spatial organizations. PNCs with individually dispersed NPs showed a shift of more than one order of magnitude to longer failure times with the same slope of the dependence as for the neat PMMA, while PNCs with clusters and aggregates were shifted to shorter times and steeper slope suggesting a different mechanism of the long-term response for different NP spatial organizations.

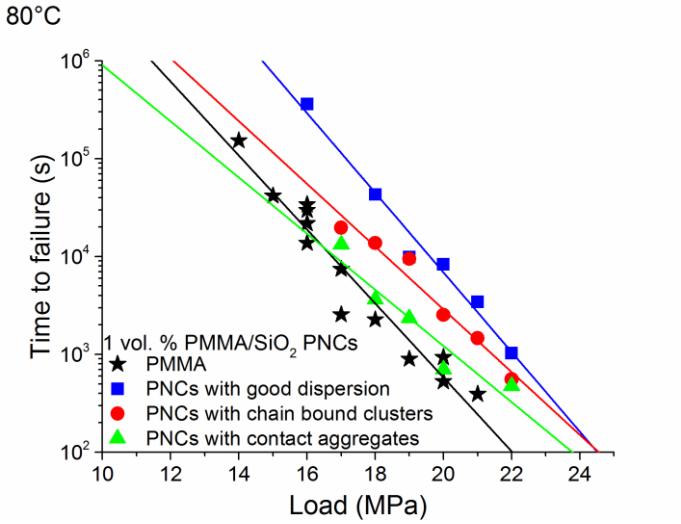

Figure 55: Dependence of time to failure on load of neat PMMA matrix and PNCs with various NP spatial organizations measured in tensile creep at 80 °C.

Neat PMMA and PMMA/5 vol. % SiO_2 with individually dispersed NPs were measured in compression at true stress–true strain conditions to investigate the effect of NPs on the intrinsic deformation behavior. Deformation curves and strain rate dependence of the yield stress, lower yield stress, yield drop, and strain hardening modulus are shown in Figure 56. The crossover between α and $\alpha + \beta$ regime was observed near the strain rate of 10^{-3} s^{-1} for both the neat PMMA and the 5 vol. % PNC with individually dispersed NPs. Both the upper and the lower yield stress of PMMA/5 vol. % SiO_2 were enhanced compared to the neat PMMA. The yield stress enhancement was caused by NP altered chain packing and dynamics. Strain softening responsible for localization phenomena in polymer glasses[143, 160-162] can be characterized by the yield drop – difference between upper and lower yield stress. Three different yield drop regions can be find in complex polymer liquids dependent on strain rate and temperature variation of α and β processes of the upper and the lower yield dependences[143]. The yield drop of the neat PMMA and the PMMA/5 vol. % SiO_2 increased with strain rate in the measured region. It suggests that II region controls the response, where the upper yield stress is governed by the both α and β processes, whereas the lower yield stress is only controlled by the α process. The region II with non-constant strain rate dependence of the yield drop lies between I and II regimes with constant strain rate dependence. Upper and lower yield stresses are controlled with the same α or $\alpha + \beta$ processes in these regions[143]. The yield drop of the 5 vol. % PNC differed slightly from the neat PMMA. Smaller yield drop of PNC could be caused by the enhanced liquid like disorder and packing frustration of NP affected polymer matrix[89]. It could significantly alter the density fluctuations in PNCs, which are responsible for the yielding response according to the polymer nonlinear Langevin equation (PNLE) model[163-166]. Enhancement of the strain hardening modulus of 5 vol. % PNC compared to the neat PMMA was significant. The enhancement of the yield stresses and the strain hardening modulus is related to the increase of energy required to activate the rearrangement of polymer segments that were influenced by NPs.

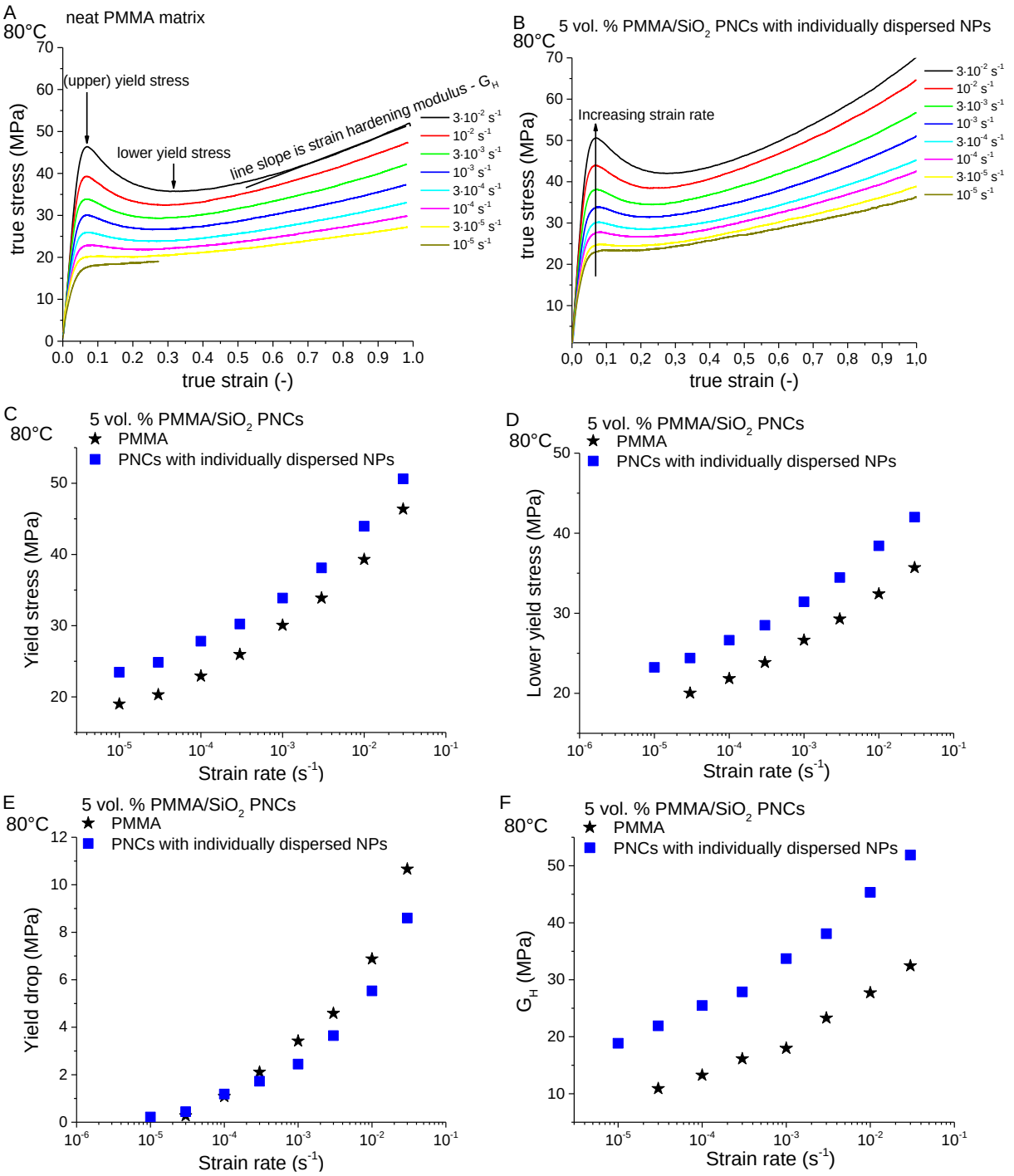

Figure 56: Dependence of true stress on true strain of (A) neat PMMA matrix and (B) PNCs with individually dispersed NPs with volume fraction of 5 vol. % measured in compression at 80°C and various strain rates. Dependence of (C) upper and (D) lower yield stress, (E) yield drop, and (F) strain hardening modulus on strain rate of neat PMMA matrix and PNCs with individually dispersed NPs with volume fraction of 5 vol. % measured in compression at 80°C.

The dependence of the yield stress on the strain rate of the PMMA matrix and the 5 vol. % PNC with individually dispersed NPs measured at various temperatures was fitted with the Ree-

Eyring equation[142, 148-150] (Figure 57). The Ree-Eyring model[142, 148-150] was developed to describe thermally activated processes with more contributions:

$$\sigma_y = \left[\frac{kT}{V_\alpha^*} sinh^{-1}\left(\frac{\dot{\varepsilon}}{\varepsilon_\alpha} exp\frac{\Delta U_\alpha}{RT}\right)\right] + \left[\frac{kT}{V_\beta^*} sinh^{-1}\left(\frac{\dot{\varepsilon}}{\varepsilon_\beta} exp\frac{\Delta U_\beta}{RT}\right)\right], \quad (10)$$

where k is the Boltzmann constant, T the temperature, V^* the activation volume, ε the pre-exponential factor dependent on the thermomechanical history, $\dot{\varepsilon}$ the strain rate, ΔU the activation energy, and R the universal gas constant. Activation volumes and energies calculated from the Ree-Eyring equation are listed in Table M2. The determined activation volumes and energies for the neat PMMA are in good accordance with the literature[88, 89, 142, 143, 150]. Results obtained showed the different influence of NPs on the α and β process. Whereas the more local β process seems to be unchanged by NPs, the more cooperative α process exhibited an increase of both the activation volume and energy. It suggests that NPs affect preferably or in greater amount the chain dynamic at longer time and length scales. It could lead to a conclusion that the frustrated layer between the immobilized and bulk chains has a greater impact on the large strain deformation behavior than the immobilized layer at interface. The results are in good accordance with the literature[88] which confirm the pronounced effect of polymer–NP interactions on the α process involving the entire backbone chain compared to the β process presumably involving only few segments[135, 136, 139-141, 167].

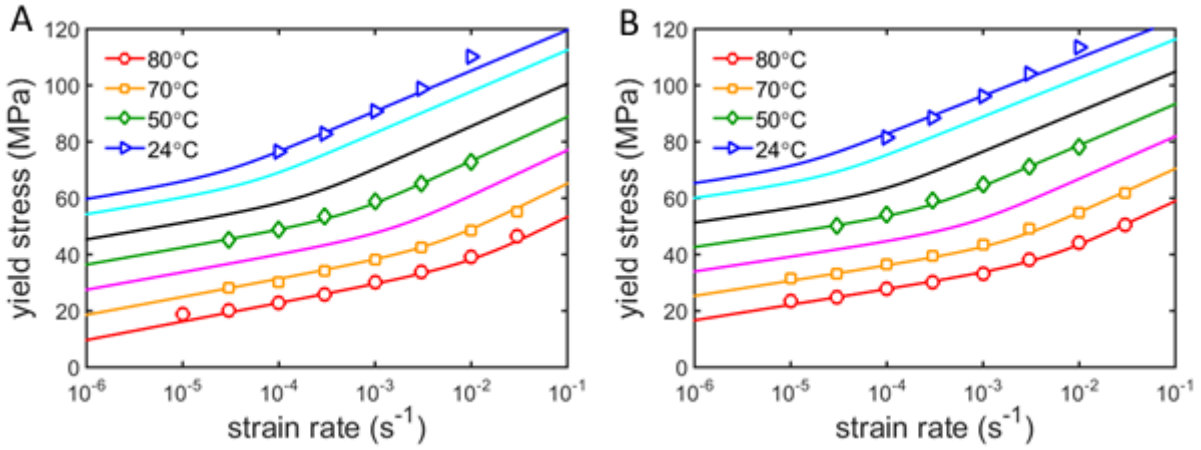

Figure 57: Dependence of yield stress on strain rate fitted by Ree-Eyring equation of (A) neat PMMA matrix and (B) 5 vol. % PNCs with individually dispersed NPs.

Table 11: Activation volumes and energies of pure PMMA matrix and 5 vol. % PNCs with individually dispersed NPs calculated by Ree-Eyring equation (Equation 10).

Sample	V_α^* (nm^3)	ΔU_α (kJ·mol^{-1})	ε_α (s^{-1})	V_β^* (nm^3)	ΔU_β (kJ·mol^{-1})	ε_β (s^{-1})
PMMA	1.71	334	$1.70 \cdot 10^{42}$	1.06	93.9	$1.49 \cdot 10^{12}$
5 vol. % PNC with individual NPs	2.03	395	$5.61 \cdot 10^{49}$	1.07	91.2	$2.47 \cdot 10^{11}$

The dependence of the relative composite modulus on the filler volume fraction was similar for both of the investigated molecular weights (Figure 58A) while more enhanced yield stresses were found for PNCs with the higher molecular weight (Figure 58B). It suggests that higher molecular weight and different tacticity had a minor influence on the nanocomposite stiffness while the yielding process was more affected. A single *B* parameter of the Pukanszky model cannot describe the increase of the yield stress with increasing filler volume fraction suggesting a worsening dispersion state or saturation. In the case of the higher molecular weight, the less pronounced decrease of the *B* parameter suggested stronger interactions or better dispersion state durability.

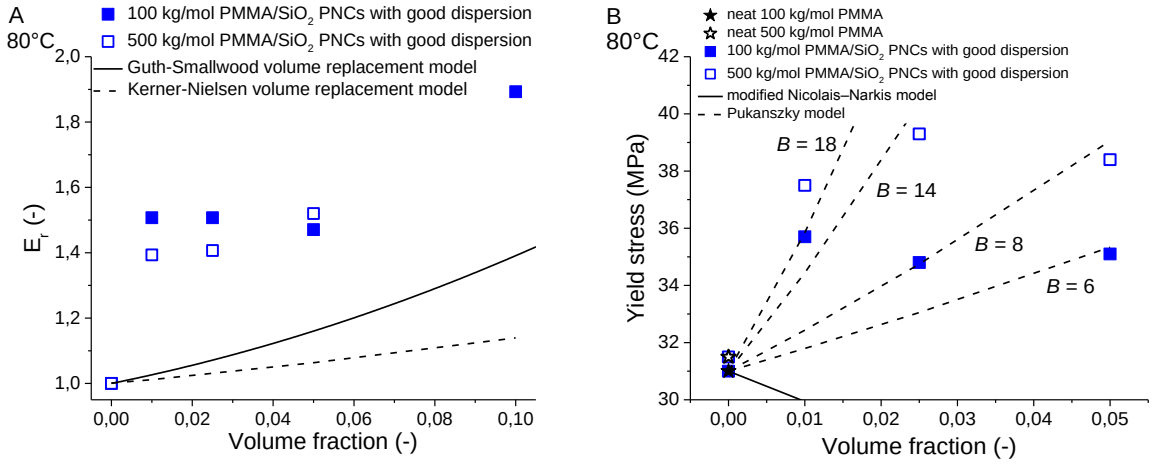

Figure 58: Volume fraction dependence of (A) relative composite modulus and (B) yield stress of PMMA/SiO_2 PNCs with two various molecular weights.

Significant relative modulus enhancement of PMMA/AZO PNCs against the volume replacement continuum mechanics models[74-76, 153-155] was found similarly with PMMA/SiO_2 PNCs (Figure 59A). The nanostructure dependent trend of enhanced properties with improved dispersion state was maintained also in PMMA/AZO system. Difference of relative modulus was significant between SiO_2 and AZO NPs filled PNCs with individually dispersed NPs, but other dispersion states had almost identical values of relative modulus. The difference in mechanical properties between PMMA SiO_2 and AZO NPs was caused by the different interaction strength between used NPs and matrix. Relative moduli of PMMA and PC filled by colloidal nanosilica organized into mixture of contact aggregates and individually dispersed NPs were compared (Figure 59B). The enhancement of the relative modulus was less pronounced for PC compared to PMMA matrix due to the weaker NP–polymer interaction strength. Although PC–SiO_2 interactions were weaker than PMMA–SiO_2, they still sufficed to induce a significant immobilization that changed the molecular packing and dynamics of the NP-surrounding matrix and cause the volume replacement continuum models[74-76, 153-155] unable to describe the dependence of the relative modulus on the filler volume fraction.

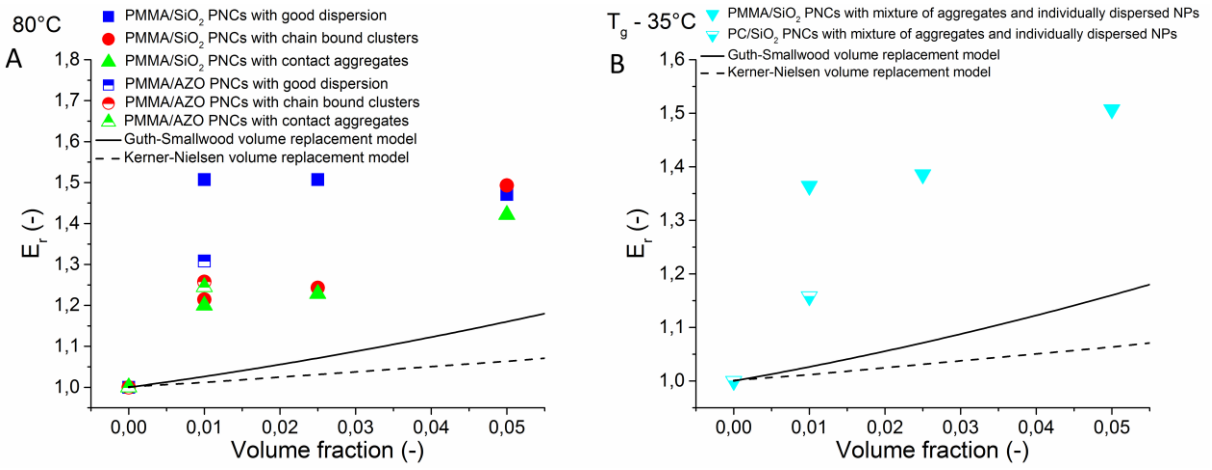

Figure 59: Dependence of relative modulus on volume fraction of (A) PMMA SiO_2 and AZO PNCs at 80 °C and (B) PMMA and PC SiO_2 PNCs at T_g – 35 °C.

5.4 Correlation between relaxation and mechanical properties

The enhancement of the yield stress by NPs introduced into the polymer matrix was reported in previous chapters (Figure 60A). The yield stress was reduced to the distance from the glass transition temperature ($T_g - T$) to further investigate this phenomenon (Figure 60B). It was found that the strain rate dependence of the reduced yield stress of the neat PMMA matrix and PNCs converged into a single curve. It suggests that the distance from the glass transition distance controls the investigated yield behavior. Chains were further from its T_g in PNC than in PMMA matrix, occupying a different location in energy landscape, when measured at a single temperature. NPs significantly altered the packing and dynamics of the surrounding chains compared to the bulk. A similar effect of NPs on the glass transition temperature and yield stress showed that the dynamics responsible for the vitrification process is crucial also in the yielding phenomenon operating at the same length and time scale.

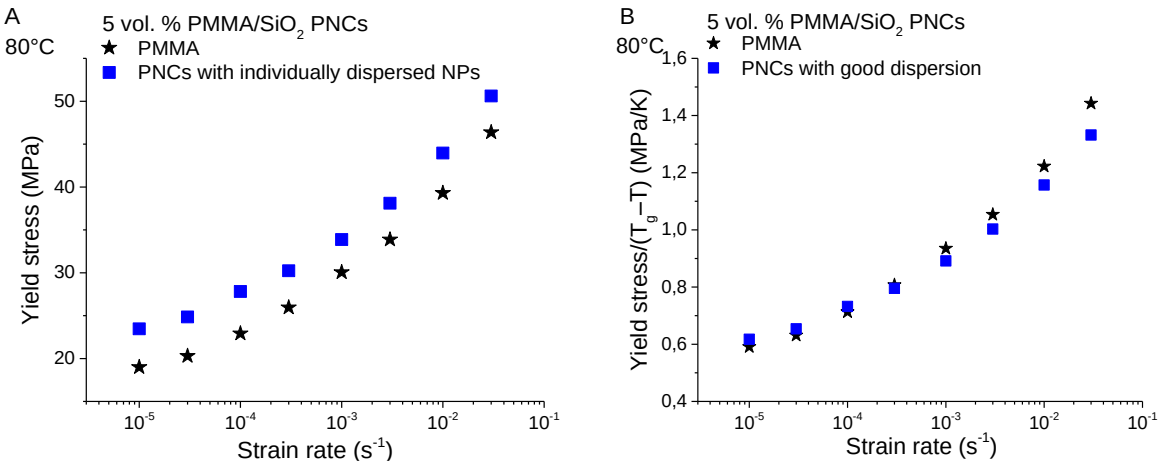

Figure 60: Dependence of (A) yield stress and (B) yield stress reduced to distance from glass transition temperature on strain rate of PMMA matrix and 5 vol. % PMMA/SiO_2 PNCs with individually dispersed NPs measured in compression at 80 °C.

The pronounced increase of the strain hardening modulus of PNCs with individually dispersed NPs compared to the neat PMMA matrix was also reported in previous chapters (Figure 61A). Strain hardening modulus was reduced to the distance from the glass transition ($T_g - T$) similarly as in the previous case, but no convergence of the PNC and the matrix strain rate dependence was found (Figure 61B). It means that the dynamics at strain hardening regime is not similar with the local segmental dynamics responsible for glass transition. The strain hardening modulus was also reduced to the number of entanglements per one chain (Figure 61C) which caused the PNC and the neat matrix data converged into a single curve. NPs act as entanglements attractors altering the polymer dynamics in plateau region. The results suggests that the dynamics responsible for the strain hardening response lies in the same time and length scale as the dynamics in the plateau region.

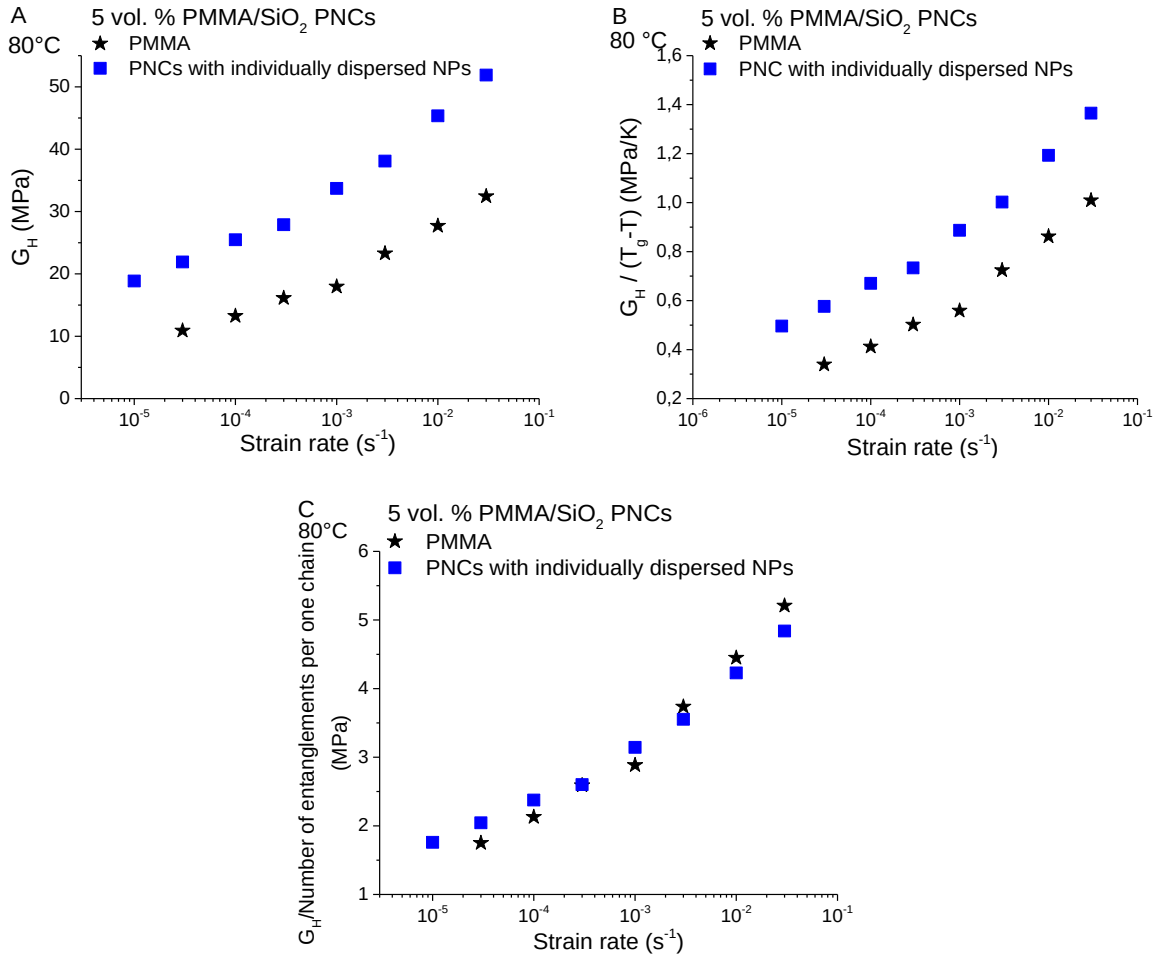

Figure 61: Dependence of (A) strain hardening modulus, (B) strain hardening modulus reduced to distance from glass transition, and (C) strain hardening modulus reduced to number of entanglements per one chain on strain rate of neat PMMA matrix and 5 vol. % PMMA/SiO_2 PNCs with individually dispersed NPs measured in compression at 80 °C.

6. Conclusions

Nanostructure control, relaxation and mechanical properties of nanocomposites with polymer glass matrix and ceramic nanoparticles were investigated. A deep investigation was performed on PMMA/SiO_2 model system and subsequently broadened to systems with another matrices and NPs to generalize the obtained results. First, a method enabling to control the NPs spatial organization was devised. Subsequently, properties of polymer nanocomposites with governed dispersion state were investigated. Relaxational and mechanical properties of PNCs with precisely determined nanostructure were determined to provide valuable data characterizing this promising class of materials. Furthermore, NPs were utilized as probes that affect molecular packing and dynamics of polymer chains. The determined relaxational and mechanical properties were linked to provide information about the molecular processes behind deformation response of polymer glasses and their nanocomposites.

Polymer nanocomposites with controlled NP dispersion state were prepared by solution blending technique with fast solvent evaporation. Individually dispersed NPs, chain bound clusters, contact aggregates and mixture of individually dispersed NPs and contact aggregates were identified by TEM and USAXS techniques. Solvent–particle interactions were suggested as the dominant structure governing factor among the complex interplay of particle–polymer–solvent interactions at investigated conditions. The solvent–particle interaction strength was quantified by Drago´s donor-acceptor interaction enthalpy[56-61]. Matrix and solvent had basic character and particle surface functional groups had acidic character. Influence of NP volume fraction on NP dispersion was also investigated. Worsening of dispersion state of individually dispersed NPs was found with increasing volume fraction of NPs due to shortening of the interparticle distance – increase of the particle–particle attractive interaction strength. Phase diagram of acid-base interaction enthalpy dependence on the volume fraction were constructed for the PMMA/SiO_2 model system. Only narrow window for achievement of individually dispersed NPs was found. It was found that the two observed cases of contact aggregates has different origin. The aggregates prepared from a solvent with the highest acid-base interaction enthalpy had the origin in a depletion attraction and thermodynamic character while the aggregates prepared from a solvent with the lowest acid-base interaction enthalpy were formed due to an insufficient solvation of NPs by the solvent and had kinetic character.

Higher molecular weight and change of tacticity improved the dispersion state due to better steric stabilization[51] of longer chains and stronger adsorption of iso form of PMMA onto silica surface[105, 106]. Influence of NP–polymer and NP–NP interactions on final dispersion state was investigated on PNCs with various composition. Influence of various NPs was investigated in PNC with PMMA matrix. It was found that the dispersion state of NPs worsened in the order SiO_2, AZO, and Fe_2O_3 due to the increase of NP–NP interaction strength and decrease of NP–polymer interaction strength. Attractive NP–polymer interactions were mediated by acid–base interactions between acidic NP surface groups and basic PMMA functional groups. Therefore

strength of NP–polymer interactions decreased with the strengthening acidic character of NPs. These results suggest that the NP–polymer interaction strength decreases in the order PMMA, PC, and PS due to the weakening of the polymer´s basic character.

A precise NP spatial organization control brought unique opportunity to study the influence of the PNC nanostructure on the relaxational and mechanical properties independently of the system chemical composition – NP–polymer interaction strength. Systems with individually dispersed NPs enhanced the investigated properties the most followed by systems with chain bound clusters and systems with contact aggregates influenced the properties the least with some exceptions discussed later. Structure-independent correlation between glass transition temperature, reptation time, elastic modulus of PNCs and interfacial area was found. It was found that NPs significantly influence chain behavior in plateau region increasing number of entanglements per chain and therefore act as entanglement attractors. The existing volume replacement continuum mechanics models[74-76, 153-155] for the composition dependence of the elastic and plateau modulus were unable to describe the dependence of the relative modulus on the NP volume fraction. It is a clear evidence for bringing another segment scale reinforcing mechanism into consideration. The results support the immobilization concept, where adsorbed layer of polymer segments on NP surface and the surrounding frustrated layer of polymer chains are assumed. The adsorption of polymer segments onto the particle surface increased their hydrodynamic size that influenced the viscosity of PNCs melts. The adsorption coefficient was found to be the highest in PNCs with individually dispersed NPs and the lowest in PNCs with contact aggregates due to the effective surface area. PNCs with chain bound clusters showed the highest particle interaction coefficient due to strong interactions of particles in closely packed clusters mediated by the adsorbed chains. Although PNCs with individually dispersed NPs showed the most pronounced increase of the yield stress in the ductile flow controlled regime, the macroscopically ductile response broadened to lower temperatures and over larger range of strain rates in PNCs with chain bound clusters due to their hierarchical nature. Structure-related differences were found in long term mechanical properties. Structure-related differences were also found in the long term mechanical properties such that PNCs with individually dispersed NPs, in contrast with the other NP organizations, significantly improved the time to failure compared to the neat PMMA matrix.

Greater enhancement of reptation time and plateau modulus was determined for PMMA/SiO_2 PNCs with 500 kg/mol compared to 100 kg/mol matrix. Pronounced NP influence on relaxation properties of 500 kg/mol PNCs in terminal zone was probably caused by stronger adsorption of isotactic PMMA chains[105, 106] contained in greater amount in 500 kg/mol PMMA matrix. Also, larger frustrated layer is expected due to more preferable interparticle distance to polymer coil ratio. Therefore, more entanglements were induced by NPs and chain reptation was significantly slowed down because more chains had to pass through more and larger areas with affected dynamics. Minor influence of molecular weight and tacticity on stiffness was found while pronounced increase of yield stress was found for PNCs with 500 kg/mol PMMA. It suggest

stronger influence of the molecular weight and tacticity on the processes operating at longer time scale.

The greatest enhancement of properties was found for PMMA/SiO_2 system, where moderate-strong interaction are expected due to polar interactions and possible hydrogen bonding. PMMA acts as Lewis base due to its ester side groups. Silica, on the other hand, acts as Lewis acid due to silanol groups onto its surface. The properties were less influenced in the case of AZO NPs due to less acidic character of their surface. Only weak dipole–dipole interactions are expected in PS/SiO_2 PNCs in contrast with PMMA/SiO_2 PNCs, therefore only small influence on final properties was found in PS based PNCs. Properties of PC/SiO_2 PNCs were less enhanced than PMMA/SiO_2 PNCs due to weaker NP–polymer interaction strength.

Different influence of NPs on α and β processes of yielding was found. The more local β process was almost unchanged. Increase of activation volume and energy of the cooperative α process was found. It means that NPs affect preferably or in greater amount the chain dynamic at longer time and length scales. It led to a conclusion that frustrated layer between the immobilized segments and bulk chains has a greater impact on the large strain deformation behavior than surface immobilized layer. Polymer–NP interactions had stronger effect on α process involving the entire backbone compared to β process presumably involving only few segments.

Correlation between relaxational and mechanical properties of PNCs was investigated. It was found that the strain rate dependence of neat PMMA matrix and PNCs converges into a single curve when reduced to the distance from the glass transition temperature. PNC samples were further from its glass transition, occupying a different location in energy landscape, than the neat PMMA matrix when measured at the same temperature. NPs significantly alter packing and dynamics of surrounding chains from the bulk state. A correlation of glass transition temperature and yield stress enhancement showed that the dynamics these processes operate at the same length and time scale. Strain hardening modulus did not correlate with glass transition. It means that dynamics at strain hardening regime is not similar with the local segmental dynamics. Strain hardening modulus was reduced to the number of entanglements per one chain. The PNC and the matrix data converged into a single curve. NPs act as entanglements attractors altering polymer dynamics in the plateau region. The results suggest that the dynamics responsible for the strain hardening response lies in the same time and length scale as the dynamics in the plateau region.

7. References

1.Kao, J.; Thorkelsson, K.; Bai, P.; Rancatore, B. J.; Xu, T. Toward functional nanocomposites: taking the best of nanoparticles, polymers, and small molecules. *Chemical Society Reviews* **2013,** 42 (7), 2654-2678 DOI: 10.1039/c2cs35375j.

2.Wegst, U. G. K.; Bai, H.; Saiz, E.; Tomsia, A. P.; Ritchie, R. O. Bioinspired structural materials. *Nature Materials* **2015,** 14 (1), 23-36 DOI: 10.1038/nmat4089.

3.Nie, Z.; Petukhova, A.; Kumacheva, E. Properties and emerging applications of self-assembled structures made from inorganic nanoparticles. *Nature Nanotechnology* **2010,** 5 (1), 15-25 DOI: 10.1038/nnano.2009.453.

4.Espinosa, H. D.; Rim, J. E.; Barthelat, F.; Buehler, M. J. Merger of structure and material in nacre and bone - Perspectives on de novo biomimetic materials. *Progress in Materials Science* **2009,** 54 (8), 1059-1100 DOI: 10.1016/j.pmatsci.2009.05.001.

5.Wang, J.; Cheng, Q.; Tang, Z. Layered nanocomposites inspired by the structure and mechanical properties of nacre. *Chemical Society Reviews* **2012,** 41 (3), 1111-1129 DOI: 10.1039/c1cs15106a.

6.Yao, H. B.; Fang, H. Y.; Wang, X. H.; Yu, S. H. Hierarchical assembly of micro-/nano-building blocks: bio-inspired rigid structural functional materials. *Chemical Society Reviews* **2011,** 40 (7), 3764-3785 DOI: 10.1039/c0cs00121j.

7.Meyers, M. A.; Chen, P. Y.; Lopez, M. I.; Seki, Y.; Lin, A. Y. M. Biological materials: A materials science approach. *Journal of the Mechanical Behavior of Biomedical Materials* **2011,** 4 (5), 626-657 DOI: 10.1016/j.jmbbm.2010.08.005.

8.Chen, P. Y.; Lin, A. Y. M.; Lin, Y. S.; Seki, Y.; Stokes, A. G.; Peyras, J.; Olevsky, E. A.; Meyers, M. A.; McKittrick, J. Structure and mechanical properties of selected biological materials. *Journal of the Mechanical Behavior of Biomedical Materials* **2008,** 1 (3), 208-226 DOI: 10.1016/j.jmbbm.2008.02.003.

9.Dimas, L. S.; Bratzel, G. H.; Eylon, I.; Buehler, M. J. Tough Composites Inspired by Mineralized Natural Materials: Computation, 3D printing, and Testing. *Advanced Functional Materials* **2013,** 23 (36), 4629-4638 DOI: 10.1002/adfm.201300215.

10.Akcora, P.; Liu, H.; Kumar, S. K.; Moll, J.; Li, Y.; Benicewicz, B. C.; Schadler, L. S.; Acehan, D.; Panagiotopoulos, A. Z.; Pryamitsyn, V.; Ganesan, V.; Ilavsky, J.; Thiyagarajan, P.; Colby, R. H.; Douglas, J. F. Anisotropic self-assembly of spherical polymer-grafted nanoparticles. *Nature Materials* **2009,** 8 (4), 354-U121 DOI: 10.1038/nmat2404.

11.Kumar, S. K.; Jouault, N.; Benicewicz, B.; Neely, T. Nanocomposites with Polymer Grafted Nanoparticles. *Macromolecules* **2013,** 46 (9), 3199-3214 DOI: 10.1021/ma4001385.

12.Jouault, N.; Lee, D.; Zhao, D.; Kumar, S. K. Block-Copolymer-Mediated Nanoparticle Dispersion and Assembly in Polymer Nanocomposites. *Advanced Materials* **2014,** 26 (24), 4031-4036 DOI: 10.1002/adma.201305641.

13.Lin, Y. L.; Chiou, C. S.; Kumar, S. K.; Lin, J. J.; Sheng, Y. J.; Tsao, H. K. Self-Assembled Superstructures of Polymer-Grafted Nanoparticles: Effects of Particle Shape and Matrix Polymer. *Journal of Physical Chemistry C* **2011,** 115 (13), 5566-5577 DOI: 10.1021/jp112088x.

14.Akcora, P.; Kumar, S. K.; Moll, J.; Lewis, S.; Schadler, L. S.; Li, Y.; Benicewicz, B. C.; Sandy, A.; Narayanan, S.; Illavsky, J.; Thiyagarajan, P.; Colby, R. H.; Douglas, J. F. "Gel-like" Mechanical Reinforcement in Polymer Nanocomposite Melts. *Macromolecules* **2010,** 43 (2), 1003-1010 DOI: 10.1021/ma902072d.

15.Maillard, D.; Kumar, S. K.; Fragneaud, B.; Kysar, J. W.; Rungta, A.; Benicewicz, B. C.; Deng, H.; Brinson, L. C.; Douglas, J. F. Mechanical Properties of Thin Glassy Polymer Films Filled with Spherical Polymer-Grafted Nanoparticles. *Nano Letters* **2012,** 12 (8), 3909-3914 DOI: 10.1021/nl301792g.

16.Jancar, J.; Douglas, J. F.; Starr, F. W.; Kumar, S. K.; Cassagnau, P.; Lesser, A. J.; Sternstein, S. S.; Buehler, M. J. Current issues in research on structure-property relationships in polymer nanocomposites. *Polymer* **2010,** 51 (15), 3321-3343 DOI: 10.1016/j.polymer.2010.04.074.

17.Hashemi, A.; Jouault, N.; Williams, G. A.; Zhao, D.; Cheng, K. J.; Kysar, J. W.; Guan, Z.; Kumart, S. K. Enhanced Glassy State Mechanical Properties of Polymer Nanocomposites via Supramolecular Interactions. *Nano Letters* **2015,** 15 (8), 5465-5471 DOI: 10.1021/acs.nanolett.5b01859.

18.Jordan, J.; Jacob, K. I.; Tannenbaum, R.; Sharaf, M. A.; Jasiuk, I. Experimental trends in polymer nanocomposites - a review. *Materials Science and Engineering a-Structural Materials Properties Microstructure and Processing* **2005,** 393 (1-2), 1-11 DOI: 10.1016/j.msea.2004.09.044.

19.Mackay, M. E.; Tuteja, A.; Duxbury, P. M.; Hawker, C. J.; Van Horn, B.; Guan, Z. B.; Chen, G. H.; Krishnan, R. S. General strategies for nanoparticle dispersion. *Science* **2006,** 311 (5768), 1740-1743 DOI: 10.1126/science.1122225.

20.Jouault, N.; Vallat, P.; Dalmas, F.; Said, S.; Jestin, J.; Boue, F. Well-Dispersed Fractal Aggregates as Filler in Polymer-Silica Nanocomposites: Long-Range Effects in Rheology. *Macromolecules* **2009,** 42 (6), 2031-2040 DOI: 10.1021/ma801908u.

21.Jouault, N.; Dalmas, F.; Boue, F.; Jestin, J. Multiscale characterization of filler dispersion and origins of mechanical reinforcement in model nanocomposites. *Polymer* **2012,** 53 (3), 761-775 DOI: 10.1016/j.polymer.2011.12.001.

22.Chevigny, C.; Jouault, N.; Dalmas, F.; Boue, F.; Jestin, J. Tuning the Mechanical Properties in Model Nanocomposites: Influence of the Polymer-Filler Interfacial Interactions. *Journal of Polymer Science Part B-Polymer Physics* **2011,** 49 (11), 781-791 DOI: 10.1002/polb.22246.

23.Jouault, N.; Zhao, D.; Kumar, S. K. Role of Casting Solvent on Nanoparticle Dispersion in Polymer Nanocomposites. *Macromolecules* **2014,** 47 (15), 5246-5255 DOI: 10.1021/ma500619g.

24.Zhao, D.; Schneider, D.; Fytas, G.; Kumar, S. K. Controlling the Thermomechanical Behavior of Nanoparticle/Polymer Films. *Acs Nano* **2014,** 8 (8), 8163-8173 DOI: 10.1021/nn503486e.

25.Harton, S. E.; Kumar, S. K.; Yang, H.; Koga, T.; Hicks, K.; Lee, E.; Mijovic, J.; Liu, M.; Vallery, R. S.; Gidley, D. W. Immobilized Polymer Layers on Spherical Nanoparticles. *Macromolecules* **2010,** 43 (7), 3415-3421 DOI: 10.1021/ma902484d.

26.Schadler, L. S.; Kumar, S. K.; Benicewicz, B. C.; Lewis, S. L.; Harton, S. E. Designed interfaces in polymer nanocomposites: A fundamental viewpoint. *Mrs Bulletin* **2007,** 32 (4), 335-340 DOI: 10.1557/mrs2007.232.

27.Kim, S. Y.; Zukoski, C. F. Role of Polymer Segment-Particle Surface Interactions in Controlling Nanoparticle Dispersions in Concentrated Polymer Solutions. *Langmuir* **2011,** 27 (17), 10455-10463 DOI: 10.1021/la201704u.

28.Kim, S. Y.; Zukoski, C. F. Particle Restabilization in Silica/PEG/Ethanol Suspensions: How Strongly do Polymers Need To Adsorb To Stabilize Against Aggregation? *Langmuir* **2011,** 27 (9), 5211-5221 DOI: 10.1021/la200022j.

29.Kim, S. Y.; Zukoski, C. F. Super- and sub-Einstein intrinsic viscosities of spherical nanoparticles in concentrated low molecular weight polymer solutions. *Soft Matter* **2012,** 8 (6), 1801-1810 DOI: 10.1039/c2sm06807a.

30.Kim, S. Y.; Schweizer, K. S.; Zukoski, C. F. Multiscale Structure, Interfacial Cohesion, Adsorbed Layers, and Thermodynamics in Dense Polymer-Nanoparticle Mixtures. *Physical Review Letters* **2011,** 107 (22), DOI: 10.1103/PhysRevLett.107.225504.

31.Meth, J. S.; Zane, S. G.; Chi, C.; Londono, J. D.; Wood, B. A.; Cotts, P.; Keating, M.; Guise, W.; Weigand, S. Development of Filler Structure in Colloidal Silica-Polymer Nanocomposites. *Macromolecules* **2011,** 44 (20), 8301-8313 DOI: 10.1021/ma201714u.

32.Janes, D. W.; Moll, J. F.; Harton, S. E.; Durning, C. J. Dispersion Morphology of Poly(methyl acrylate)/Silica Nanocomposites. *Macromolecules* **2011,** 44 (12), 4920-4927 DOI: 10.1021/ma200205j.

33.Bansal, A.; Yang, H. C.; Li, C. Z.; Cho, K. W.; Benicewicz, B. C.; Kumar, S. K.; Schadler, L. S. Quantitative equivalence between polymer nanocomposites and thin polymer films. *Nature Materials* **2005,** 4 (9), 693-698 DOI: 10.1038/nmat1447.

34.Hamming, L. M.; Qiao, R.; Messersmith, P. B.; Brinson, L. C. Effects of dispersion and interfacial modification on the macroscale properties of TiO(2) polymer-matrix nanocomposites. *Composites Science and Technology* **2009,** 69 (11-12), 1880-1886 DOI: 10.1016/j.compscitech.2009.04.005.

35.Hub, C.; Harton, S. E.; Hunt, M. A.; Fink, R.; Ade, H. Influence of sample preparation and processing on observed glass transition temperatures of polymer nanocomposites. *Journal of Polymer Science Part B-Polymer Physics* **2007,** 45 (16), 2270-2276 DOI: 10.1002/polb.21249.

36.Becker, C.; Krug, H.; Schmidt, H. In Tailoring of thermomechanical properties of thermoplastic nanocomposites by surface modification of nanoscale silica particles, 7th MRS Symposium on Better Ceramics Through Chemistry, San Francisco, Ca, 1996

Apr 08-12, 1996; San Francisco, Ca, 1996; pp 237-242.

37.Bansal, A.; Yang, H.; Li, C.; Benicewicz, R. C.; Kumar, S. K.; Schadler, L. S. Controlling the thermornechanical properties of polymer nanocomposites by tailoring the polymer-particle interface. *Journal of Polymer Science Part B-Polymer Physics* **2006,** 44 (20), 2944-2950 DOI: 10.1002/polb.20926.

38.Sen, S.; Xie, Y.; Bansal, A.; Yang, H.; Cho, K.; Schadler, L. S.; Kumar, S. K. Equivalence between polymer nanocomposites and thin polymer films: Effect of processing conditions and molecular origins of observed behavior. *European Physical Journal-Special Topics* **2007,** 141, 161-165 DOI: 10.1140/epjst/e2007-00034-x.

39.Castrillo, P. D.; Olmos, D.; Amador, D. R.; Gonzalez-Benito, J. Real dispersion of isolated fumed silica nanoparticles in highly filled PMMA prepared by high energy ball milling. *Journal of Colloid and Interface Science* **2007,** 308 (2), 318-324 DOI: 10.1016/j.jcis.2007.01.022.

40.Hu, Y. H.; Chen, C. Y.; Wang, C. C. Viscoelastic properties and thermal degradation kinetics of silica/PMMA nanocomposites. *Polymer Degradation and Stability* **2004,** 84 (3), 545-553 DOI: 10.1016/j.polymdegradstab.2004.02.001.

41.Chau, J. L. H.; Hsieh, C.-C.; Lin, Y.-M.; Li, A.-K. Preparation of transparent silica-PMMA nanocomposite hard coatings. *Progress in Organic Coatings* **2008,** 62 (4), 436-439 DOI: 10.1016/j.porgcoat.2008.02.005.

42.Stojanovic, D. B.; Brajovic, L.; Orlovic, A.; Dramlic, D.; Radmilovic, V.; Uskokovic, P. S.; Aleksic, R. Transparent PMMA/silica nanocomposites containing silica nanoparticles coating

under supercritical conditions. *Progress in Organic Coatings* **2013,** 76 (4), 626-631 DOI: 10.1016/j.porgcoat.2012.12.002.

43.Sargsyan, A.; Tonoyan, A.; Davtyan, S.; Schick, C. The amount of immobilized polymer in PMMA SiO(2) nanocomposites determined from calorimetric data. *European Polymer Journal* **2007,** 43 (8), 3113-3127 DOI: 10.1016/j.eurpolymj.2007.05.011.

44.Etienne, S.; Becker, C.; Ruch, D.; Grignard, B.; Cartigny, G.; Detrembleur, C.; Calberg, C.; Jerome, R. Effects of incorporation of modified silica nanoparticles on the mechanical and thermal properties of PMMA. *Journal of Thermal Analysis and Calorimetry* **2007,** 87 (1), 101-104 DOI: 10.1007/s10973-006-7827-4.

45.Triebel, C.; Muenstede, H. Temperature dependence of rheological properties of poly(methyl methacrylate) filled with silica nanoparticles. *Polymer* **2011,** 52 (7), 1596-1602 DOI: 10.1016/j.polymer.2011.02.014.

46.Hedayati, M.; Salehi, M.; Bagheri, R.; Panjepour, M.; Maghzian, A. Ball milling preparation and characterization of poly (ether ether ketone)/surface modified silica nanocomposite. *Powder Technology* **2011,** 207 (1-3), 296-303 DOI: 10.1016/j.powtec.2010.11.011.

47.Weickmann, H.; Delto, R.; Thomann, R.; Brenn, R.; Doell, W.; Muelhaupt, R. PMMA nanocomposites and gradient materials prepared by means of polysilsesquioxane (POSS) self-assembly. *Journal of Materials Science* **2007,** 42 (1), 87-92 DOI: 10.1007/s10853-006-1044-1.

48.Cangialosi, D.; Boucher, V. M.; Alegria, A.; Colmenero, J. Enhanced physical aging of polymer nanocomposites: The key role of the area to volume ratio. *Polymer* **2012,** 53 (6), 1362-1372 DOI: 10.1016/j.polymer.2012.01.033.

49.Neikirk, C. C.; Chung, J. W.; Priestley, R. D. Thermomechanical behavior of hydrogen-bond based supramolecular poly(epsilon-caprolactone)-silica nanocomposites. *Rsc Advances* **2013,** 3 (37), 16686-16696 DOI: 10.1039/c3ra42031k.

50.Hooper, J. B.; Schweizer, K. S.; Desai, T. G.; Koshy, R.; Keblinski, P. Structure, surface excess and effective interactions in polymer nanocomposite melts and concentrated solutions. *Journal of Chemical Physics* **2004,** 121 (14), 6986-6997 DOI: 10.1063/1.1790831.

51.Hooper, J. B.; Schweizer, K. S. Contact aggregation, bridging, and steric stabilization in dense polymer-particle mixtures. *Macromolecules* **2005,** 38 (21), 8858-8869 DOI: 10.1021/ma051318k.

52.Hooper, J. B.; Schweizer, K. S. Theory of phase separation in polymer nanocomposites. *Macromolecules* **2006,** 39 (15), 5133-5142 DOI: 10.1021/ma060577m.

53.Hooper, J. B.; Schweizer, K. S. Real space structure and scattering patterns of model polymer nanocomposites. *Macromolecules* **2007,** 40 (19), 6998-7008 DOI: 10.1021/ma071147e.

54.Hall, L. M.; Jayaraman, A.; Schweizer, K. S. Molecular theories of polymer nanocomposites. *Current Opinion in Solid State & Materials Science* **2010,** 14 (2), 38-48 DOI: 10.1016/j.cossms.2009.08.004.

55.Vanderbeek, G. P.; Stuart, M. A. C.; Fleer, G. J.; Hofman, J. E. SEGMENTAL ADSORPTION ENERGIES FOR POLYMERS ON SILICA AND ALUMINA. *Macromolecules* **1991,** 24 (25), 6600-6611 DOI: 10.1021/ma00025a009.

56.Drago, R. S.; Vogel, G. C.; Needham, T. E. 4-PARAMETER EQUATION FOR PREDICTING ENTHALPIES OF ADDUCT FORMATION. *Journal of the American Chemical Society* **1971,** 93 (23), 6014-& DOI: 10.1021/ja00752a010.

57.Marmo, M. J.; Mostafa, M. A.; Jinnai, H.; Fowkes, F. M.; Manson, J. A. ACID-BASE INTERACTION IN FILLER-MATRIX SYSTEMS. *Industrial & Engineering Chemistry Product Research and Development* **1976,** 15 (3), 206-211 DOI: 10.1021/i360059a014.

58.Fowkes, F. M.; Mostafa, M. A. ACID-BASE INTERACTIONS IN POLYMER ADSORPTION. *Industrial & Engineering Chemistry Product Research and Development* **1978,** 17 (1), 3-7 DOI: 10.1021/i360065a002.

59.Fowkes, F. M. ACID-BASE CONTRIBUTIONS TO POLYMER-FILLER INTERACTIONS. *Rubber Chemistry and Technology* **1984,** 57 (2), 328-343 DOI: 10.5254/1.3536012.

60.Allara, D. L.; Fowkes, F. M.; Noolandi, J.; Rubloff, G. W.; Tirrell, M. V. BONDING AND ADHESION OF POLYMER INTERFACES. *Materials Science and Engineering* **1986,** 83 (2), 213-226 DOI: 10.1016/0025-5416(86)90339-3.

61.Fowkes, F. M. QUANTITATIVE CHARACTERIZATION OF THE ACID-BASE PROPERTIES OF SOLVENTS, POLYMERS, AND INORGANIC SURFACES. *Journal of Adhesion Science and Technology* **1990,** 4 (8), 669-691 DOI: 10.1163/156856190x00595.

62.Zidek, J.; Kucera, J.; Jancar, J. Model of Random Spatial Packing of Rigid Spheres with Controlled Macroscopic Homogenity. *Cmc-Computers Materials & Continua* **2010,** 16 (1), 51-73.

63.Zidek, J.; Kucera, J.; Jancar, J. Nearest Particle Distance and the Statistical Distribution of Agglomerates from a Model of a Finite Set of Particles. *Cmc-Computers Materials & Continua* **2011,** 24 (3), 183-208.

64.Kalfus, J.; Jancar, J. Relaxation processes in PVAc-HA nanocomposites. *Journal of Polymer Science Part B-Polymer Physics* **2007,** 45 (11), 1380-1388 DOI: 10.1002/polb.21139.

65.Kalfus, J.; Jancar, J. Immobilization of polyvinylacetate macromolecules on hydroxyapatite nanoparticles. *Polymer* **2007,** 48 (14), 3935-3937 DOI: 10.1016/j.polymer.2007.04.049.

66.Kalfus, J.; Jancar, J. Elastic response of nanocomposite poly(vinylacetate)-hydroxyapatite with varying particle shape. *Polymer Composites* **2007,** 28 (3), 365-371 DOI: 10.1002/pc.20273.

67.Kalfus, J.; Jancar, J. Viscoelastic response of nanocomposite poly(vinyl acetate)-hydroxyapatite with varying particle shape-dynamic strain softening and modulus recovery. *Polymer Composites* **2007,** 28 (6), 743-747 DOI: 10.1002/pc.20331.

68.Debenedetti, P. G.; Stillinger, F. H. Supercooled liquids and the glass transition. *Nature* **2001,** 410 (6825), 259-267 DOI: 10.1038/35065704.

69.Paul, D. R.; Robeson, L. M. Polymer nanotechnology: Nanocomposites. *Polymer* **2008,** 49 (15), 3187-3204 DOI: 10.1016/j.polymer.2008.04.017.

70.Rittigstein, P.; Torkelson, J. M. Polymer-nanoparticle interfacial interactions in polymer nanocomposites: Confinement effects on glass transition temperature and suppression of physical aging. *Journal of Polymer Science Part B-Polymer Physics* **2006,** 44 (20), 2935-2943 DOI: 10.1002/polb.20925.

71.Moll, J.; Kumar, S. K. Glass Transitions in Highly Attractive Highly Filled Polymer Nanocomposites. *Macromolecules* **2012,** 45 (2), 1131-1135 DOI: 10.1021/ma202218x.

72.Ash, B. J.; Schadler, L. S.; Siegel, R. W. Glass transition behavior of alumina/polymethylmethacrylate nanocomposites. *Materials Letters* **2002,** 55 (1-2), 83-87 DOI: 10.1016/s0167-577x(01)00626-7.

73.Riggleman, R. A.; Toepperwein, G.; Papakonstantopoulos, G. J.; Barrat, J.-L.; de Pablo, J. J. Entanglement network in nanoparticle reinforced polymers. *Journal of Chemical Physics* **2009,** 130 (24), DOI: 10.1063/1.3148026.

74.Guth, E.; Gold, O. On the hydrodynamic theory of the viscosity of suspensions. *Phys. Rev.* **1938,** 53, 322.

75.Smallwood, H. M. Limiting law of the reinforcement of rubber. *J. Appl. Phys.* **1944,** 15, 758.

76.Guth, E. Theory of filler reinforcement. *Appl. Phys.* **1945,** 16, 20.

77.Sarvestani, A. S.; Picu, C. R. Network model for the viscoelastic behavior of polymer nanocomposites. *Polymer* **2004,** 45 (22), 7779-7790 DOI: 10.1016/j.polymer.2004.08.060.

78.Sarvestani, A. S.; Picu, C. R. A frictional molecular model for the viscoelasticity of entangled polymer nanocomposites. *Rheologica Acta* **2005,** 45 (2), 132-141 DOI: 10.1007/s00397-005-0002-1.

79.Picu, C. R.; Sarvestani, A. S.; Palade, L. I. Molecular Constitutive Model for Entangled Polymer Nanocomposites. *Materiale Plastice* **2012,** 49 (3), 133-142.

80.Tannenbaum, R.; Zubris, M.; David, K.; Ciprari, D.; Jacob, K.; Jasiuk, W.; Dan, N. FTIR characterization of the reactive interface of cobalt oxide nanoparticles embedded in polymeric matrices. *Journal of Physical Chemistry B* **2006,** 110 (5), 2227-2232 DOI: 10.1021/jp054469y.

81.Ciprari, D.; Jacob, K.; Tannenbaum, R. Characterization of polymer nanocomposite interphase and its impact on mechanical properties. *Macromolecules* **2006,** 39 (19), 6565-6573 DOI: 10.1021/ma0602270.

82.Jouault, N.; Moll, J. F.; Meng, D.; Windsor, K.; Ramcharan, S.; Kearney, C.; Kumar, S. K. Bound Polymer Layer in Nanocomposites. *Acs Macro Letters* **2013,** 2 (5), 371-374 DOI: 10.1021/mz300646a.

83.Anderson, B. J.; Zukoski, C. F. Rheology and Microstructure of Entangled Polymer Nanocomposite Melts. *Macromolecules* **2009,** 42 (21), 8370-8384 DOI: 10.1021/ma9011158.

84.Anderson, B. J.; Zukoski, C. F. Rheology and Microstructure of Polymer Nanocomposite Melts: Variation of Polymer Segment-Surface Interaction. *Langmuir* **2010,** 26 (11), 8709-8720 DOI: 10.1021/la9044573.

85.Jouault, N.; Crawford, M. K.; Chi, C. Z.; Smalley, R. J.; Wood, B.; Jestin, J.; Melnichenko, Y. B.; He, L. L.; Guise, W. E.; Kumar, S. K. Polymer Chain Behavior in Polymer Nanocomposites with Attractive Interactions. *Acs Macro Letters* **2016,** 5 (4), 523-527 DOI: 10.1021/acsmacrolett.6b00164.

86.Cheng, S. W.; Carroll, B.; Lu, W.; Fan, F.; Carrillo, J. M. Y.; Martin, H.; Holt, A. P.; Kang, N. G.; Bocharova, V.; Mays, J. W.; Sumpter, B. G.; Dadmun, M.; Sokolov, A. P. Interfacial Properties of Polymer Nanocomposites: Role of Chain Rigidity and Dynamic Heterogeneity Length Scale. *Macromolecules* **2017,** 50 (6), 2397-2406 DOI: 10.1021/acs.macromol.6b02816.

87.Jancar, J.; Recman, L. Particle size dependence of the elastic modulus of particulate filled PMMA near its T-g. *Polymer* **2010,** 51 (17), 3826-3828 DOI: 10.1016/j.polymer.2010.06.041.

88.Jancar, J.; Hoy, R. S.; Lesser, A. J.; Jancarova, E.; Zidek, J. Effect of Particle Size, Temperature, and Deformation Rate on the Plastic Flow and Strain Hardening Response of PMMA Composites. *Macromolecules* **2013,** 46 (23), 9409-9426 DOI: 10.1021/ma400965c.

89.Jancar, J.; Hoy, R. S.; Jancarova, E.; Zidek, J. Effect of temperature, strain rate and particle size on the yield stresses and post-yield strain softening of PMMA and its composites. *Polymer* **2015,** 63, 196-207 DOI: 10.1016/j.polymer.2015.03.001.

90.Dorigato, A.; Sebastiani, M.; Pegoretti, A.; Fambri, L. Effect of Silica Nanoparticles on the Mechanical Performances of Poly(Lactic Acid). *Journal of Polymers and the Environment* **2012,** 20 (3), 713-725 DOI: 10.1007/s10924-012-0425-6.

91.Turcsanyi, B.; Pukanszky, B.; Tudos, F. COMPOSITION DEPENDENCE OF TENSILE YIELD STRESS IN FILLED POLYMERS. *Journal of Materials Science Letters* **1988,** 7 (2), 160-162 DOI: 10.1007/bf01730605.

92.Pukanszky, B. INFLUENCE OF INTERFACE INTERACTION ON THE ULTIMATE TENSILE PROPERTIES OF POLYMER COMPOSITES. *Composites* **1990,** 21 (3), 255-262 DOI: 10.1016/0010-4361(90)90240-w.

93.Vorod, G.; Pukansky, B. Prediction of the yield stress of composites containing particles with an interlayer of changing properties. *Composites Part a-Applied Science and Manufacturing* **2002,** 33 (10), 1317-1322 DOI: 10.1016/s1359-835x(02)00168-9.

94.Moczo, J.; Pukanszky, B. Polymer micro and nanocomposites: Structure, interactions, properties. *Journal of Industrial and Engineering Chemistry* **2008,** 14 (5), 535-563 DOI: 10.1016/j.jiec.2008.06.011.

95.Jancar, J.; Dianselmo, A.; Dibenedetto, A. T. THE YIELD STRENGTH OF PARTICULATE REINFORCED THERMOPLASTIC COMPOSITES. *Polymer Engineering and Science* **1992,** 32 (18), 1394-1399 DOI: 10.1002/pen.760321809.

96.Zhao, D.; Gimenez-Pinto, V.; Jimenez, A. M.; Zhao, L. X.; Jestin, J.; Kumar, S. K.; Kuei, B.; Gomez, E. D.; Prasad, A. S.; Schadler, L. S.; Khani, M. M.; Benicewicz, B. C. Tunable Multiscale Nanoparticle Ordering by Polymer Crystallization. *Acs Central Science* **2017,** 3 (7), 751-758 DOI: 10.1021/acscentsci.7b00157.

97.Khan, J.; Harton, S. E.; Akcora, P.; Benicewicz, B. C.; Kumar, S. K. Polymer Crystallization in Nanocomposites: Spatial Reorganization of Nanoparticles. *Macromolecules* **2009,** 42 (15), 5741-5744 DOI: 10.1021/ma900794t.

98.Jancar, J.; Fiore, K. Molecular weight scaling of the spherulite growth rate in isothermally melt crystallized polyethylene nanocomposites. *Polymer* **2011,** 52 (25), 5851-5857 DOI: 10.1016/j.polymer.2011.10.026.

99.Zhou, Y.; He, J. L.; Hu, J.; Dang, B. Surface-modified MgO nanoparticle enhances the mechanical and direct-current electrical characteristics of polypropylene/polyolefin elastomer nanodielectrics. *Journal of Applied Polymer Science* **2016,** 133 (1), DOI: 10.1002/app.42863.

100.Fox, T. G.; Flory, P. J. 2ND-ORDER TRANSITION TEMPERATURES AND RELATED PROPERTIES OF POLYSTYRENE .1. INFLUENCE OF MOLECULAR WEIGHT. *Journal of Applied Physics* **1950,** 21 (6), 581-591 DOI: 10.1063/1.1699711.

101.Fox, T. G.; Flory, P. J. THE GLASS TEMPERATURE AND RELATED PROPERTIES OF POLYSTYRENE - INFLUENCE OF MOLECULAR WEIGHT. *Journal of Polymer Science* **1954,** 14 (75), 315-319 DOI: 10.1002/pol.1954.120147514.

102.Gourari, A.; Bendaoud, M.; Lacabanne, C.; Boyer, R. F. INFLUENCE OF TACTICITY ON T-BETA, T-G, AND T-LL IN POLY(METHYL METHACRYLATE)S BY THE METHOD OF THERMALLY STIMULATED CURRENT (TSC). *Journal of Polymer Science Part B-Polymer Physics* **1985,** 23 (5), 889-916 DOI: 10.1002/pol.1985.180230505.

103.Denny, L. R.; Boyer, R. F.; Elias, H. G. DEPENDENCE OF TG AND TLL ON TACTICITY OF PMMA BY DIFFERENTIAL SCANNING CALORIMETRY. *Journal of Macromolecular Science-Physics* **1986,** B25 (3), 227-265 DOI: 10.1080/00222348608248039.

104.Starr, F. W.; Douglas, J. F.; Glotzer, S. C. Origin of particle clustering in a simulated polymer nanocomposite and its impact on rheology. *Journal of Chemical Physics* **2003,** 119 (3), 1777-1788 DOI: 10.1063/1.1580099.

105.Hamieh, T.; Schultz, J. New approach to characterise physicochemical properties of solid substrates by inverse gas chromatography at infinite dilution II. Study of the transition temperatures of poly(methyl methacrylate) at various tacticities and of poly(methyl methacrylate) adsorbed on alumina and silica. *Journal of Chromatography A* **2002,** 969 (1-2), 27-36 DOI: 10.1016/s0021-9673(02)00358-8.

106.Hamieh, T.; Fadlallah, M. B.; Schultz, J. New approach to characterise physicochemical properties of solid substrates by inverse gas chromatography at infinite dilution III. Determination of the acid-base properties of some solid substrates (polymers, oxides and carbon fibres): a new model. *Journal of Chromatography A* **2002,** 969 (1-2), 37-47 DOI: 10.1016/s0021-9673(02)00369-2.

107.TANABE, K.; YAMAGUCHI, T. JOURNAL OF THE RESEARCH INSTITUTE FOR CATALYSIS HOKKAIDO UNIVERSITY **1964,** 11 (3), 179-184.

108.Huang, Y. C.; Fowkes, F. M.; Lloyd, T. B. ACIDIC AND BASIC NATURE OF FERRIC-OXIDE SURFACES - ADSORPTION, ADHESION, ZETA-POTENTIALS AND DISPERSIBILITY IN MAGNETIC INKS FOR HARD DISKS. *Journal of Adhesion Science and Technology* **1991,** 5 (1), 39-56.

109.Williams, M. L.; Landel, R. F.; Ferry, J. D. TEMPERATURE DEPENDENCE OF RELAXATION MECHANISMS IN AMORPHOUS POLYMERS AND OTHER GLASS-FORMING LIQUIDS. *Physical Review* **1955,** 98 (5), 1549-1549.

110.Williams, M. L.; Landel, R. F.; Ferry, J. D. MECHANICAL PROPERTIES OF SUBSTANCES OF HIGH MOLECULAR WEIGHT .19. THE TEMPERATURE DEPENDENCE OF RELAXATION MECHANISMS IN AMORPHOUS POLYMERS AND OTHER GLASS-FORMING LIQUIDS. *Journal of the American Chemical Society* **1955,** 77 (14), 3701-3707 DOI: 10.1021/ja01619a008.

111.Ferry, J. D., Viscoelastic properties of polymers. third edition ed.; John Wiley & Sons: 1980; p 640.

112.Liu, C.; He, J.; van Ruymbeke, E.; Keunings, R.; Bailly, C. Evaluation of different methods for the determination of the plateau modulus and the entanglement molecular weight. *Polymer* **2006,** 47 (13), 4461-4479 DOI: 10.1016/j.polymer.2006.04.054.

113.Wu, S. CHAIN STRUCTURE AND ENTANGLEMENT. *Journal of Polymer Science Part B-Polymer Physics* **1989,** 27 (4), 723-741 DOI: 10.1002/polb.1989.090270401.

114.van Melick, H. G. H.; Govaert, L. E.; Meijer, H. E. H. On the origin of strain hardening in glassy polymers. *Polymer* **2003,** 44 (8), 2493-2502 DOI: 10.1016/s0032-3861(03)00112-5.

115.Kremer, K.; Sukumaran, S. K.; Everaers, R.; Grest, G. S. Entangled polymer systems. *Computer Physics Communications* **2005,** 169 (1-3), 75-81 DOI: 10.1016/j.cpc.2005.03.019.

116.Kavassalis, T. A.; Noolandi, J. THE ENTANGLEMENT CONCEPT IN POLYMER PHYSICS REVISITED. *New Trends in Physics and Physical Chemistry of Polymers* **1989**, 419-453.

117.Cross, M. M. RHEOLOGY OF NON-NEWTONIAN FLUIDS - A NEW FLOW EQUATION FOR PSEUDOPLASTIC SYSTEMS. *Journal of Colloid Science* **1965,** 20 (5), 417-& DOI: 10.1016/0095-8522(65)90022-x.

118.Fetters, L. J.; Lohse, D. J.; Richter, D.; Witten, T. A.; Zirkel, A. CONNECTION BETWEEN POLYMER MOLECULAR-WEIGHT, DENSITY, CHAIN DIMENSIONS, AND MELT VISCOELASTIC PROPERTIES. *Macromolecules* **1994,** 27 (17), 4639-4647 DOI: 10.1021/ma00095a001.

119.Fetters, L. J.; Lohse, D. J.; Graessley, W. W. Chain dimensions and entanglement spacings in dense macromolecular systems. *Journal of Polymer Science Part B-Polymer Physics* **1999,** 37 (10), 1023-1033 DOI: 10.1002/(sici)1099-0488(19990515)37:10<1023::aid-polb7>3.0.co;2-t.

120.Graessley, W. W.; Edwards, S. F. ENTANGLEMENT INTERACTIONS IN POLYMERS AND THE CHAIN CONTOUR CONCENTRATION. *Polymer* **1981,** 22 (10), 1329-1334 DOI: 10.1016/0032-3861(81)90231-7.

121.Gibbs, J. H.; Dimarzio, E. A. NATURE OF THE GLASS TRANSITION AND THE GLASSY STATE. *Journal of Chemical Physics* **1958,** 28 (3), 373-383 DOI: 10.1063/1.1744141.

122.Adam, G.; Gibbs, J. H. ON TEMPERATURE DEPENDENCE OF COOPERATIVE RELAXATION PROPERTIES IN GLASS-FORMING LIQUIDS. *Journal of Chemical Physics* **1965,** 43 (1), 139-& DOI: 10.1063/1.1696442.

123.Glotzer, S. C.; Coniglio, A. FRUSTRATION, CONNECTIVITY, AND THE GLASS-TRANSITION. *Computational Materials Science* **1995,** 4 (4), 325-333 DOI: 10.1016/0927-0256(95)00042-5.

124.Robertson, C. G.; Santangelo, P. G.; Roland, C. M. Comparison of glass formation kinetics and segmental relaxation in polymers. *Journal of Non-Crystalline Solids* **2000,** 275 (3), 153-159 DOI: 10.1016/s0022-3093(00)00260-x.

125.Stillinger, F. H.; Debenedetti, P. G. Glass Transition Thermodynamics and Kinetics. *Annual Review of Condensed Matter Physics, Vol 4* **2013,** 4, 263-285 DOI: 10.1146/annurev-conmatphys-030212-184329.

126.McKenna, G. B.; Simon, S. L. 50th Anniversary Perspective: Challenges in the Dynamics and Kinetics of Glass-Forming Polymers. *Macromolecules* **2017,** 50 (17), 6333-6361 DOI: 10.1021/acs.macromo1.7b01014.

127.Hamieh, T.; Toufaily, J.; Fadlallah, M. B. Study of superficial properties of some polymers and oxides. *Advanced Powder Technology* **2003,** 14 (5), 547-558 DOI: 10.1163/156855203322448336.

128.Schneider, G. J. Dynamics of nanocomposites. *Current Opinion in Chemical Engineering* **2017,** 16, 65-77 DOI: 10.1016/j.coche.2017.04.006.

129.Berriot, J.; Montes, H.; Lequeux, F.; Long, D.; Sotta, P. Evidence for the shift of the glass transition near the particles in silica-filled elastomers. *Macromolecules* **2002,** 35 (26), 9756-9762 DOI: 10.1021/ma0212700.

130.Mujtaba, A.; Keller, M.; Ilisch, S.; Radusch, H. J.; Beiner, M.; Thurn-Albrecht, T.; Saalwachter, K. Detection of Surface-Immobilized Components and Their Role in Viscoelastic Reinforcement of Rubber-Silica Nanocomposites. *Acs Macro Letters* **2014,** 3 (5), 481-485 DOI: 10.1021/mz500192r.

131.Merabia, S.; Sotta, P.; Long, D. R. A Microscopic Model for the Reinforcement and the Nonlinear Behavior of Filled Elastomers and Thermoplastic Elastomers (Payne and Mullins Effects). *Macromolecules* **2008,** 41 (21), 8252-8266 DOI: 10.1021/ma8014728.

132.Sotta, P.; Albouy, P. A.; Abou Taha, M.; Long, D. R.; Grau, P.; Fayolle, C.; Papon, A. Nonentropic Reinforcement in Elastomer Nanocomposites. *Macromolecules* **2017,** 50 (16), 6314-6322 DOI: 10.1021/acs.macromol.7b00698.

133.Anderson, B. J.; Zukoski, C. F. Rheology and Microstructure of an Unentangled Polymer Nanocomposite Melt. *Macromolecules* **2008,** 41 (23), 9326-9334 DOI: 10.1021/ma801415e.

134.Mueller, S.; Llewellin, E. W.; Mader, H. M. The rheology of suspensions of solid particles. *Proceedings of the Royal Society a-Mathematical Physical and Engineering Sciences* **2010,** 466 (2116), 1201-1228 DOI: 10.1098/rspa.2009.0445.

135.Johari, G. P.; Goldstei.M. VISCOUS LIQUIDS AND GLASS TRANSITION .2. SECONDARY RELAXATIONS IN GLASSES OF RIGID MOLECULES. *Journal of Chemical Physics* **1970,** 53 (6), 2372-& DOI: 10.1063/1.1674335.

136.Johari, G. P. Localized molecular motions of beta-relaxation and its energy landscape. *Journal of Non-Crystalline Solids* **2002,** 307, 317-325 DOI: 10.1016/s0022-3093(02)01491-6.

137.Muzeau, E.; Cavaille, J. Y.; Vassoille, R.; Perez, J.; Johari, G. P. EFFECTS OF SUB-T(G) ANNEALINGS ON THE ANELASTIC RELAXATION IN POLY(METHYL METHACRYLATE). *Macromolecules* **1992,** 25 (19), 5108-5110 DOI: 10.1021/ma00045a043.

138.Perez, J.; Cavaille, J. Y.; David, L. New experimental features and revisiting the alpha and beta mechanical relaxation in glasses and glass-forming liquids. *Journal of Molecular Structure* **1999,** 479 (2-3), 183-194 DOI: 10.1016/s0022-2860(98)00869-2.

139.Beiner, M.; Garwe, F.; Schroter, K.; Donth, E. AGING EFFECTS ON DYNAMIC SHEAR MODULI AT THE ONSET OF THE DYNAMIC GLASS-TRANSITION IN 2 POLY(ALKYL METHACRYLATE)S. *Polymer* **1994,** 35 (19), 4127-4132 DOI: 10.1016/0032-3861(94)90586-x.

140.Garwe, F.; Schonhals, A.; Lockwenz, H.; Beiner, M.; Schroter, K.; Donth, E. Influence of cooperative alpha dynamics on local beta relaxation during the development of the dynamic glass transition in poly(n-alkyl methacrylate)s. *Macromolecules* **1996,** 29 (1), 247-253 DOI: 10.1021/ma9506142.

141.Beiner, M. Relaxation in poly(alkyl methacrylate)s: Crossover region and nanophase separation. *Macromolecular Rapid Communications* **2001,** 22 (12), 869-895 DOI: 10.1002/1521-3927(20010801)22:12<869::aid-marc869>3.0.co;2-r.

142.Roetling, J. A. Yield Stress Behavior of Polymethylmethacrylate. *Polymer* **1965,** 6, 311.

143.van Breemen, L. C. A.; Engels, T. A. P.; Klompen, E. T. J.; Senden, D. J. A.; Govaert, L. E. Rate- and temperature-dependent strain softening in solid polymers. *Journal of Polymer Science Part B-Polymer Physics* **2012,** 50 (24), 1757-1771 DOI: 10.1002/polb.23199.

144.Varghese, A. G.; Batra, R. C. Constitutive equations for thermomechanical deformations of glassy polymers. *International Journal of Solids and Structures* **2009,** 46 (22-23), 4079-4094 DOI: 10.1016/j.ijsolstr.2009.08.006.

145.Govaert, L. E.; Tervoort, T. A. Strain hardening of polycarbonate in the glassy state: Influence of temperature and molecular weight. *Journal of Polymer Science Part B-Polymer Physics* **2004,** 42 (11), 2041-2049 DOI: 10.1002/poplb.20095.

146.Ngai, K. L.; Rendell, R. W.; Yee, A. F.; Plazek, D. J. ANTIPLASTICIZATION EFFECTS ON A SECONDARY RELAXATION IN PLASTICIZED GLASSY POLYCARBONATES. *Macromolecules* **1991,** 24 (1), 61-67 DOI: 10.1021/ma00001a010.

147.Senden, D. J. A.; Krop, S.; van Dommelen, J. A. W.; Govaert, L. E. Rate- and temperature-dependent strain hardening of polycarbonate. *Journal of Polymer Science Part B-Polymer Physics* **2012,** 50 (24), 1680-1693 DOI: 10.1002/polb.23165.

148.Eyring, H. Viscosity, Plasticity, and Diffusion as Examples of Absolute Reaction Rates. *The Journal of Chemical Physics* **1936,** 4, 283.

149.Ree, T.; Eyring, H. THEORY OF NON-NEWTONIAN FLOW .2. SOLUTION SYSTEM OF HIGH POLYMERS. *Journal of Applied Physics* **1955,** 26 (7), 800-809 DOI: 10.1063/1.1722099.

150.Bauwens-Crowet. The compression yield behaviour of polymethyl methacrylate over wide range of temperatures and strain-rates. *Journal of Materials Science* **1973,** 8, 968-979.

151.Nicolais, L.; Narkis, M. STRESS-STRAIN BEHAVIOR OF STYRENE-ACRYLONITRILE/GLASS BEAD COMPOSITES IN GLASSY REGION. *Polymer Engineering and Science* **1971,** 11 (3), 194-& DOI: 10.1002/pen.760110305.

152.Lavengoo.Re; Nicolais, L.; Narkis, M. DEFORMATIONAL MECHANISM IN PARTICULATE-FILLED GLASSY POLYMERS. *Journal of Applied Polymer Science* **1973,** 17 (4), 1173-1185 DOI: 10.1002/app.1973.070170414.

153.Kerner, E. H. The elastic and thermoelastic properties of composite media. *Proceedings of the Physical Society* **1956,** 69B, 808.

154.Nielsen, L. E. GENERALIZED EQUATION FOR ELASTIC MODULI OF COMPOSITE MATERIALS. *Journal of Applied Physics* **1970,** 41 (11), 4626-& DOI: 10.1063/1.1658506.

155.Nielsen, L. E.; Landel, R. F., *Mechanical properties of polymers and composites*. New York, 1994.

156.Bellemare, S. C.; Bureau, M. N.; Denault, J.; Dickson, J. I. Fatigue crack initiation and propagation in polyamide-6 and in polyamide-6 nanocomposites. *Polymer Composites* **2004,** 25 (4), 433-441 DOI: 10.1002/pc.20036.

157.Jen, M. H. R.; Tseng, Y. C.; Wu, C. H. Manufacturing and mechanical response of nanocomposite laminates. *Composites Science and Technology* **2005,** 65 (5), 775-779 DOI: 10.1016/j.compscitech.2004.10.010.

158.Ormsby, R.; McNally, T.; O'Hare, P.; Burke, G.; Mitchell, C.; Dunne, N. Fatigue and biocompatibility properties of a poly(methyl methacrylate) bone cement with multi-walled carbon nanotubes. *Acta Biomaterialia* **2012,** 8 (3), 1201-1212 DOI: 10.1016/j.actbio.2011.10.010.

159.Takeda, T.; Shindo, Y.; Wei, Z. J.; Kuronuma, Y.; Narita, F. Fatigue failure and electrical resistance behaviors of carbon nanotube-based polymer composites under uniaxial tension-tension loading in a cryogenic environment. *Journal of Composite Materials* **2015,** 49 (4), 457-463 DOI: 10.1177/0021998314521059.

160.van Melick, H. G. H.; Govaert, L. E.; Meijer, H. E. H. Localisation phenomena in glassy polymers: influence of thermal and mechanical history. *Polymer* **2003,** 44 (12), 3579-3591 DOI: 10.1016/s0032-3861(03)00089-2.

161.Meijer, H. E. H.; Govaert, L. E. Multi-scale analysis of mechanical properties of amorphous polymer systems. *Macromolecular Chemistry and Physics* **2003,** 204 (2), 274-288 DOI: 10.1002/macp.200290080.

162.Meijer, H. E. H.; Govaert, L. E. Mechanical performance of polymer systems: The relation between structure and properties. *Progress in Polymer Science* **2005,** 30 (8-9), 915-938 DOI: 10.1016/j.progpolymsci.2005.06.009.

163.Chen, K.; Schweizer, K. S. Microscopic constitutive equation theory for the nonlinear mechanical response of polymer glasses. *Macromolecules* **2008,** 41 (15), 5908-5918 DOI: 10.1021/ma800778v.

164.Chen, K.; Schweizer, K. S. Suppressed Segmental Relaxation as the Origin of Strain Hardening in Polymer Glasses. *Physical Review Letters* **2009,** 102 (3), DOI: 10.1103/PhysRevLett.102.038301.

165.Chen, K.; Schweizer, K. S. Theory of aging, rejuvenation, and the nonequilibrium steady state in deformed polymer glasses. *Physical Review E* **2010,** 82 (4), DOI: 10.1103/PhysRevE.82.041804.

166.Chen, K.; Schweizer, K. S. Theory of Yielding, Strain Softening, and Steady Plastic Flow in Polymer Glasses under Constant Strain Rate Deformation. *Macromolecules* **2011,** 44 (10), 3988-4000 DOI: 10.1021/ma200436w.

167.Garwe, F.; Schonhals, A.; Beiner, M.; Schroter, K.; Donth, E. MOLECULAR COOPERATIVITY AGAINST LOCALITY AT GLASS-TRANSITION ONSET IN POLY(N-BUTYL METHACRYLATE). *Journal of Physics-Condensed Matter* **1994,** 6 (35), 6941-6945 DOI: 10.1088/0953-8984/6/35/005.

8. Author Outputs

Publications:

(1) Ondreas, F.; Lepcio, P.; Zarybnicka, K.; Zboncak, M.; Govaert, L.E.; Jancar, J. The effect of the nanoparticle organization on the relaxation and mechanical properties of polymer nanocomposites. Submitted to Macromolecules **2018**.

(2) Ondreas, F.; Jancar, J. Temperature, Frequency, And Small Static Stress Dependence Of The Molecular Mobility In Deformed Amorphous Polymers Near Their Glass Transition. *Macromolecules* **2015**, *48*, 4702-4716.

(3) Lepcio, P.; Ondreas, F.; Zarybnicka, K.; Zboncak, M.; Caha, O.; Jancar, J. Bulk polymer nanocomposites with preparation protocol governed nanostructure: the origin and properties of aggregates and polymer bound clusters. Soft Matter **2018**, 14 (11), 2094-2103.

(4) Cech, V.; Knob, A.; Hosein, H. -A.; Babik, A.; Lepcio, P.; Ondreas, F.; Drzal, L. T. Enhanced Interfacial Adhesion Of Glass Fibers By Tetravinylsilane Plasma Modification. *Composites Part A: Applied Science and Manufacturing* **2014**, *58*, 84-89.

(5) Lepcio, P.; Ondreas, F.; Jancar, J. Rheological Behavior Of Polystyrene-Based Nanocomposite Suspensions Under Laos. *Materials Science Forum* **2016**, *851*, 215-220.

(6) Zboncak, M.; Ondreas, F.; Jancar, J. Force-Assembled Fe3O4 Particle Chains In Polyurethane Matrix. *Materials Science Forum* **2016**, *851*, 221-225.

(7) Ondreas, F.; Lepcio, P.; Zarybnicka, K.; Zboncak, M.; Pasthukov, L.; Govaert, L.E.; Jancar, J. Mechanical properties of nanostructure controlled polymer nanocomposites. *DYFP* 2018 *Book of Abstracts*. Eindhoven, **2018**. p. 292-295.

(8) Ondreas, F.; Lepcio, P.; Zboncak, M.; Jancar, J. Thermo-Mechanical Behavior of Polymer Nanocomposites with Controlled Nanostructure. *Curie - Pasteur - CEITEC joint young scientist retreat*. Brno, **2017**. p. 86-86.

(9) Ondreas, F.; Lepcio, P.; Zboncak, M.; Jancar, J. Thermo-mechanical response of polymer nanocomposites with governed structure. *CEITEC PhD Retreat II, Book of abstracts*. Brno, **2017**. p. 94-94. ISBN: 978-80-210-8550-3.

(10) Ondreas, F.; Lepcio, P.; Zboncak, M.; Jancar, J. Reologické a termomechanické vlastnosti polymerních skel a jejich nanokompozitů. *TA Instruments User meeting*, **2016**.

(11) Ondreas, F.; Lepcio, P.; Zboncak, M.; Jancar, J. Thermo-mechanical behavior of polymer nanocomposites with governed structure. *CEITEC Science Mixer* **2016**.

(12) Ondreas, F.; Jancar, J. Response of polymer glasses to simultaneous static and dynamic loading. *Book of Abstracts of 16th International Conference of Deformation Yield and Fracture of Polymers.* Eindhoven, **2015**. P.193-196.

(13) Ondreas, F.; Jancar, J. Influence of nanoparticle- chain interactions on supermolecular structure and deformation behavior of glassy polymer nanocomposites. *Structure and Dynamics of Polymer Nanocomposites*. Montpellier: Laboratoire Charles Coulomb Montpellier, **2015**.

(14) Ondreas, F.; Lepcio, P.; Zboncak, M.; Jancar, J. Thermo-Mechanical Behavior of Polymer Glasses Probed by Nano- Particles. *Chemistry & Life 2015 – Book of Abstracts*. Brno: Brno University of Technology, **2015**. p. 188-189. ISBN: 978-80-214-5228- 2.

(15) Ondreas, F.; Jancar, J. Response of PMMA to simultaneous static and dynamic loading near glass transition. *CEITEC PHD RETREAT*. 1. Brno: Masaryk University, **2015**. p. 108-108. ISBN: 978-80-210-7825- 3.

(16) Ondreas, F.; Lepcio, P.; Cech, Analysis of a-SiOC:H films by selected spectroscopic techniques. In *Student conference Chemistry is Life.* Brno University of Technology, Faculty of Chemistry, **2012**.

Projects:

(1) TA62804000 – Recycling of waste polycarbonates and development of advanced thermoplastic blends with polycarbonate part usable in primary production application – 2018-2019 – coinvestigator

(2) STI-J-17-4204 – Mechanical properties of polymer nanocomposites with controlled structure – 2017 – principal investigator

(3) STI-J-16-3650 – Governing of nanoparticle self-assembly in polymer liquids and influence of formed nanostructure on thermomechanical behavior of final nanocomposites – 2016 – principal investigator

(4) STI-J-17-4295 – Magnetic field directed self-assembly as rout for bottom-up build-up approach inspired by nature – 2017 – coinvestigator

(5) STI-J-15-2856 Influence of kinetic and thermodynamic preparation conditions on dispersion states of polymer nanocomposites and their thermomechanical properties – 2015 – coinvestigator